A Doctoral Dissertation

The role of minor faults in the upper crust along the high strain-rate zones: topographical and geological approaches

ひずみ集中帯の上部地殻における小規模断層の役割:

地形・地質学的アプローチ

March 2022

Tomonori TAMURA

Graduate School of Sciences and Technology for Innovation, Yamaguchi University

Abstract

In high strain-rate zones, active regions of ongoing crustal deformation, earthquakes occur frequently, the total slip rates of active faults are in the zone not consistent to strain rate detected by geodesy. This difference is one of the most significant issues for crustal deformation, and is known as “strain-rate paradox”. Previous crustal deformation models are mainly constructed with major active faults alone, whereas minor faults are often recognized in the high strain-rate zones. The aims of this thesis are to solve the strain-rate paradox and propose a new image of the crustal deformation by focusing on the minor faults. In order to accomplish these goals, the representative high strain-rate zones such as San-in Shear Zone (SSZ) and Niigata-Kobe Tectonic Zone (NKTZ) were targeted. As a result of the topographical and geological approaches, universal model, origin, deformation process and mechanism of the high strain-rate zone were clarified. The main outcomes are as follows:

(1) Minor faults in the NKTZ, which are mostly NE–SW to ENE–WSW-trending, have a few mm to a few dozens of cm in width and exhibit dextral sense of shear. These minor faults are distributed in the vicinity and/or away from the major active faults. In addition, the active fault, whose core zone has 5 m in thickness, were found. Such fault showed dextral sense of shear and has the latest slip event after AD 1521–1658, suggesting that the fault clearly contribute to the dextral deformation of the NKTZ. The origins of such faults are thought to be tensile cracks formed in Cretaceous, suggesting that the faults contribute to the dextral deformation of the NKTZ after repeated faulting along the cracks. The minor faults away from the major active faults are also thought to contribute to the deformation of the NKTZ, whereas minor faults outside of the NKTZ cannot contribute to that of the NKTZ.

(2) Minor faults in the SSZ, which are mostly ENE–WSW to NE–SW-trending, have a few mm to a few dozens of cm in width and exhibit dextral sense of shear. These other minor faults trending NW–SE ~ NNW–SSE direction with steep dips, are sinistral sense of shear. The minor faults, which is trending E–W direction with steep dips, showed dextral sense of shear. Active faults, whose attitude are nearly parallel to the SSZ, are also newly recognized. The thickness of the fault is a few cm and thought to show dextral-reverse oblique slip after 18648-16313 cal. BC. The frameworks of the major active faults in the SSZ are thought to prepared along the geological boundaries and such faults have grown by the repeated activities since Paleogene. It is considered that not only major active faults but also minor faults away from

the major active faults can contribute to the dextral motion of the SSZ. On the contrary, there are only reverse fault was recognized in the area outside of the SSZ.

(3) The minor fault in the high strain-rate zones, which includes the minor fault away from the major active fault, can contribute to the dextral deformation of the high strain-rate zones because of their attitudes and sense of shears. On the other hand, the minor faults outside of the high strain-rate zones cannot contribute to the dextral deformation of the zone due to their attitudes and sense of shears. Thus, there are noteworthy difference between minor faults in and outside of the high strain-rate zones. Combining these outcomes, a hierarchical structure of the high strain-rate zones can be constructed as follows: (I) fault core of major active faults, (II) damage zone of major active faults, (III) brittle shear zone (or active background; the area beyond the damage zone but in the SSZ), (IV) inactive background (outside of the high strain-rate zone). This new model enables to partly solve the strain rate paradox for both zones, whereas an occurrence of faults differs between the zones. The NKTZ is characterized by NE–SW to ENE–WSW-trending minor faults and their thickness ranging from a few mm to a few dozens of cm. The active faults possess fault core with > 5 m in thickness. The SSZ are characterized by NW–SE or E–W-trending minor faults and their thickness ranging from a few mm to a few dozens of cm. Some faults show the Quaternary activities, whereas fault core with a few meters in thickness were not found. These differences on fault occurrence are considered to be derived from the evolutional processes. It is thought that the repeated activities along the pre-existed structures lead to present active faults. Thus, it can be considered that the faults are assigned in response to the local geological background, which result in dextral contribution to the high strain-rate zones.

This study clarified universal model, origin, deformation process and mechanism of the high strain-rate zone by focusing on the minor faults. These achievements can constrain the modeling of the crustal deformation and interpretations of the geodetical observations and can contribute to assessments of large-scale constructions and seismic hazards.

要旨

地殻変動が活発な領域であり大地震がしばしば発生することで知られるひずみ集中帯では，活断層の平均変位速度の合計（長期的変位速度）と測地観測によって得られる変形レート（短期的ひずみ速度）は一致しない．このような違いはひずみパラドックス問題と呼ばれ，地殻変形に関する第一級の未解決問題である．これまでの地殻変動モデルでは，主要活断層の変形に基づいて説明されるが，ひずみ集中帯には小規模断層も認められている．本博士論文の目的は，小規模断層に着目することでひずみパラドックス問題を解決し，地殻変動の新たな描像を提案することにある．この目的を達成するため，国内の代表的な 2 つのひずみ集中帯（新潟-神戸ひずみ集中帯と山陰ひずみ集中帯）を対象とし，地形・地質学的研究を行った．結果として，ひずみ集中帯の一般像，それぞれの起源と形成過程，小規模断層を含めた地殻変形メカニズムを解明した．主な成果は次のとおりである．

（1）新潟-神戸ひずみ集中帯では，ENE–WSW〜NE–SW 走向で数 mm〜数十 cm 幅の右横ずれセンスを示す小規模断層が発達しており，主要活断層の周辺や離れた場所に分布する．また，5 m 幅の断層コアを有する活断層を新たに発見した．本活断層はひずみ集中帯の方向に調和的な走向を持ち，AD 1521–1658 以降に右横ずれ運動が生じたと考えられる．この活動は明らかに新潟-神戸ひずみ集中帯の右横ずれ変形に寄与する．これら断層の起源は後期白亜紀の引張性クラックであると考えられ，その後の活動を繰り返しながら現在はひずみ集中帯の右横ずれ変形を担っていると考えられる．主要活断層から離れた地域の断層もひずみ集中帯の変形に寄与すると考えられるが，ひずみ集中帯の外側では左横ずれセンスを示し，ひずみ集中帯の変形には参加しない．

（2）山陰ひずみ集中帯では，数 mm~数十 cm 幅の小規模断層が発達しており，主要活断層の周辺や離れた場所に分布する．山陰ひずみ集中帯の小規模断層は，NW–SE〜NNW–SSE 走向で高角傾斜の左横ずれセンスないし，E–W 走向で高角傾斜の右横ずれセンスを有する傾向が認められる．本地域でもひずみ集中帯の走向に調和的な活断層を新たに発見した．断層コアは厚さ数 cm であり，18648–16313 cal. BC 以降の右横ずれ逆断層運動が生じたと考えられる．山陰ひずみ集中帯における主要活断層は新生代火山岩の貫入境界を利用してその骨格が準備され，活動を繰り返すことで成長したと考えられる．主要活断層だけでなく，そこから離れた地域の断層もひずみ集中帯の右横ずれ変形に寄与すると考えられるが，ひずみ集中帯の外側では逆断層運動を示す断層のみが認められた．

（3）両ひずみ集中帯の小規模断層は，主要活断層から離れたものも含まれ，右横ずれ変形に寄与する姿勢・運動センスを有する．一方で，両ひずみ集中帯の外側に位置する小規

模断層は，その姿勢や運動センスからひずみ集中帯の変形に寄与していない．したがって，ひずみ集中帯の内外には明確な違いがあり，ひずみ集中帯の変形階層構造は次のように想定される：(I) 主要活断層の断層コア，(II) 主要活断層のダメージゾーン，(III) 脆性せん断帯（活動的な背景領域; ダメージゾーンの外側かつひずみ集中帯の内側），(IV) 非活動的な背景領域（ひずみ集中帯の外側）．このような地殻変形モデルを導入することで，ひずみパラドックス問題を解決に導くことができるだろう．一方，各々の断層の産状はひずみ集中帯によって異なる．新潟-神戸ひずみ集中帯では，ENE–WSW〜NE–SW 走向で数 mm〜数十 cm 幅の断層ガウジ帯を特徴とするが，中には数 m にも及ぶ断層コアを有する活断層も認められる．山陰ひずみ集中帯では，NW–SE 走向ないし E-W 走向高角傾斜で数 mm〜数十 cm 幅の断層ガウジ帯を特徴とする．活断層露頭も認められるが数 m に及ぶ断層コアはほとんど認められない．これら断層の産状的違いは各地で発達した既存の弱面に規制されて断層が配置され，断層沿いで固有の活動を繰り返すことで成長し現在に至ったと考えられる．このように，地域の局所的な地質学的背景に応じて各断層が配置され・成長し，結果としてひずみ集中帯の右横ずれ変形に寄与していると考えられる．

本研究は小規模断層の変形を考慮することで，ひずみ集中帯の一般的な変形モデルや発達過程，ひずみパラドックス問題の解決案を提示し，地殻変形の描像を刷新するに至った．本成果は，地殻の変形モデリングや測地観測結果の解釈に制約を与えるとともに，大型構造物の建設や地域の地震防災の面でも貢献すると期待される．

Contents

List of figures and tables

Chapter 1. Introduction

Chapter 2. Comprehensive study for constructing a deformation model across Niigata-Kobe Tectonic Zone, central Japan

Chapter 3. Distribution and occurrence of faults for the upper crustal deformation beneath

1. Introduction

1.1. Backgrounds

High strain-rate zones are identified by the Global Navigation Satellite System (GNSS) observations in last few decades. It is thought that geodetically observed high strain rate is associated with inland earthquakes which are frequently occurred in the zone (e.g. Nishimura, 2017). There are four representative high strain-rate zones in Japan: the Niigata-Kobe Tectonic Zone (NKTZ: Sagiya, 2000), the San-in Shear Zone (SSZ: Nishimura and Takada, 2017), strain concentration zone along the Ou-Backbone Range (OBR: Miura et al., 2002; Miura et al., 2004), Southern Kyushu Shear Zone (SKSZ: Sueoka et al., 2021) (Fig.1.1).

Upper crust is thought to behave in an elastic manner according to "elastic rebound theory" (Reid, 1910) involving accumulation and release of stress and strain for crustal faults. This implies that the short-term strain rate in an area surrounding faults should agree with the sum of the long-term slip rates of the faults. However, the discrepancy between the geodesy and geology have been seen across the high strain-rate zones (See Section 1.2 for details). Crustal deformation triggered by infrequent, large-magnitude earthquake (M >9.0) is proposed as a possible explanation for the strain-rate paradox (Ikeda et al., 2012). For example, elastic strain in northeastern Japan crust was released during the 2011 Tohoku-Oki earthquake (M 9.0) (Ikeda et al., 2012). This might result in the long-term strain rate (i.e., for periods greater than a few kyr, longer than the recurrence interval of great earthquakes) falling below the short-term strain rate (for periods of a few decades) (Ikeda et al., 2012). On the other hand, a state of E–W-trending contractions before and after the 2011 Tohoku-Oki earthquake (M 9.0) was confirmed by separating short- and long-wavelength components on the basis of the GNSS observations, indicating that the high strain-rate zones should include inelastic deformation (e.g., Menesess-Gutierrez and Sagiya, 2016). Thus, only the elastic behavior of the crust along with "Armageddon earthquake" cannot explain whole deformation of the crust beneath the high strain-rate zones. Menesess-Gutierrez and Sagiya (2016) and Menesess-Gutierrez et al. (2018) inferred that such strain concentration is arisen from ductile deformation of a deep crustal fault, which is one explanation of the inelastic deformation driven by the lower crustal viscous deformation. In contrast, it remains unclear what factors are involved to upper crustal deformation in the high strain rate zones. As shown in Ohzono et al. (2011), inelastic deformation due to uncountable minor faults, cracks and the effects of

volcanos are listed as possible factors. As other explanations of inelastic strain stored in the upper and lower crust, block rotations, microcracking, tensile/shear fractures, shifted/deformed veins (sigmoidal carbonate vein), granular flow, folding, pressure solution and dislocation creep may be also possible candidate (Shelef and Oskin, 2010; Ohzono et al., 2011; Otsubo et al., 2020; Karabacak et al., 2020).

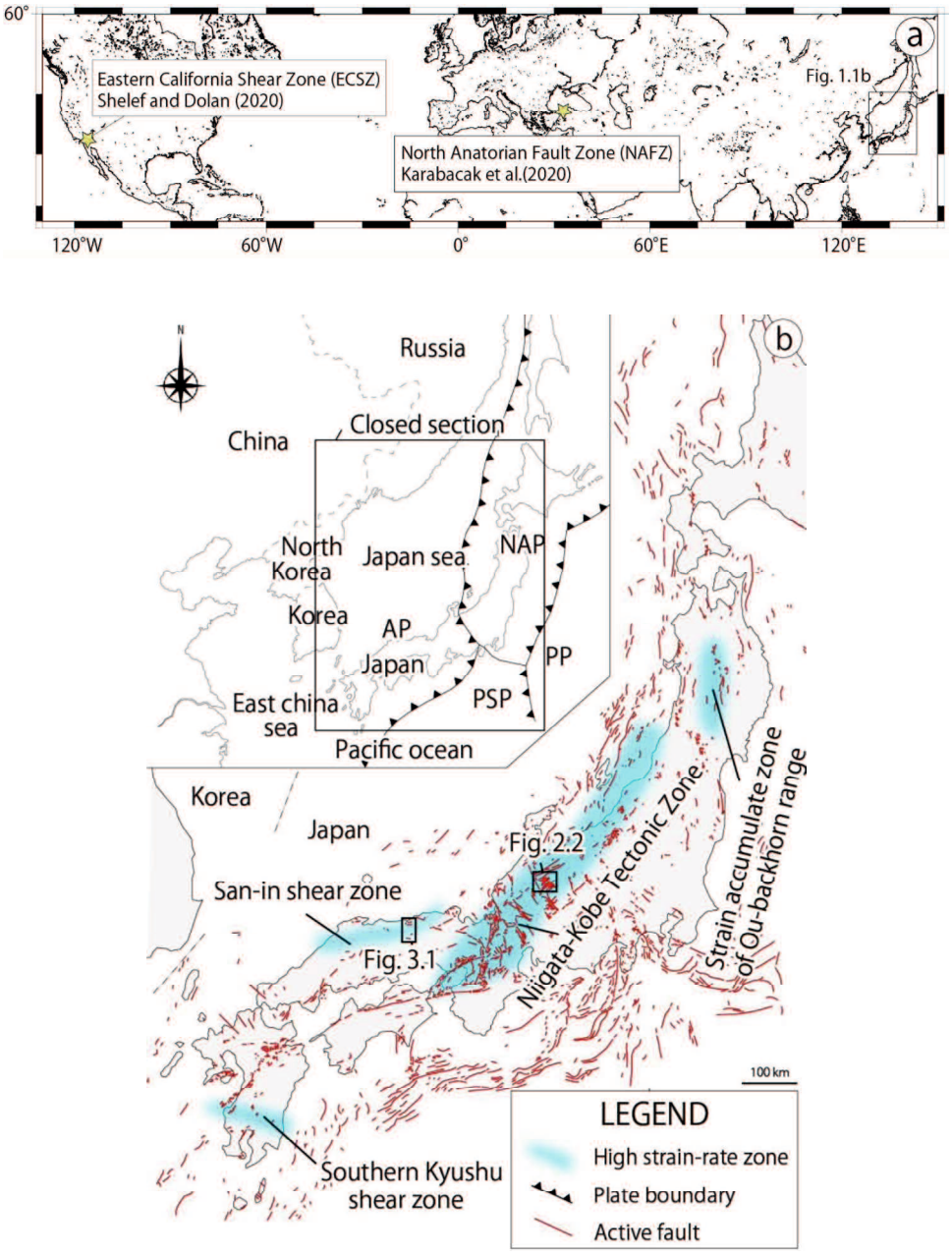

Figure 1. 1. Distribution of worldwide high strain-rate zones.

(a) A compilation of high strain-rate zones reported in the world. (b) Configuration of plates, high strain-rate zones and active faults. Dotted black lines indicate national borders. The fine red lines are active faults

given by Research Group for Active faults of Japan (1991). Small rectangles denote study areas of the NKTZ and SSZ. The extent of the high strain-rate zone follows those of Sagiya et al. (2000), Miura et al. (2004), Nishimura and Takata (2017) and Sueoka et al. (2021).

1.2. Reports on characteristic structures from worldwide high strain-rate zones

Recent studies have quantified the long-term deformation rate of off-fault deformation based on the displacement along minor faults, or that inferred from deformed pre-existing structure (such as sigmoidal vein or curved mylonite lineation). Eastern California Shear Zone (ECSZ) is one of the major high strain-rate zones, extending from Palm Springs (lied to the east of Los Angeles) to Sierra Nevada range (lied to the east of San Francisco) adjacent to the San Andreas fault (Fig. 1.1a). Shelef and Oskin (2010) anticipated that the potential discrepancy between fast geodetic rates (e.g., ~ 13 mm/y; Millinar et al., 2001) to slow slip rates (e.g., 6.2±1.9 mm/y; Oskin et al., 2008) may be at least a part due to unaccounted distributed displacement. Focusing on off-fault deformation (block rotations and offsets of secondary faults) in the ECSZ, Shelef and Oskin (2010) found that distributed displacement accommodates ~ 25 % of total displacements of the zone. This study indicates that the deformation of not only the master fault, but also minor faults obviously contribute to the observed motion of the high strain-rate zone.

North Anatolian Fault Zone (NAFZ) is also high strain-rate zone and located in the northern part of Turkey (Fig. 1.1a). In this area, it is known that the total slip rate of the fault (18 ± 3.5 mm/y; Hurbert-Ferrari et al., 2002) is much lower than the strain rate obtained by GPS observations (25.5 mm/y; Reilinger et al., 2006). Karabacak et al. (2020) paid close attention to the distributed deformation of the eastern North Anatolian Fault and compared the displacement data of the sigmoidal carbonate vein with isotopic age results, indicating the off-fault deformation rate of 15.9 ± 3.19 mm/y (corresponding to at least 50 % of the geodetically estimated annual slip rate across the fault).

In addition to the worldwide high strain-rate zones, field observations, topographic interpretations, zircon fission-track and zircon U-Pb datings are also conducted along high strain-rate zones in Japan (e.g., Tamura, 2018 MS; Tamura et al., 2020; Goto et al., 2020; Sueoka et al., 2021). In order to detect unclear tectonic landforms in the SKSZ, Goto et al. (2020) performed detailed topographic analysis and identified 1327 lineaments. Fault outcrops are also found on the lineaments (Mukoyoshi et al., 2019; Sueoka et al. 2021), suggesting that some of the lineaments are corresponding to the faults in the SKSZ. Minor

faults are also reported in the NKTZ, which provide a positive deformation for dextral motion of the NKTZ. Tamura (2018 MS) paid attention to the presence of the minor faults and quantified these total slip rate of 1.3–8.2 mm/y, indicating that crustal strain is also sufficiently stored in minor faults even away from the damage zone of major active faults. Thus, it appears that the role of minor faults for the upper crustal deformation in the high strain-rate zone cannot be negligible. Moreover, Tamura (2018 MS) assumed an active zone of concentrated minor faults as a tentative deformation model in the NKTZ (Fig. 1.2).

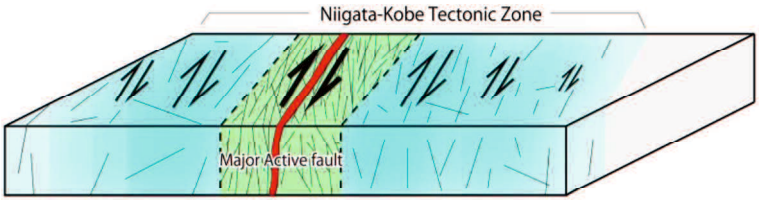

Figure 1. 2. Tentative structural model in the NKTZ (modified after Tamura, 2018 MS)

Blue zone shows active zone of concentrated minor faults. Reddish line and fine black lines denote major active fault and minor faults, respectively.

1.3. The implications for engineering geology to investigate high strain-rate zones

Although the earthquakes frequently occur in the high strain-rate zones (c.f. Nishimura et al., 2017), topographical and geological investigations for active fault evaluation have not been sufficiently conducted. The long-term evaluation of the major active fault has been investigated on a preferential basis because those of high potentials to cause destructive earthquakes. In most case, it is easy to determine trench site of the major active faults because major active faults create clear tectonic landforms. The trenching survey, which is conducted after detecting tectonic landforms, is one of the effective evaluation methods for the major active faults (e.g., Okada, 2008), providing beneficial information for the assessment of seismic hazard (e.g., latest activity and recurrence interval). However, trench survey will be difficult to excavate the minor active faults due to lack of tectonic landforms. In addition, Tamura (2018 MS) thought that some of the minor faults in the NKTZ may be active while most of the minor faults did not express the tectonic landforms. Thus, these faults bear a problem on detectability and it is difficult to evaluate them, it often cause middle to large-scale earthquakes. For example, the 2000 Western Tottori earthquake (M 7.3) and 2016 Central Tottori earthquake (M 6.6) were occurred in the SSZ due to the activity of the undetected faults. If these faults have been evaluated prior to the earthquakes, some extent of

the damage might be mitigated. Thus, understanding the feature of the minor faults in the high strain-rate zone will be needed for basic information of regional seismic hazards.

Analyzing minor faults in the high strain-rate zone are needed for not only regional seismic hazard but also construction of large-scale structures (e.g., nuclear power plant, dam and tunnel construction). In addition, recent studies in Japan Atomic Energy Agency (JAEA) pay attention to such minor faults in the high strain-rate zones to develop a new method or technology for deep nuclear waste repository of high-level radioactive waste (Goto et al., 2021; Sueoka et al., 2021). Therefore, it can be expected that the investigation of the minor faults in the high strain-rate zone can contribute to the field of the engineering geology.

High strain-rate zone	Width	Geodetic rate	Discrepancy	Major active faults
NKTZ	100 km	~ 12 mm/y	~6 mm/y	Atotsugawa fault
SSZ	17.5 ~44.5 km	4.0 ~ 6.0 mm/y	~5.7 mm/y	Shikano fault
ECSZ		13.5 ~18 mm/y	7 ~12 mm/y	Harper Lake fault
NAFZ		25.5 mm/y	4.0 ~ 10 mm/y	Northern Anatolia fault

Table 1. 1. The characteristics of the high strain-rate zones.

The geodetic rates are from Ohzono et al. (2011), Nishimura and Takada (2017), Reilinger et al. (2006), Meade and Hager (2005) and Millinar et al. (2001). Referred geologic rates are shown in Tamura et al. (2020), Shelef and Oskin (2010) and Karabacak et al. (2020).

1.4. Aims of this study

Main contents of this thesis are: (1) completing the field works and analysis in and outside of the NKTZ, (2) characterizing major and minor faults distributed in the SSZ, and (3) constructing general deformation model by integrating datum obtained from this study.

Tamura (2018 MS) reported distribution and occurrences of major active and minor faults in the NKTZ and discuss the existence of the active zone of concentrated minor faults (Fig. 1.2). However, such tentative model and the actual activities of faults cannot adequately be explained due to lack of fieldwork outside of the NKTZ and clear evidence for faulting during the Quaternary in the NKTZ. Accomplishing such uncompleted issue would enable this study to construct enhanced and comprehensive deformation model of the NKTZ. In chapter 2, major outcomes are shown as follows: (1) I have conducted further investigations and analyses of the area outside of the NKTZ, (2) I have clarified the Quaternary activity of one of the

faults in the NKTZ. Integrating these further investigations and previous thesis (Tamura, 2018 MS), enhanced and comprehensive structure model across the NKTZ will be illustrated. Note that the contents of this chapter partly include in Tamura et al. (2020).

Secondary, I also targeted upper crustal deformation in the SSZ from topographical and geological points of view, since geodetical and geophysical studies have been antecedently carried out along the SSZ to reveal its deformation especially in the lower crust. Although the San-in district is well-known area for immaturity and low activity of active faults due to lack of fault-related landforms (e.g., Okada, 2002), minor faults were frequently confirmed around the major active faults and/or aftershock areas in the San-in district (Kobayashi, 2004; Aizawa et al., 2005; Uchida et al., 2021). Some of them showed the present stress fields obtained from the fault-slip data (Uchida et al., 2021). Such facts, therefore, suggest that the SSZ seems to be deformed by the minor faults within the zone as well as NKTZ. The SSZ can be an appropriate zone to compare NKTZ because both zones have been researched intensively and are located in inland areas, which allows me to perform fieldworks and topographic analysis and to compare this study with previous studies of Tamura (2018 MS). Previous research for active faults in the SSZ (e.g., Kobayashi, 2004; Aizawa et al., 2005; Uchida et al., 2021) does not pay attention to the existence of minor faults away from the major active fault, whereas effects of such minor faults may not be negligible. In this thesis, not only major active faults but also minor faults away from the major active faults are paid attention as one explanation of inelastic deformation in the high strain-rate zones. In an effort to assess such minor faults, broader area where no active faults have previously been identified was also targeted even if it is apart from the aftershock areas and damage zones. In chapter 3, distribution and occurrences of major active and minor faults in and outside of the SSZ will be reported and discuss the hierarchical structure model of the SSZ.

In order to specify the role of minor faults for upper crustal deformation in high strain-rate zones, chapter 4 made the following discussions: (1) general hierarchical structure model and evolutional process based on comparison between the high strain-rate zones, (2) implication for the seismic hazard involving effects of minor faults.

2. Comprehensive study for constructing a deformation model across Niigata-Kobe Tectonic Zone, central Japan

2.1. Introduction

The Niigata-Kobe Tectonic Zone (NKTZ) possess not only faults within the damage zone and fault core zone of the Ushikubi faults and the Atotsugawa faults, but also minor faults outside of the damage zones (Oohashi and Kobayashi, 2008; Niwa et al., 2011). These minor faults can be expected to be one of the explanations to solve the strain-rate paradox. Thus, Tamura (2018 MS) paid attention to the existence of minor faults within the NKTZ and mapped the distribution and occurrence of the minor faults based on aerial topographic interpretations and field survey. Tamura (2018 MS) estimated that the total long-term slip rate of the minor faults in the NKTZ is 1.3–8.2 mm/y. In addition, an active zone of minor faults outside of the damage zone as a tentative deformation model of the NKTZ was proposed (Tamura, 2018 MS). However, such topographic interpretations and field survey only in the NKTZ cannot always provide enough data to construct a deformation model of the NKTZ. The area outside of the NKTZ have yet to be conducted, that is, I have yet to fully understand the order and sophisticated hierarchy of NKTZ constructed by the presence of the minor faults. For reconstructing the deformation model of the NKTZ, the distribution, occurrence of the faults and comparison between fault characteristics in the areas inside and outside of the NKTZ are needed. Thus, the area outside of the NKTZ (Kurumijima area), which is 40 km away from the Atotsugawa fault, was investigated. Hence, this chapter reports the minor faults outside of the NKTZ and reconstructs the enhanced version of the deformation model of the NKTZ.

In addition, actual activities (e.g., latest activities) of the studied faults remain unclear because of the insufficient assessment of the faults in the NKTZ although Tamura (2018 MS) proposed active zone of minor faults. Tamura (2018 MS) investigated around the Inagoe fault and recognized a fault outcrop sandwiching sand-gravel mixtures, suggesting that at least one of the studied faults is likely to be active. However, the activity of the fault has not been clearly demonstrated since the age of the sand-gravel mixtures uncomfortably overlying the fault outcrop have not been determined. The fault outcrop is located in the vicinity of the Inagoe fault trace (see Section 2.2 for detail), suggesting that it is related to the Inagoe fault. If the latest activity is well estimated, the outcrop would be a good example of faults in the NKTZ

showing the latest activity during the Quaternary. Therefore, this chapter also reports the detailed redescription of the fault outcrop and surrounding region for the purpose of determining whether it is fault core zone or not, and when is the latest activity.

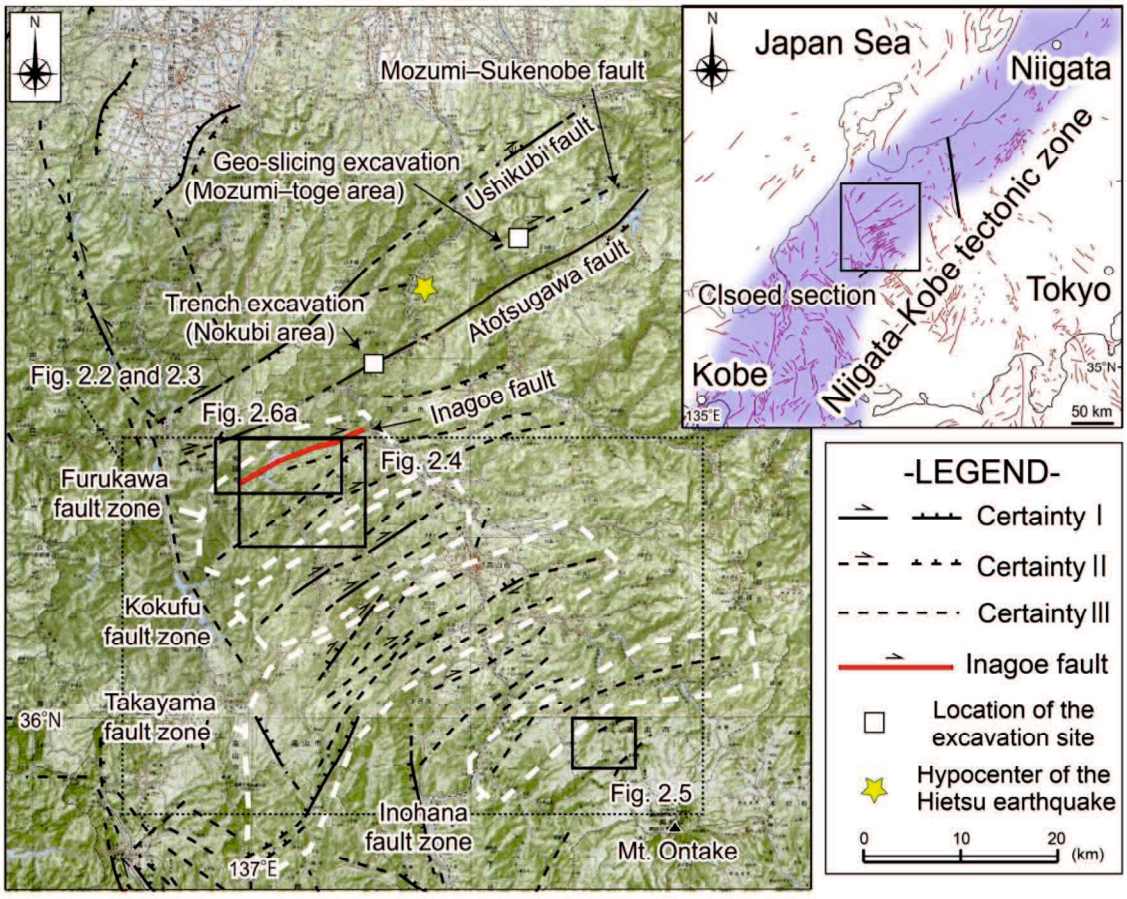

Figure 2. 1. Distribution of active faults in the NKTZ

The study area corresponds to the black rectangle. The inset shows the location of the Niigata–Kobe tectonic zone (Sagiya et al., 2000) and the major active faults in central Japan. Hypocenter of Hietsu earthquakes from Usami et al. (2013) is also shown. The topographic map was created using the Geospatial Information Authority of Japan 1:200,000 topographic map series. Active fault traces and lineaments detected by Research Group for Active Faults of Japan (1991) were subdivided into three ranks (Certainties I, II, and III), which refer the reliability of the existence of active faults. Note that Takayama-Oppara fault zone is composed of the Furukawa fault zone, the Kokufu fault zone, the Takayama fault zone and the Inohana fault zone [URL 3].

2.2. Overview of topography and geology

NE–SW trending NKTZ is well known shear zone from Niigata area to Kobe area, which

is 50–100 km in width (e.g., Sagiya et al., 2000). The zone traverses the Itoigawa-Shizuoka Tectonic Zone (ISTL), the boundary between Eurasia plate and North American plate (Fig. 1.1). The approximate topography in the NKTZ is characterized by active fault traces and lineaments by applying aerial photograph analysis (Tamura, 2018 MS; Fig. 2.2). Active fault traces are subdivided into two categories: Certainty I and II. Certainty I is assigned to faults when it is certain beyond doubt (clear evidences for the location and the sense of the displacement) that the fault was active during the Quaternary. Certainty II is assigned when it is not definitely certain but it is possible to infer the sense of the displacement. Certainty III is assigned when a fault is a lineament (without displacement marker) suspected being a fault was active during the Quaternary. Tamura (2018 MS) found that most of the active fault traces and lineaments are composed of offsets and fault saddles. It is known that the density of the active fault traces and lineaments are decreasing with increasing the distance from the Atotsugawa fault system (Tamura, 2018 MS). In addition, some active fault traces and lineaments are partly pass through the geological boundary and location of fault outcrops (Tamura, 2018 MS; Fig. 2.2 ~ 2.4). Broad scale geology within and around the NKTZ is characterized by three belts form south to north: the Hida belt, the Hida marginal belt and the Mino belt (e.g., Isozaki et al., 2010; Wakita, 2013; Fig 2.3). Hida belt comprises metamorphic rocks and granite from northern part of the Gifu Prefecture to the Hokuriku district. These lithologic distribution in the area are not always everywhere since other younger rocks and deposits overlie these metamorphic rocks and granite, resulting in limited distribution. The metamorphic rocks are thought to be suffered no less than three metamorphisms at 330 Ma, 230 Ma and 180 Ma (Soma and Kunugiza, 1993). A granite accompanied with foliations in the Hida belt is the Funatsu granite, including mylonite rocks (Kano, 1983). Hida marginal belt, distributed along the southern margin between the Furukawa area and Takayama area, is composed of middle to upper Paleozoic shallow marine formations including the metamorphosed facies of the Unazuki belt (e.g., Tsukada et al., 2004). The Mino belt is mainly composed of various types of melanges, broken formations, turbidites and tectonic slabs (e.g., Wakita, 2000). The Nohi Rhyolite (tuff, tuff breccia and rhyolite) covers these terranes and is widespread in the NKTZ. The study area is from central NKTZ (southern part of the Atotsugawa fault) to outside of the zone (approximately 45 km southeast from the Atotsugawa fault), including the Hida belt, the Hida marginal belt and the Mino belt. Although original distribution of the basement rocks is thought to be complicated due to wide variety of the rocks, actual main exposure of the study area is the widespread Nohi

Rhyolite unconformably overlain these belts. Local geology of the Kurumijima area is composed of the Nohi Rhyolite, Suzuran-Kogen basalts (early Pleisocene) and granites which intrudes into the Nohi Rhyolite (Yamada et al., 1985; Fig. 2.5).

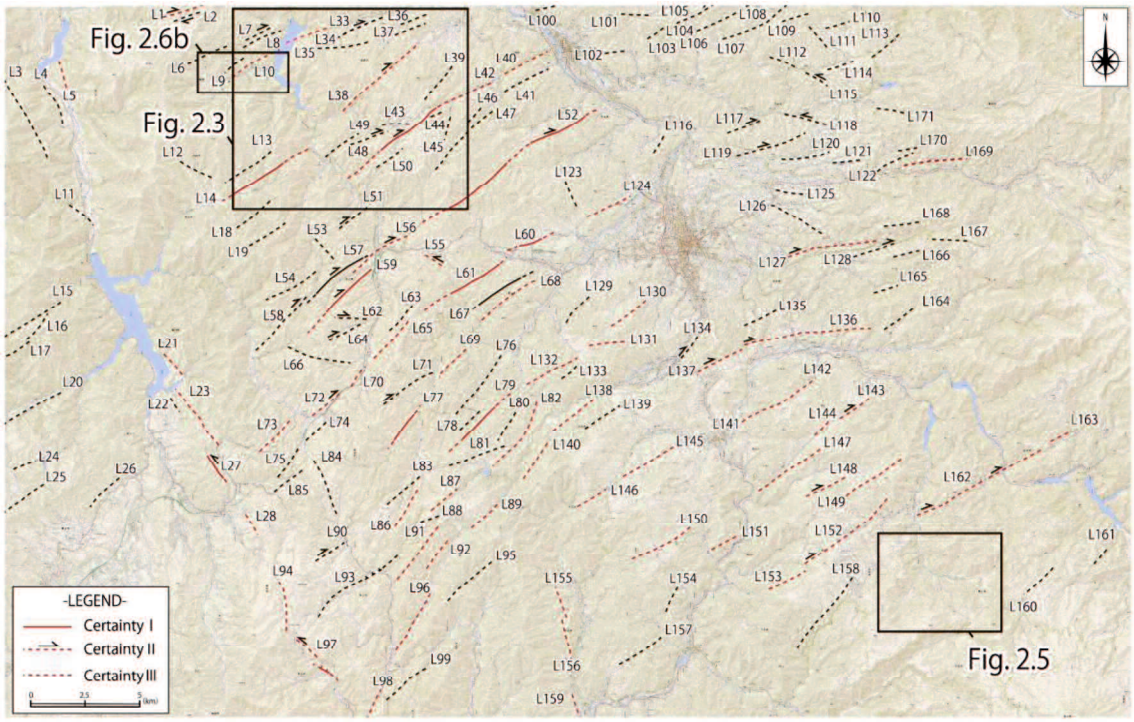

Figure 2. 2. Active fault traces and lineaments in the NKTZ

This figure is modified after Tamura (2018 MS). The red lines shows the detected active fault traces and lineaments, corresponding to the distribution of active fault traces and lineaments given by Research Group for Active Fault of Japan (1991). The black lines denotes newly detected active fault traces and lineaments in Tamura (2018 MS). The broad scale geology of this figure is corresponding to Fig.2.3.

The Inagoe fault is constituting the Furukawa fault zone (Fig. 2.1), which includes Unehata fault and Toichigawa fault. Tamura (2018 MS) investigated the Inobuseyama area (Fig. 2.4) and discovered the fault core zone of the Unehata fault. Although Tamura (2018 MS) also recognized fault outcrops around the southwestern part of the Toichigawa fault, the fault core zone of the Toichigawa fault have not been recognized. Numerous topographic detections of the active faults have been performed since 1980s. Research Group for Active Faults of Japan (1980) and Research Group for Active Faults of Japan (1991) conducted traditional topographic interpretations (40,000 ~ 50,000 scale), mapping the ENE-WSW trending lineaments from Ho pass to Inagoe region. Because the fault outcrop, located on the

lineaments, was confirmed in the Inagoe region, the lineament was regarded as an active fault trace of active fault (so-called Inagoe fault; Research Group for Active Faults of Gifu Prefecture, 2008; Fig. 2.6). Although Nakata and Imaizumi (2002) did not traced the active fault along the lineament, Suzuki and Sugito (2010), Imaizumi et al. (2018) and Kumahara et al. (2019) mapped the revised version of Inagoe fault trace, which extends from Kurigatani river to Inagoe region via Ho pass (Fig. 2.6). Although the western part of the Inagoe fault is interpretated as active fault (site indistinct) on the basis of topographic analysis, the latest activity of the fault is unknown owing to lack of direct evidence. As for the local landforms in the western part of the Inagoe fault, the Kurigatani river is running to the shimo-odori lake and is surrounded by Mt. Mominuka (1744 m), Mt. Gozen (1816 m), Mt. Kurigadake (1728 m). Middle terrace (50-160 m in height from the river), lower terrace (0-50 m in height from the river) and landslide scarps are distributed around the Kurigatani river. The Inagoe fault trace trends NE-SW to ENE-WSW orientations. The active fault trace crosses the Kurigatani river, which is located in 1 km away from the Hida-Kawai parking area to the southwest. The local geology of around the Inagoe fault is composed of Hida metamorphic rocks, Tetori group, Nohi Rhyolite and Hokuriku group (Fig. 2.3 and 2.6). The Hida metamorphic rocks are composed of limestone, granitic gneiss, calcareous gneiss, dioritic gneiss, augen gneiss and ultramylonite, mainly distributed around the western part of the Inagoe fault. Tetori group, one of the upper Jurassic to lower Cretaceous sedimentary rocks, is mainly distributed in Hokuriku district and Hida district (e.g., Matsukawa et al., 2003). The group is composed of sandstone, shale and conglomerate and often found around the eastern part of the Inagoe fault. Upper Cretaceous Nohi Rhyolite subdivided into Odorigawa rhyolite, Gero ash-flow sheet, granite porphyry dike, Shitsutani formation and Miboro ring dike, which are widely distributed around the southern side of the Inagoe fault. Hokuriku group (Pliocene to Pleistocene) constitutes sandstone, shale and conglomerate (e.g., Tamura et al., 2010). The group is also mainly distributed in Hokuriku district and Hida district, unconformably overlying the Hida metamorphic rocks around the western part of the Inagoe fault. The orientations of geologic fault are trending NE–SW, ENE–WSW or NW–SE directions (Nozawa, 1975), and the Inagoe fault is traced along one of the NE-SW-trending geologic faults. Niwa et al. (2011) investigated around the Kurigatani river and observed minor faults near the western part of the Inagoe fault trace. In addition to the field survey, a geologic section created through tunneling excavation of Hida tunnel, the third longest road tunnel in Japan (10.7 km in length) running Tokai-Hokuriku Express Way, shows geological faults

located in a few hundred meters from the Kawai portal (e.g., Fukui et al., 2007). These geological faults can reflect the Inagoe fault since the location of the geological faults is nearly equal to that of the Inagoe fault trace. Tamura (2018 MS) investigated Inobuseyama area including the Inagoe fault and discovered faults in the area (Fig. 2.4. and 2.7). The approximate attitude of the faults in the Inobuseyama area shows NE–SW trending with steep dips (Tamura, 2018 MS). At the intersection of the active fault trace and Kurigatani river, representative the fault outcrop is exposed (Inagoe fault outcrop, hereafter), and the Inagoe fault outcrop will be mainly reported in this chapter (Fig. 2.6b).

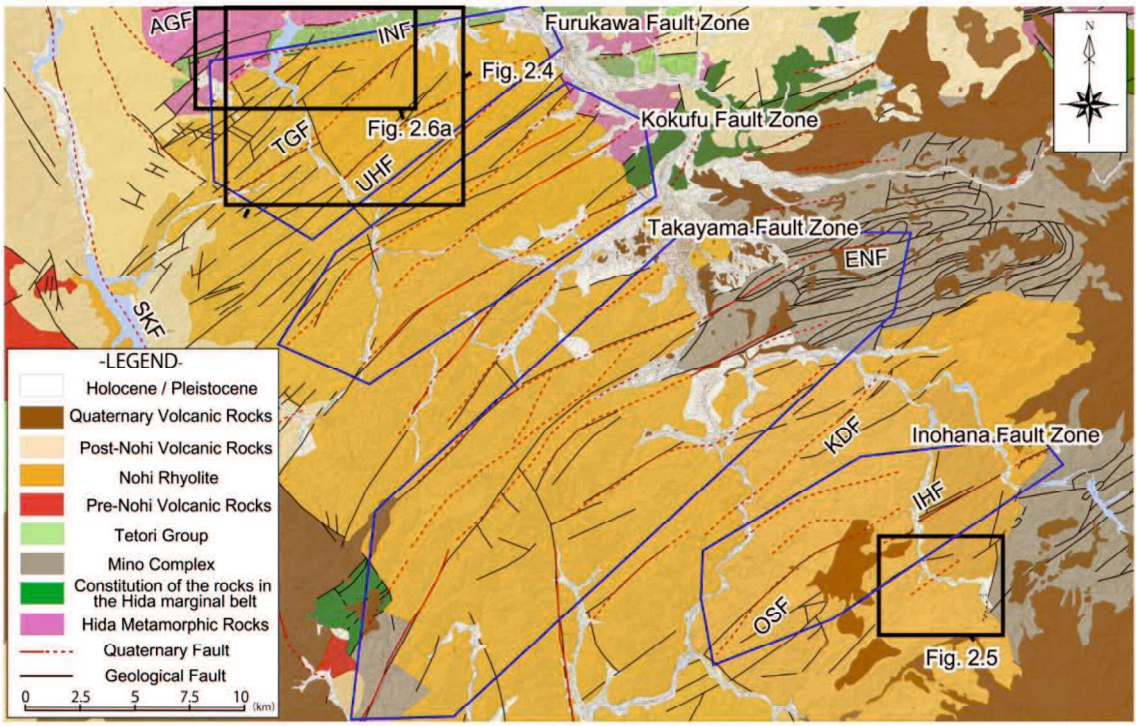

Figure 2. 3. Simplified geological map in the NKTZ (modified after Tamura et al., 2020)

The simplified geological map is from Geoland Gifu (https://geo-gifu.org/geoland/gaikan/contents_top.html). Topographic map (1:25,000) is from Geospatial Information Authority of Japan. Red lines are active faults and lineaments given by Research Group for Active Faults (1991).

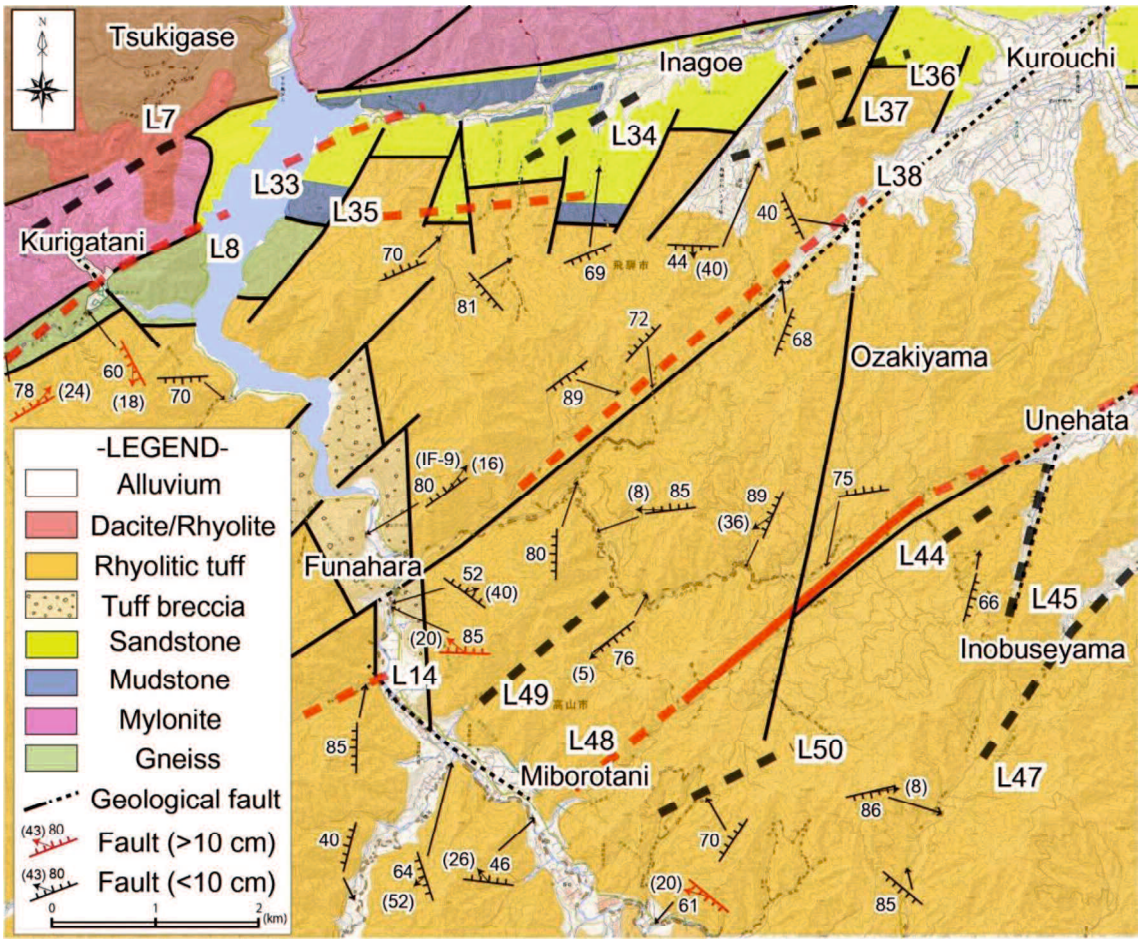

Figure 2. 4. Compiled map of the geological map and route map

This figure is modified after Tamura, 2018 MS). Thick red lines shows the detected active fault traces and lineaments, corresponding to the distribution of active fault traces and lineaments given by Research Group for Active Fault of Japan (1991). Thick black lines denotes newly detected active fault traces and lineaments in Tamura (2018 MS).

2.3. Method

The Kurumijima area was elected as the study area outside of the NKTZ since the Kurumijima area mostly has simple geology (the Nohi Rhyolite) and is not expected to be affected by Atera fault zone. Studied faults were described in terms of strikes, dips, striations, fault rocks, sense of shears, host rocks and composite planar fabrics. Observations ranging from microscopic scale to hand-specimen scale of fault rocks collected from the Kurumijima area were carried out after making polished slabs. The collected sample was cut parallel to the striations and perpendicular to the planes so that XZ planes of the fault rocks can be observed. A method for sample preparation and treatments for incohesive fault rocks (fault gouge) were

applied in accordance with the guideline of Oohashi et al. (2008).

As for the field survey inside of the NKTZ, the western part of the Inagoe fault, which is corresponding to the region of 5 km away from the Atotsugawa fault to the south, was intensively investigated. Fault outcrops were described in terms of strikes, dips, striations, sense of shears, host rocks, fault rocks. The sketch and description of the fault outcrop was reconducted (in July 2021) since its outcropping condition was changed. Macroscopic and stereoscopic observations of fault rocks collected from the field were carried out after making polished slabs. The collected sample was cut parallel to the striations and perpendicular to the planes so that XZ planes of the fault rocks can be seen. Note, however, that direction of the observation in Fig. 3.4 was shown from bottom to top. Sample preparations and treatments for incohesive fault rocks (fault gouge and fault breccia) were performed in accordance with Oohashi et al. (2008). The carbon sample for the radiocarbon measurement was dry condition. The radiocarbon measurement was conducted at the premises of Paleo Labo Co., Ltd. (Saitama, Japan) using accelerator mass spectrometry (AMS) (Paleo Lab compact AMS instrument). The radiocarbon age was measured based on a Libby half-life of 5568 years and was corrected for isotope fractionation using AMS-measured $\delta^{13}C$. The measured conventional age was calibrated using the OxCal 4.4 program (Bronk Ramsey, 2009) with the IntCal 20 calibration curve (Reimer et al., 2020). The concentrations of acids and alkali for pretreatment were 1.2 mol/L (HCl), 1.0 mol/L (NaOH), and 1.2 mol/L (HCl), respectively.

2.4. Results

2.4.1. Fault occurrences in the Kurumijima area

A total of 14 faults, consisting of fault gouge and/or fault breccia were recognized in the Kurumijima area (Fig. 2.7 and 2.8). These faults have NE–SW to ENE–WSW trending strikes with low to moderate dips. Except for three minor faults KF-5, KF-6 and KF-7 located in the central Kurumijima area, minor faults are found within ~500 m of geological faults. The majority of the fault widths range from a few millimeters to a few centimeters with the exception of fault KF-1 in the northwestern part of the Kurumijima area. Such evidences suggest that most of the minor faults in the Kurumijima area are related to the geological faults. On the other hand, KF-1 is located on geological fault in the central northern part of the Kurumijima area and comprise of the 10 cm thick gouge zone (Fig. 2.8a). The orientation of the gouge zone is N56° E/73° N and striations plunge 20° to the west, whose fault plane is accompanied with comet marks indicate sinistral–reverse oblique slip. Thus, the KF-1 is

interpretated as a fault core zone of the geological fault in the central northern part of the Kurumijima area since this fault is enough thick to express map-scale faults and has same attitude as that of the geological fault. As for geological fault-related minor ones, KF-2, for example, is oriented N77° E/50° N, contains a gouge zone that is ~1 cm wide (Fig. 2.8b and c), and the slickenlines on the fault plane plunge 39° to the west. The composite planar fabrics of the fault gouge marked by P-foliations and R1 shears indicate sinistral–normal oblique slip (Fig. 2.8d).

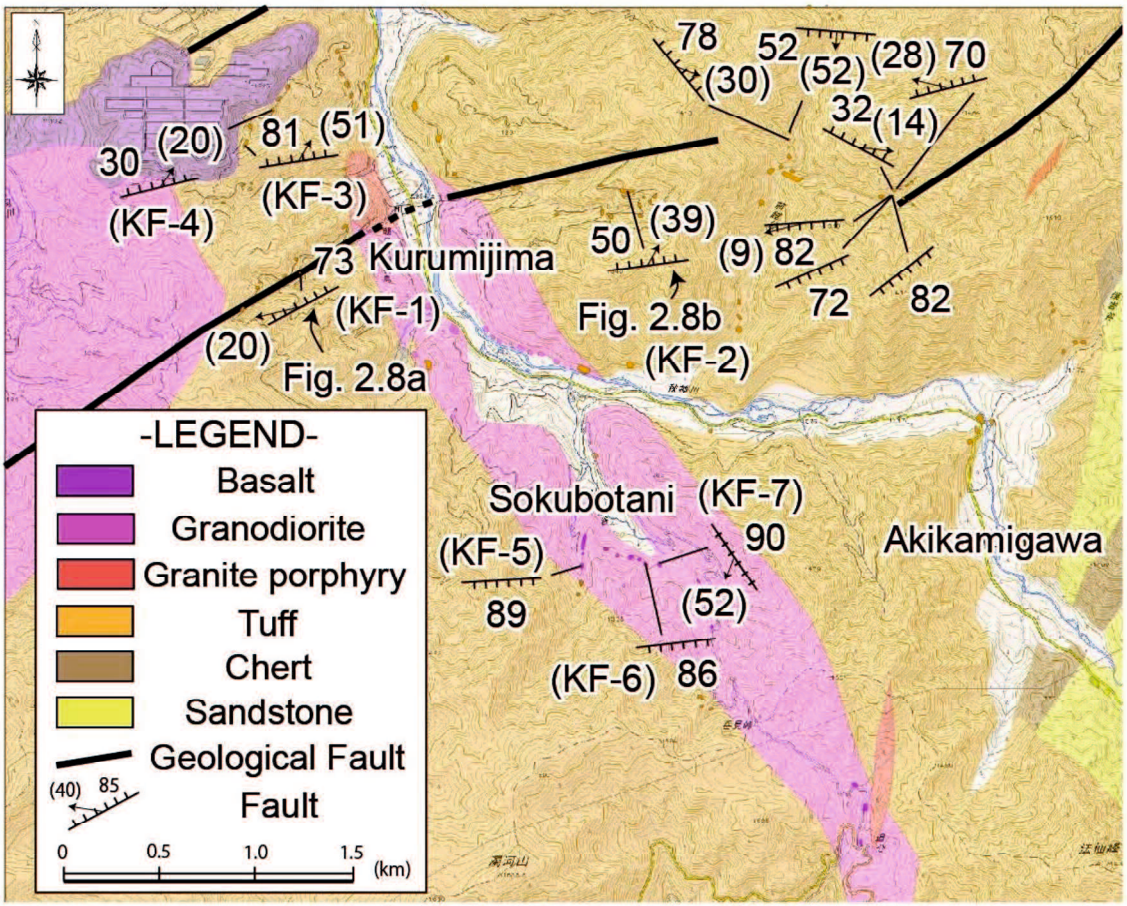

Figure 2. 5. Detailed geological map in the Kurumijima area

This figure is modified after Tamura et al. (2020). The geological map is from Yamada et al. (1985). Topographic map (1:25,000) is from Geospatial Information Authority of Japan.

Two minor faults (KF-3 and KF-4) located ~500 m from geological faults in the northwestern part of the area trend NE–SW and are marked by gouge zones varying in width from a few millimeters to about one centimeter. These minor faults can be also related to the

southwestern part of the Inohana fault since KF-3 and KF-4 are also located ~500 m from the Inohana fault trace shown in Imaizumi et al. (2018). The minor faults KF-5, KF-6, and KF-7 strikeing ENE–WSW or NW–SE and are characterized by a few millimeters thick fault gouge zones. The striations on the fault plane of KF-7 plunging southwest at 52° , whereas those on the fault planes of KF-5 and KF-6 could not be observed.

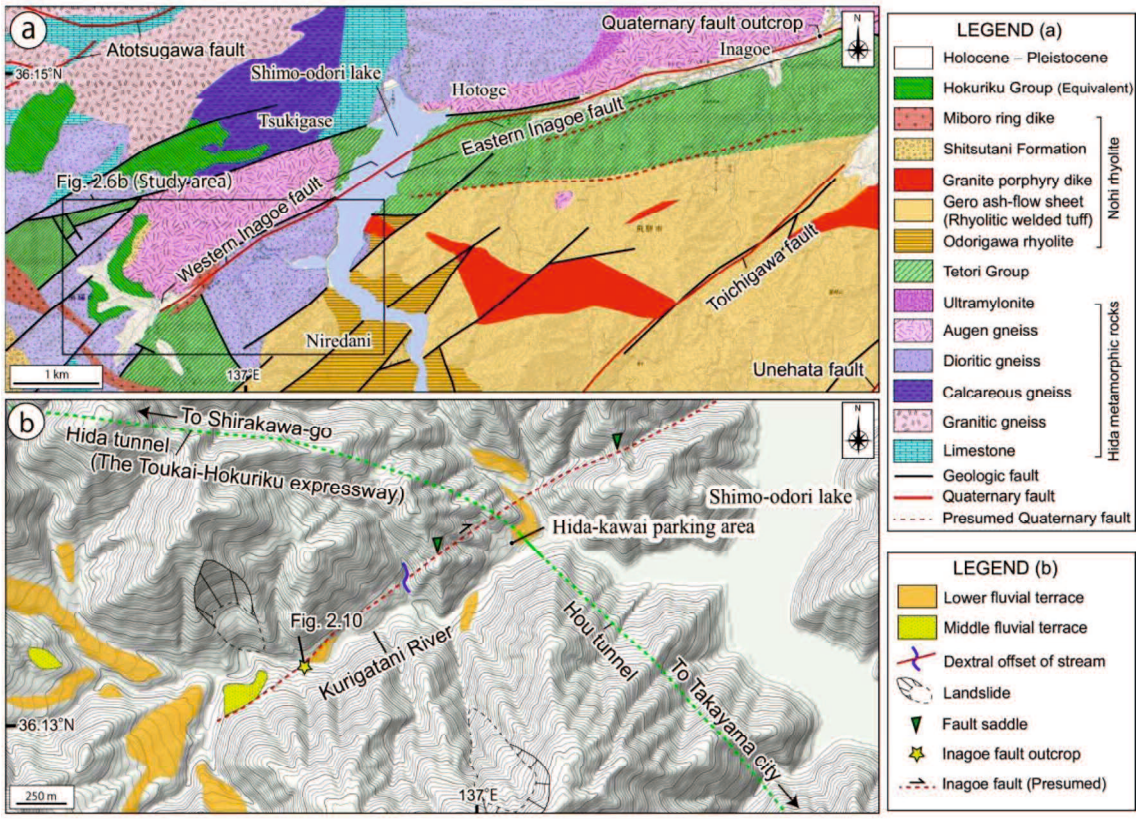

Figure 2. 6. Geology around the Inagoe fault and its landforms.

(a) Detailed geological map around the Inagoe fault. Geological map is modified after Gioland Gifu [URL4].

(b) Topographic map around the western part of the Inagoe fault. The topographic map was created using 10 m grid-cell DEM provided by Geospatial Information Authority of Japan. Topographic interpretations are referred from Kumahara et al. (2019).

In the Kurumijima area, minor faults, consistent with the present stress field (i.e., I found no NE–SW-trending faults with a dextral sense of shear or NW–SE-trending faults with a sinistral sense of shear), have not been confirmed. Thus, it appears that there is clear difference between the minor faults in the Inobuseyama area and those of the Kurumijima area. This implies that the faults in the Kurumijima area were activated under a different stress

field from that of the present day, unlike the Inobuseyama area.

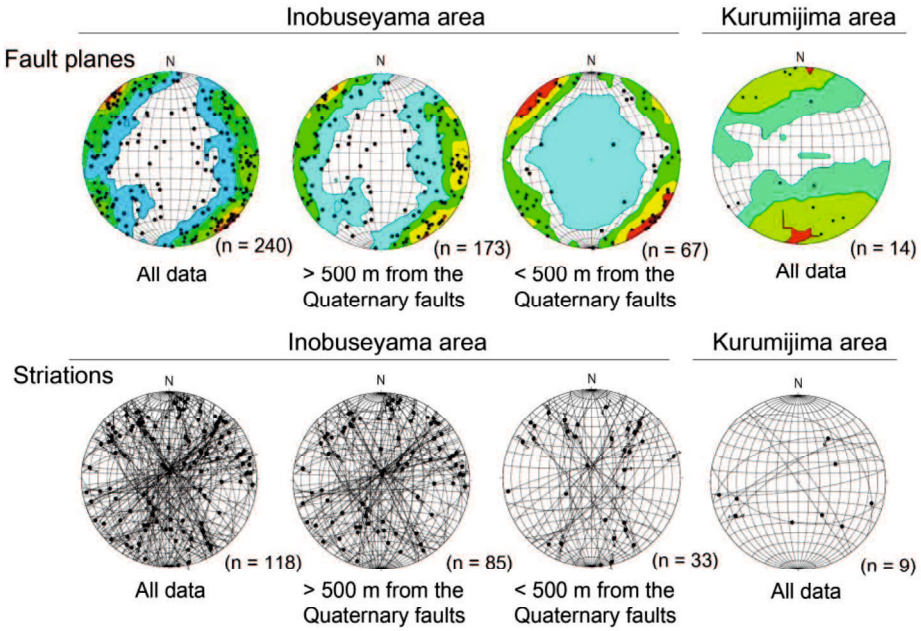

Figure 2. 7. Equal area, lower hemisphere projection of the poles of faults in the NKTZ

This figure is after Tamura et al. (2020). The Inobuseyama area is corresponding to the field area of Fig. 2.4. The Kurumijima area is corresponding to the field area of Fig. 2.5.

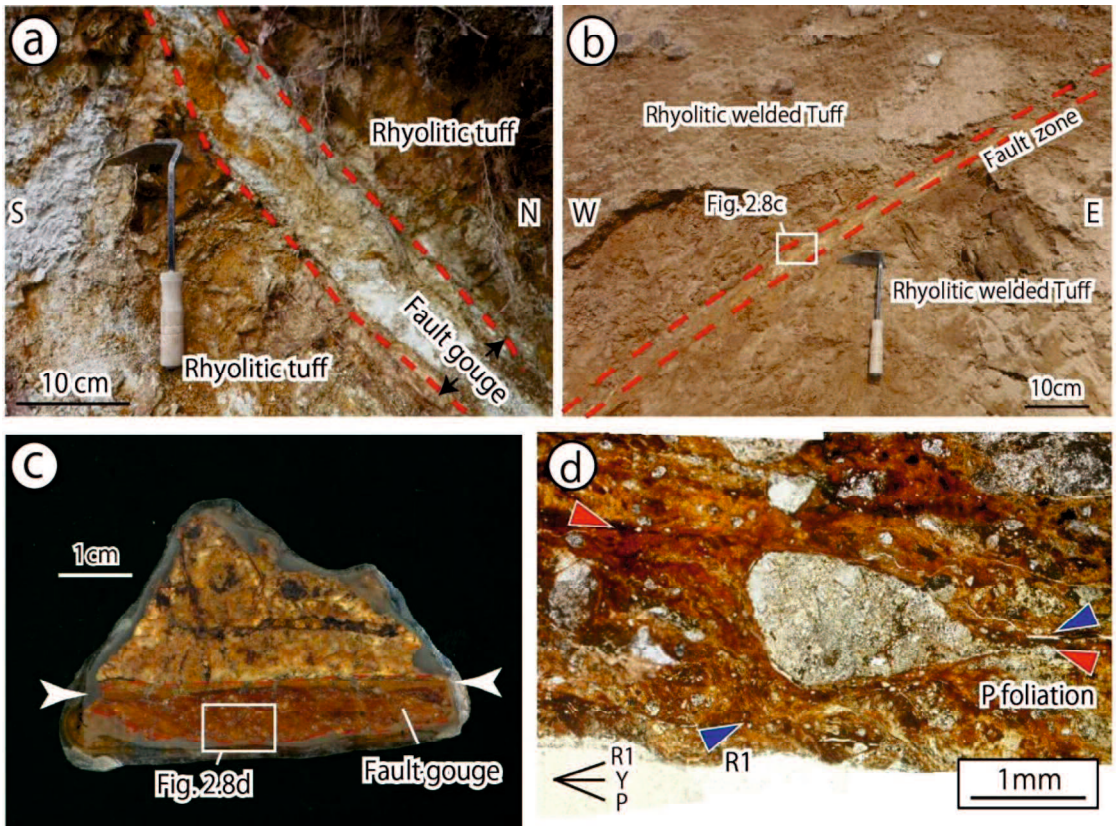

Figure 2. 8. Representative fault occurrences in the Kurumijima area

This figure is modified after Tamura et al. (2020). (a) Fault core zone of the geological fault. (b) Photograph of a minor fault. (c) Hand-specimen photograph of the minor fault. (d) Photomicrograph of gouge zone with P-foliations defined by clast alignment. R1=Riedel shear; Y=Y plane; P=P-foliation of composite planar fabric.

2.4.2. The Inagoe fault

The Inagoe fault outcrop constitutes fault gouge and fault breccia and cataclasite (Fig. 2.9 and 2.10). The fault gouge is subdivided into white fault gouge zone, black fault gouge zone, gray fault gouge zone, pale-orange gouge zone and pale blue gouge zone. Both fault breccia zone and cataclasite zone are white in color. The width of the fault zone is 5-m-wide, which is composed of at least 14 gouge zones. Most of the shear planes in the gouge zone are NE-SW trending and steeply dipping (The approximate strike and dip are N55° E85° S; Fig. 2.9c). Most of the striations on steeply dipping fault planes plunge at low to moderate angle (R0° ~ 45°). The composite planar fabrics in the fault gouge (N45° E trending P-foliation and N75° E striking Riedel shear) zone indicate a dextral sense of shear, consistent with the sense of movement of the fault inferred from stream offsets.

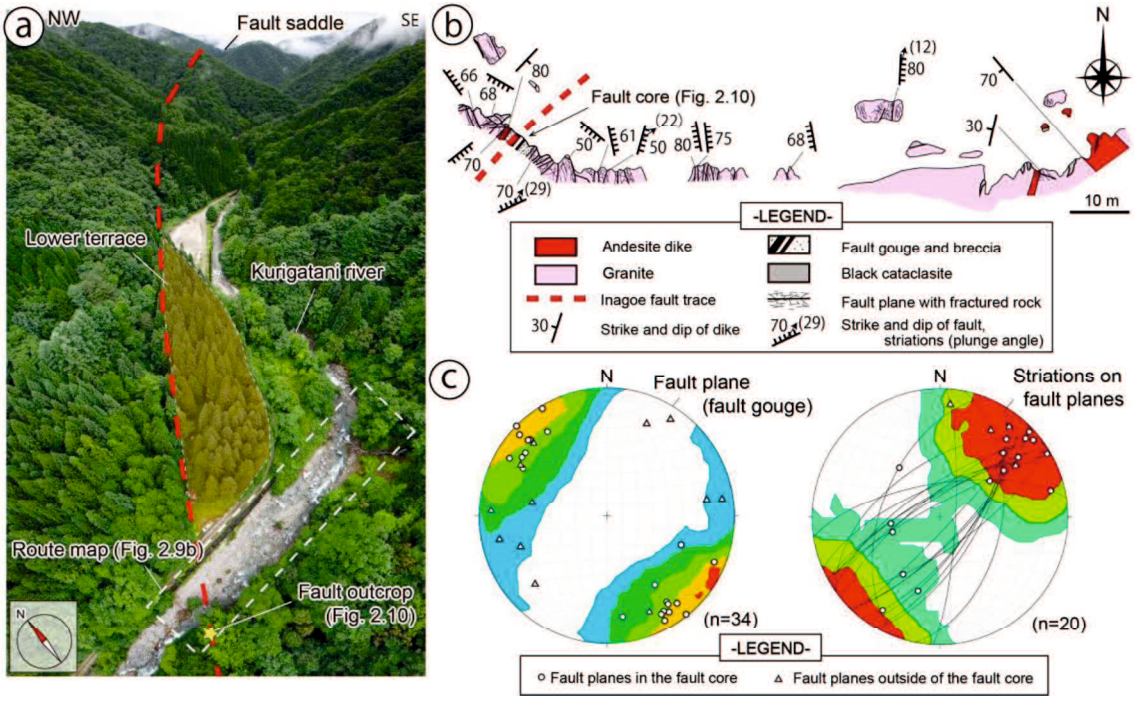

Figure 2. 9. Geologic features and landforms along the Kurigatani River

(a) Photograph showing the active fault trace, fluvial and fault-related landforms, and location of the outcrop along the Kurigatani River. The dashed red line denotes the active fault trace of the Inagoe fault. (b) Route map showing the distributions of lithologies and faults along the Kurigatani River. Approximate location of this route map is shown in Fig. 2.9a. (c) Lower-hemisphere, equal-area projections of fault planes (left) and striations on faults (right) in and around the fault core.

Incohesive gouge samples are collected from the boundary between black fault gouge zone and white fault gouge zone (Fig. 2.11b). The P-foliation of gouge fragments and Riedel shear in the gouge zone shows rotates clockwise by about 20° and strikes 20° to 30° counterclockwise with respect to Y shear, respectively (Fig. 2.11c ~ d). In addition, Fig. 2.11e shows the P-foliation of gouge fragments accompanied with σ-type clast in the zone rotates clockwise by about 10° with respect to the Y shear, indicating dextral sense of shear. Therefore, it can be summarized that the major sense of shear of the Inagoe fault is dextral faulting from the combination of field observations and sample analysis.

Unconsolidated sand-gravel mixtures unconformably overlies the granite and andesite dike. The sand-gravel mixtures, which were originally deposited above the fault zone, are also sandwiched within the fault zone. The sand-gravel mixtures are divided into upper sand-

gravel mixtures and lower sand-gravel mixtures. The lower sand-gravel mixtures mainly include andesitic, granitic and gneissic gravel, which are a few centimeters to 0.7 m in size. Matrix in the mixtures, which are coarse grain size, brownish, red brownish or ocher in color. The humus soil and silty clay was occurred at the western portion of the sand-gravel mixture. On the other hand, blackish layer and reddish silty clay were confirmed at the eastern portion of the sand-gravel mixtures. As for upper sand-gravel mixtures, andesitic, granitic and gneissic gravel, which are a few centimeters to 1.0 m in size, were included. The matrix in the mixtures, which are fine grain size, was dominant in the upper sand-gravel mixture.

The sand-gravel mixtures are also got stuck in the gouge zone. The mixtures subdivided into layer I and layer II. The layer I is composed of reddish matrix and breccia, which is matrix dominant. The layer II is composed of brownish matrix and gravel, which is gravel dominant. Major axes of gravels adjacent to the fault gouge are oriented vertically, and striations are recognized on their surfaces. On the other hand, the orientations of the axes are scattered away from the boundary between the fault gouge and the sand-gravel mixtures. Based on the distribution of the sand-gravel mixtures, existence of the striation and configuration pattern of the gravels, it is difficult to explain these geologic features of sand-gravel mixtures without faulting. Therefore, the latest activity of the fault gouge is at least after the deposition of the sand-gravel mixtures.

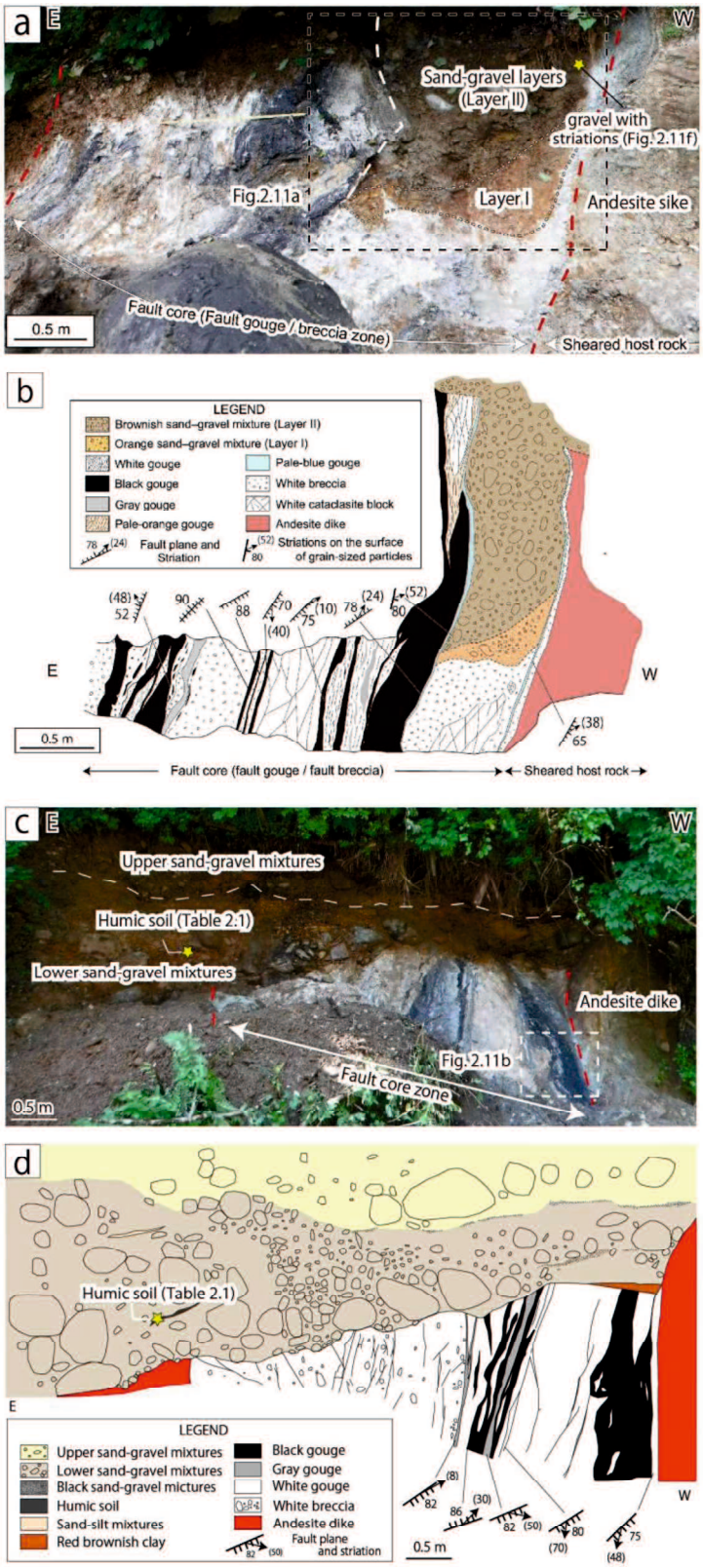

Figure 2. 10. Photographs of Inagoe fault outcrops and their sketches

(a) Snapshot of fault core zone of the Inagoe fault in 2017 (modified from Tamura (2017 MS)). (b)

Description of fault core zone of the Inagoe fault in 2017 (modified from Tamura (2017 MS). (c) Snapshot of fault core zone of the Inagoe fault in 2021. (d) Redescription of fault core zone of the Inagoe fault in 2021. The length of the yellow ruler in Fig. 3.8a is 1 m. Outcrop location is shown in Fig. 2.9a and b. Dashed red lines denote the boundary between the fault core and basement rocks.

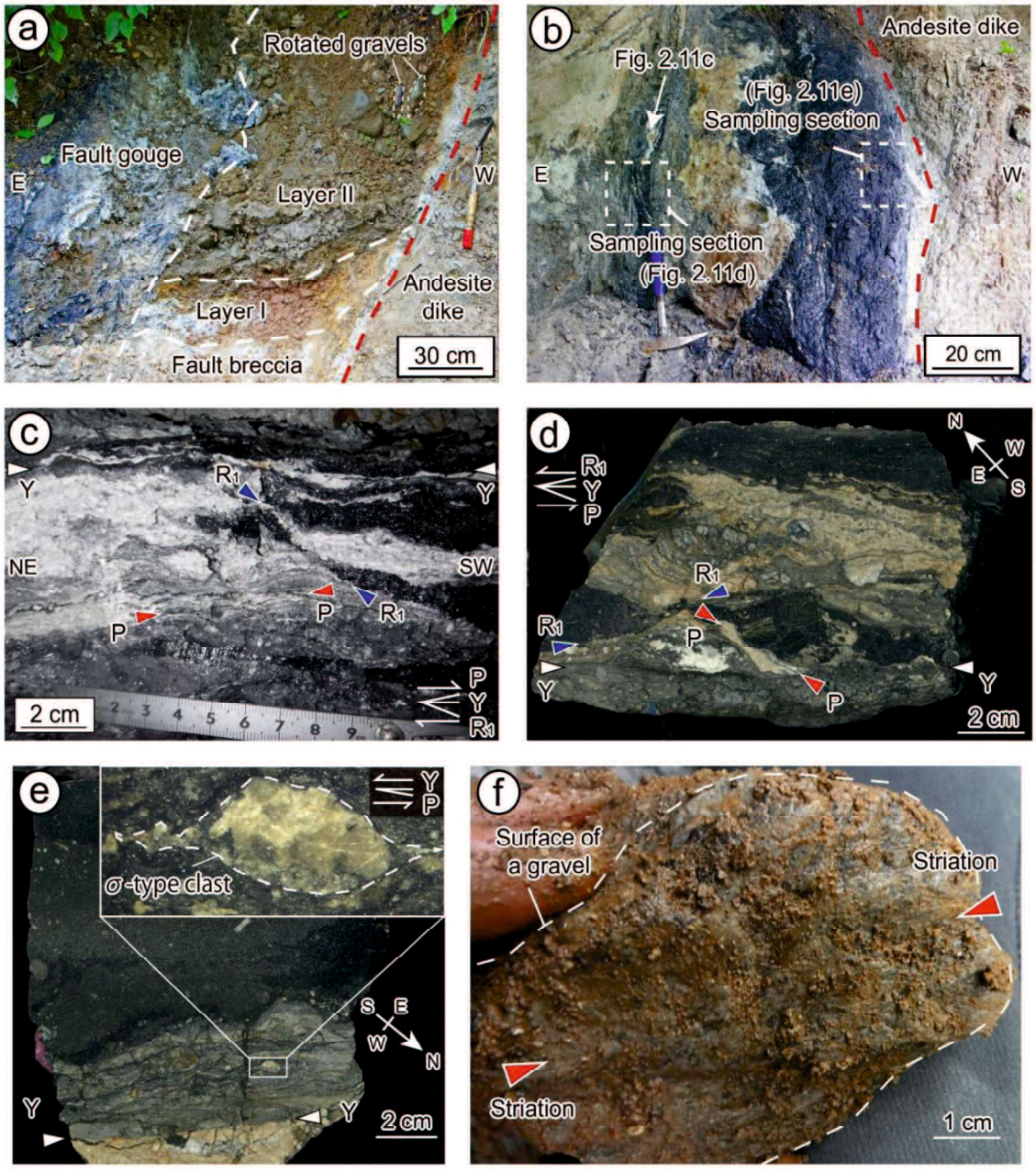

Figure 2. 11. Characteristic deformation of Inagoe fault outcrop and collected samples

(a) Photograph showing the contact between an andesite dike and the fault gouge zone. Unconsolidated sand–gravel layers (layers I and II) are sandwiched within the gouge zone. The photograph was taken in

September 2017. (b) Photograph of the contact between an andesite dike and the fault gouge zone taken in July 2020. (c) Composite planar fabrics observed in alternating layers of black and white gouge (plane view). (d and e) Scanned images of polished slabs (horizontal section) of fault gouge zone taken at the central portion (d) and western margin (e) of the fault core, with sampling section locations shown in (b). Image sections in (d) and (e) are oriented as found in the field. (f) Striations on the surface of a gravel-sized particle. R1, P, and Y denote R1 shear, P-foliation and Y shear, respectively.

In order to determine depositional age of the sand-gravel mixtures, humus soil sample was collected from the lower sand-gravel mixtures, located in 2 m high from the layer II. The humus soil was collected using stickle so that not to touch directly and cause contamination when sampling. The carbon sample from the sand-gravel mixtures yield a radiocarbon age of 285±20 yBP (AD 1521–1658; Table 2.1). As a result, the formational age of the lower sand-gravel mixtures is after 285±20 yBP.

Table 2. 1. Radiocarbon age of humus sample.

The 1 σ and 2 σ uncertainties represent the 68.27% and 95.45% confidence intervals of the calibrated age based on the high-probability density range method, respectively. The age between brackets shows conventional ^{14}C age rounded off to the nearest ten. The percentages attached with the calibrated age show the probabilities of the calibrated age on the basis of the high-probability density range method.

Sample	$\delta\ ^{13}C$ (‰)	Conventional ^{14}C age (yrBP±1σ)	^{14}C age (yrBP±1σ)	Calibrated age (Cal AD)	
				1σ	2σ
Humus soil	-29.14±0.27	285±19	285±20	1527-1552 cal AD (39.79%) 1633-1648 cal AD (28.48%)	1521-1579 cal AD (56.68%) 1585-1586 cal AD (0.19%) 1622-1658 cal AD (38.58%)

2.5. Discussion

2.5.1. The latest activity of the Inagoe fault

The location of the outcrop is approximately located on the active fault trace shown in Suzuki and Sugito (2010) and Kumahara (2019). Minor faults occurr around the fault outcrop, whereas the thickness of the faults are only a few millimeters to a few centimeters, striking NW-SE or N-S directions. Only the fault outcrop in Fig. 2.10 has large-scale fault zone (5 m in width) and shows the thickest fault zone of all the studied faults. Moreover, the composite planar fabrics in the fault gouge zone show a dextral sense of shear, consistent with the sense of shear of the fault inferred from stream offsets. Therefore, the Inagoe fault outcrop is identified as the fault core zone of the Inagoe fault.

In the previous observation, Tamura (2018 MS) confirmed the sand-gravel mixtures sandwiched within the fault core zone, suggesting that the mixtures fell into opening cracks along the fault core zone. Such sandwiched Quaternary deposits along the fault zone are frequently recognized (Okada and Tsutsumi, 1997; Fuseshima et al., 2002; Taniguchi et al., 2011). In most cases, opening cracks formed by strike-slip faulting are occurred as echelon cracks (Koide, 1983) and releasing bend (or releasing overstep) of pull-apart (Crowell, 1974; Sylvester, 1988), developing oblique to the master fault. Since the approximate direction of the sandwiched structure is along strike of the Inagoe fault, the opening cracks in the Inagoe fault cannot regard as the enchelon cracks and releasing bend (or releasing overstep) of pull-apart. On the other hand, sandbox experiments and field observation showed that small depressions and opening cracks striking along master faults also recognized (e.g., Ueta and Tani, 1999; Kim et al., 2004). Although the opening crack was identified in 2017 (Tamura, 2018 MS), the sandwiched structure cannot be observed now due to fluvial erosion, suggesting that such structure was not continued so long. Therefore, it is considered that the opening crack was formed, and the sand-gravel mixtures taken into the crack during the faulting, and subsequently such sandwiching structure locally developed within the fault zone was eroded (Fig. 2.12).

As shown in Chapter 2.4.2., the radiocarbon age of the humus soil was 285±20 yBP (AD 1521–1658), indicating that the formational age of the sand-gravel mixtures is after 285±20 yBP (AD 1521–1658). However, this radiocarbon age may not be accurate for estimating the formational age of layer I and II. Because the humus sample was collected from the 2 m higher than the deformed layer II, the radiocarbon age can indicate a little bit younger age of the depositional age of layer II. However, constitution of the lower sand-gravel mixtures resembles the layer II, suggesting that both formational ages will also be similar. Thus, the latest activity of the western part of the Inagoe fault is estimated to be after 285±20 yBP (AD 1521–1658). Such paleo-seismic event (after 285±20 yBP (AD 1521–1658)) may also correspond to historical earthquakes caused in the northern part of the Gifu Prefecture over the past a few hundred years (Fig. 2.13). According to Usami (2013), in the northern part of the Gifu Prefecture, AD 1586 Tensho earthquake (M 7.8), AD 1826 Hida-Oonogun earthquake (M 6.0), AD 1855 Hida-shirakawa earthquake (M 6.8) and AD 1858 Hietsu earthquake (M 7.0) is thought to be occurred. It remains controversial which active fault is corresponding to the source fault of the AD 1586 Tensho earthquake, one of the well-known historical earthquakes in Japan, whereas Okada (2011) summarized that there are three

possible fault system or zones as follows: Miboro fault system (Sugiyama et al., 1991), Atera fault zone (Toda et al., 1995) and Yoro-Kuwana-Yokkaichi fault zone (Matsu'ura et al., 2011). The AD 1826 Hida-Oonogun earthquake and the Hida-shirakawa earthquake are comparatively smaller magnitude than others. The former earthquake is thought to be caused around the Shirakawa-go based on the historical documents (Usami, 2013). The latter is thought to be caused around the northeastern part of the Takayama city (Nyuukawa region) on the basis of the historical documents (Usami, 2013). Although the timing of these earthquakes can be corresponding to the latest activity of the Inagoe fault, whether these earthquakes occurred surface rupture or not is unknown due to lack of historical information. In addition, Matsuda (1998) mentioned there are no source faults creating surface ruptures at $M < 6.7$ except for Matsushiro earthquake (M 5.7). The magnitude of the AD 1826 Hida-Oonogun earthquake is smaller than the M 6.7 (Usami, 2013). Although the AD 1855 Hida-shirakawa earthquake (M 6.8) is a bit larger than M 6.7 (Usami, 2013), the accurate magnitude of the earthquake is not determined due to lack of historical documents. Thus, it is difficult to identify whether latest activity of the Inagoe fault is corresponding to the AD 1826 Hida-Oonogun earthquake and/or the Hida-shirakawa earthquake. The AD 1858 Hietsu earthquake, one of the well-known historical earthquakes in Japan, was caused by the latest activity of the Atotsugawa fault. Numerous paleo-seismic studies on the Atotsugawa fault and Mozumi-Sukenobe fault demonstrated that these faults displaced in occurrence with the AD 1858 Hietsu earthquake (e.g., Research Group for the Atotsugawa fault et al., 1989; Has et al., 2000; Katagawa et al., 2002; Takeuchi et al., 2003; Takeuchi et al., 2007; Miyashita et al., 2008; Doke and Takeuchi, 2009). This supports the multiple shock of triggered by the at least two active faults, suggesting that the Inagoe fault, which is located in only 5 km away from the Atotsugawa fault and is subparallel to the Atotsugawa fault, is also possible candidate for having caused the AD 1858 Hietsu earthquake. Timber frame houses with damage around the Atotsugawa fault and the Mozumi-Sukenobe fault are > 50 % (Usami, 1979; Usami, 2013). On the other hand, the timber frame houses with damage in the Inagoe region and Hou pass are only < 20 %, which is negative evidence for activity of the Inagoe fault along with the AD 1858 Hietsu earthquake. On the other hand, Ma et al. (2003) and Soh et al. (2009) observed the 1999 Chi-Chi earthquake (M 7.8), which caused by movement of the Chelungpu fault in Taiwan and recognized significant differences in coseismic slip behavior at the single seismic event. Thus, it is also thought that different coseismic slip behavior can also generate different timber frame houses with damage depending on the sites.

It can be concluded that at least the western part of the Inagoe fault is clearly active after AD 1521–1658. Therefore, this achievement plays an important role for the regional disaster prevention. In addition, this study can contribute to the safety assessment of the Hida tunnel because the Inagoe fault passes through the Hida tunnel. In order efforts to obtain basic data (e.g., more accurate latest activity, recurrence interval and detailed distribution) for the purpose of accurate seismic hazard analysis, further investigation would be needed.

2.5.2. Enhanced version of hierarchical structure model of the NKTZ

Although minor faults in the Kurumijima area are rarely recognized (KF-5,6 and 7) apart from the geological faults, widespread minor faults are frequently observed outside of damage but within the NKTZ (Tamura, 2018 MS). The senses of shears of minor faults outside of the NKTZ are incongruous sense to those within the NKTZ, suggesting that the faults outside of the NKTZ are not active and do not contribute to the dextral motion of the NKTZ. On the other hand, the sense of movement of the NE–SW- to ENE–WSW-striking Inagoe fault located outside of the major active faults (but within the NKTZ) is dextral sense of shear, which is consistent to the dextral motion of the NKTZ. Such fault indicates a similar paleo-stress field to that of the present day (i.e., σ_1 trends E–W to ENE–WSW; σ_3 trends N–S to NNE–SSW; Tamura, 2018 MS), and especially the Inagoe fault is characterized by sandwiched structure. Therefore, it is inferred that some of the faults away from the major active faults (Atotsugawa, Ushikubi and Mozumi-Sukenobe fault) are also active and obviously contribute to the dextral motion of the NKTZ. Although the Inagoe fault, which is located away from the major active faults, is comparatively larger fault than a few millimeters to dozens of centimeters thick fault, these minor faults are also existed within the NKTZ. Oohashi and Kobayashi (2008) recognized 20 m thick fault gouge/breccia zone along the Ushikubi fault, whereas showed that the minor faults, consisting of several centimeters fault gouge zone, are also found more than 500 m away from the master fault. This suggests that the minor faults are also developed outside of the damage of the Ushikubi fault. Niwa et al. (2011) mapped the spatial distribution of minor faults around the Atotsugawa fault and demonstrates the minor faults are often found more than several km away from the Atotusgawa fault. These minor faults are obviously outside of the damage of the Atotsugawa fault. Tamura (2018 MS) also recognized minor faults in the Inobuseyama area, located more than 5 km away from the Atotugawa fault, and indicated that NE-SW- to ENE-WSW trending-minor faults have dextral senses of shears. These field investigations suggest that the minor

faults outside of the damage zone of major active faults contribute to the dextral motion of the NKTZ. Thus, Tamura (2018 MS) anticipated a zone of minor faults outside of the damage zone, which cannot explain conventional fault structure model as shown in Chester and Logan (1987) and Mitchell and Faulkner (2009). In general, fault core zones and a surrounding damage zone are constituting the internal fault zone. The fault core is the significant component of the fault and is composed of fault rocks (e.g., fault gouge, fault breccia, and cataclasite), while the damage zone, consisting of joints, cracks, and small-scale faults, is a zone suffered more damages than those in the surrounding country (host) rocks. Thus, host rocks outside of the damage zone do not almost have joints, cracks, and small-scale faults according to the conventional internal fault structure model (Chester and Logan, 1987; Mitchell and Faulkner, 2009). Since the "brittle shear zone (active background)", which is defined as a zone of minor faults outside of the damage zone, cannot be negligible owing to widespread minor faults outside of the damage zone, such background zone should be taken into account as a deformation zone of the NKTZ. On the other hand, area outside of the NKTZ should be defined an "inactive background" as one of the hierarchical structures of the NKTZ because the faults in the Kurumijima area are not active and do not contribute to the dextral motion of the NKTZ.

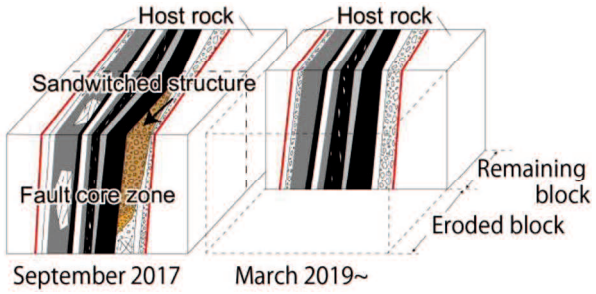

Figure 2. 12. Schematic model of the outcropping before and after erosion

The zone between the solid red lines corresponds to the Inagoe fault core zone. Brownish and orange layers are sand-gravel mixtures.

Therefore, integrating the observations in the Kurumijima area, western part of the Inagoe fault and investigations of Tamura (2018 MS), the enhanced version of the hierarchical structure model of the NKTZ can be summarized as follows (in order of decreasing deformation): 1) fault core zone of major active faults, 2) damage zones of major active faults,

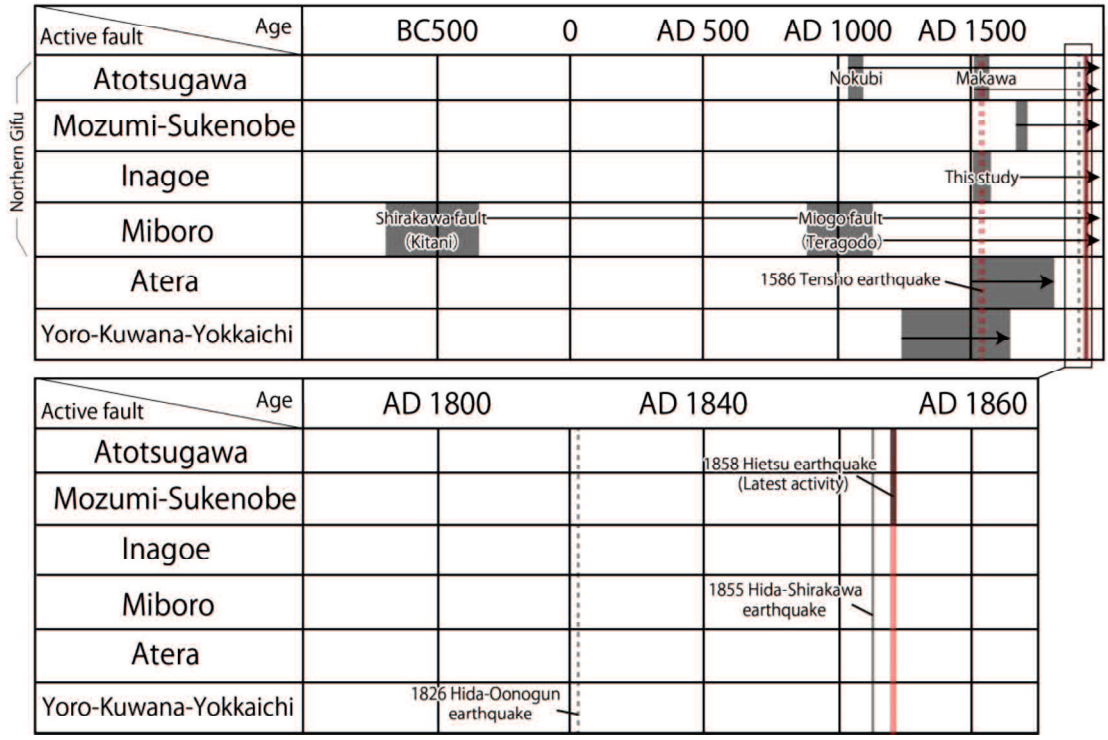

Figure 2. 13. Relationship between historical earthquakes and latest activity

Solid red line shows 1853 Hietsu earthquake. Dashed red line shows Tensho earthquake. Solid gray line shows 1855 Hida Shirakawa-Kanawaza earthquake. Dashed gray line shows 1826 Hida Oonogun earthquake. Black arrows indicate estimated age of the faulting. Gray zones denote depositional age of the humus samples. Temporal and spatial distribution of the paleo-events in the northern part of the Gifu Prefecture is compiled based on Research Group for Atostugawa Fault (1989), Sugiyama et al. (1991), Toda et al. (1995), Takeuchi et al. (2003), Okada (2011).

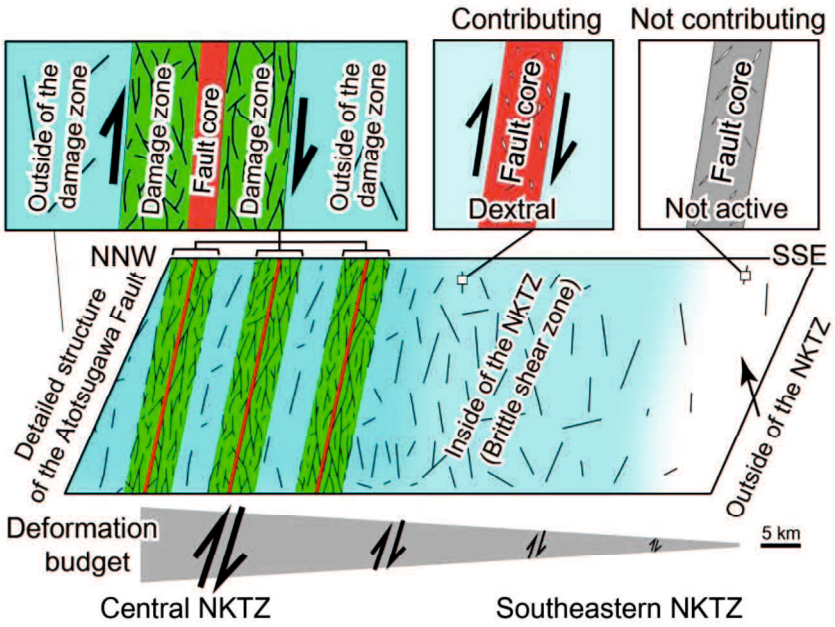

Figure 2. 14. Enhanced and comprehensive hierarchical structure model of the NKTZ

This figure is modified after Tamura et al. (2020). The black arrows denote sense of shears.

3) zones of concentrated active minor faults (incipient brittle shear zones or active background; these are beyond the damage zone but within the NKTZ), and 4) inactive background which is outside of the NKTZ (Fig. 2.14).

2.6. Conclusion

The main conclusions of this study in the NKTZ as follows:

1. As a result of the comparison between field observations in and outside of the NKTZ, brittle shear zone (or active background) that is characterized by concentrated minor faults were identified as the zone outside of the damage zone of the major active faults but in the NKTZ. As for the area outside of the NKTZ, inactive background was defined as a zone where minor faults do not contribute to the dextral motion of the NKTZ.

2. The fault outcrop along the Inagoe fault trace was reported as an example of the activity of the fault within the high strain-rate zone. The white to blackish fault zone has approximately 5 m in width, and mainly composed of fault gouge, fault breccia and cataclasite. The approximate strike of the fault is consistent with the active fault traces detected by means of the topographic analysis. Composite planar fabrics in the fault gouge

zone show a dextral sense of shear, which has good agreement with the sense of displacement of the fault inferred from stream offsets. Insight from the width, attitude, location and sense of shear, this fault outcrop is thought to be a fault core of the Inagoe fault. Dating of a carbon sample in the sand-gravel layer yields radiocarbon age of AD 1521–1658, implying that the western segment of the Inagoe fault might have ruptured during one of the four historical earthquakes in the northern part of the Gifu Prefecture.

3. Distribution and occurrence of faults for the upper crustal deformation beneath the San-in shear zone, southwest Japan

3.1. Introduction

The San-in Shear Zone (SSZ) is known for an ongoing active region of crustal deformation with high strain rate in southwest Japan (4–6 mm/y based on the observation and calculation using dislocation model; Nishimura and Takada, 2017) and shows dextral motion under E–W to NW–SE compression from focal mechanisms (Kawanishi et al., 2009; Imanishi et al., 2020, 2017; Yukutake et al., 2020). The SSZ comprises 5 major active faults, namely, Nichinanko, Shikano, Yoshioka, Amedaki-Kamato and Iwatsubo fault (Headquarters for Earthquake Research Promotion, 2016 [URL1])). Of these active faults, the Shikano, Yoshioka and Iwatsubo fault are ENE-WSW to E-W-striking dextral faults, implying that these faults can contribute to dextral motion of the SSZ because of the same strikes and sense of shears as those of the zone. In contrast, the Nichinanko and Amedaki-Kamato fault, which are NW-SE to NNW-SSE-trending active faults in the SSZ, has sinistral senses of shears and cannot contribute to the dextral motion of the SSZ.

This zone is also well-known region for microearthquake swarms, as well as inland earthquakes (e.g., 1943 Tottori earthquake (M 7.2), 2000 western Tottori earthquake (M 6.8) and 2016 central Tottori earthquake (M 6.2)). The 2000 western Tottori earthquake was occurred in the western part of the Tottori Prefecture where no active faults have been identified in the area until the 2000 western Tottori earthquake caused. Topographic interpretations detected lineaments and active fault traces (active fault and presumed active fault) around its aftershock area (e.g., Inoue et al., 2002; Takada et al., 2003), which allowed the studies focusing on the aftershock area to find small-scale faults. Paleo-seismic studies (Inoue et al., 2002; Fuseshima et al., 2002) determined the past rupture event of AD 770–1260 and ca. 27,000–7,200 through trench excavations of minor faults and radiocarbon dating. In addition to the paleo-seismic studies, it proved to be widespread minor faults distributed in aftershock area of the 2000 western Tottori earthquake based on the field surveys (Kobayashi et al., 2003; Aizawa et al., 2005; Uchida et al., 2021). The 2016 central Tottori earthquake is thought to be sinistral strike-slip fault-type earthquake caused in the central part of the Tottori Prefecture (Kurayoshi city and Misasa town) on the basis of the spatial distribution of the seismic epicenters and focal mechanisms. Field survey along the aftershock area also show the existence of minor faults (e.g., Ichimura and Mukoyoshi, 2020), which

indicates minor faults are also distributed in the central Tottori Prefecture. The 1943 Tottori earthquake, which is occurred in eastern part of the Tottori Prefecture, is triggered by the latest activity of the Shikano and Yoshioka fault. Trench survey of the Shikano fault showed that the fault has twice events over the past 8000 years, whose slip rate is estimated to be 0.2–0.4 mm/y (Okada et al., 1981). Although the fault outcrops associated with the Shikano fault are confirmed through the field surveys, the thickness of all gouge zone found during the investigation is a few millimeters to centimeters in width (Okada et al., 1981; Nishida et al., 1993). Kaneda and Okada (2002) traced the surface rupture on the 1:25,000 topographic map referring to the previous fieldworks (Tuya, 1944; Tukiji, 1948; Okada et al., 1981; Nishida et al., 1993).

Only the slip rate of the E–W to ENE–WSW-striking right-lateral major active faults cannot obviously explain the dextral motion of the SSZ. The detection of the high strain rate is mainly explained by aseismic slip in the development of flued-weakend lower crust as suggested by Iio et al. (2002). On the other hand, not only deformation in the lower crust but also deformation in the upper crust should be considered. As shown in the previous field survey around the active faults with the aftershock area in the SSZ (e.g., Tuya, 1944; Tukiji, 1948; Okada et al., 1981; Nishida et al., 1993), minor faults were frequently confirmed. In addition to the example of the SSZ, the field study of the Niigata-Kobe Tectonic Zone (NKTZ) also occurs minor faults away from the active faults, suggesting that such minor faults can also contribute to the dextral motion of the zone (Tamura, 2018 MS; Tamura et al., 2020). Hypothesizing that minor faults are widely distributed and play a role of deformation of the SSZ, not only major active faults but also minor faults in the SSZ are described and analyzed.

The purpose of study in the SSZ is to reveal the role of faults for the upper crustal deformation and propose the hierarchical deformation across the SSZ. Since the ENE-WSW to E-W-striking major active faults are significant structure to assess dextral motion of the SSZ, eastern part of the zone was targeted. The topographic interpretation is performed in and outside of the eastern part of the SSZ so that Shikano, Yoshioka and Iwatsubo faults can be analyzed (Fig. 3.1). Field investigations in the SSZ are conducted around the Shikano fault (Shikano area) and the Iwatsubo fault (Iwatsubo area), respectively (Fig. 3.1 and 3.2). To compare the faults in and outside of the SSZ, region of southern margin ~ outside of the SSZ (Kuroki area) was also investigated.

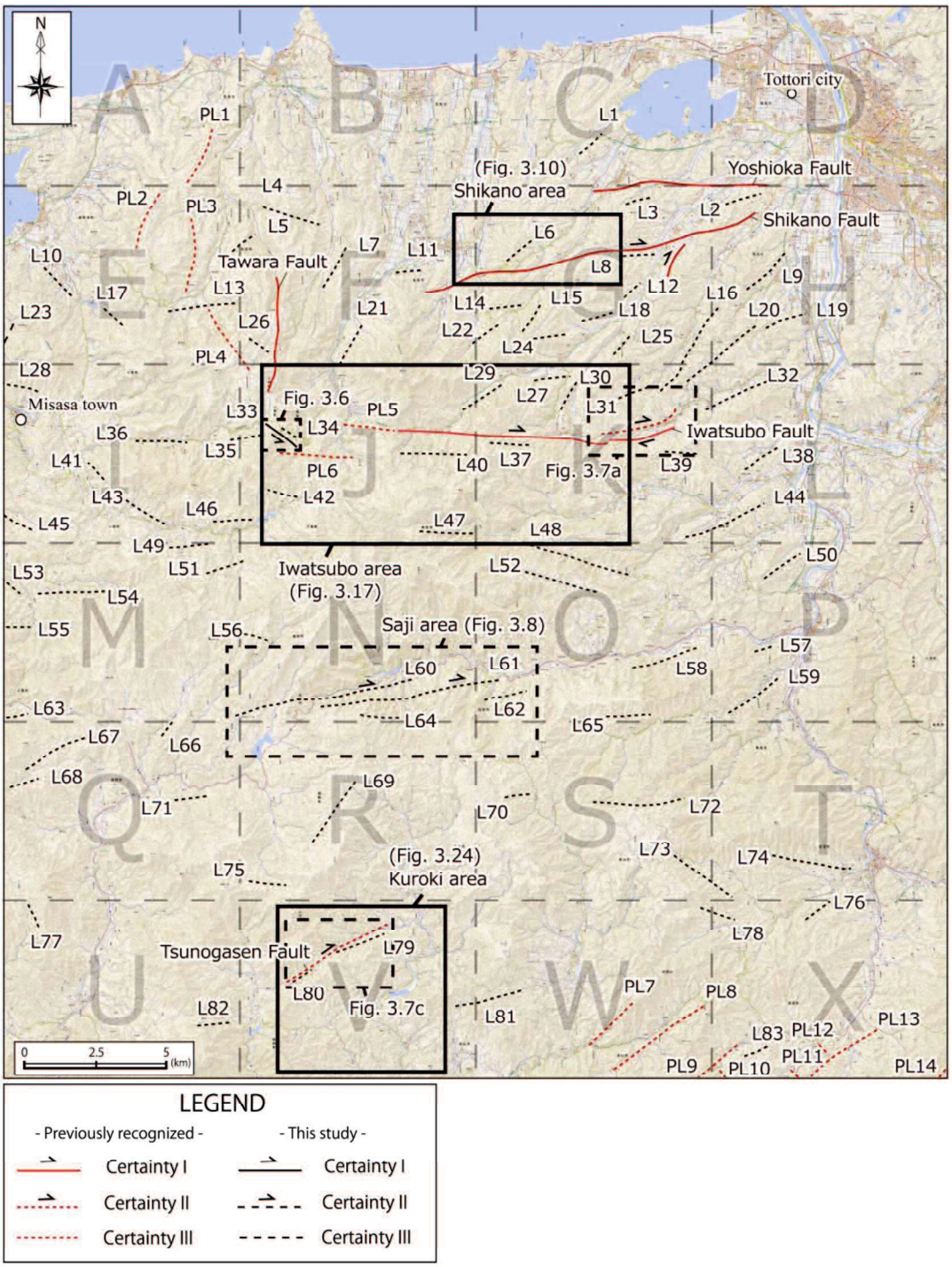

Figure 3. 1. Distribution of active fault traces and lineaments in the SSZ

Detected active fault traces and lineaments in the study area. The black lines denote the newly recognized lineaments and active fault traces through the interpretations in this study. The red lines indicate active fault traces and lineaments reported from Research Group for Active faults of Japan (1991) and Imaizumi et al. (2018). The gray dashed lines denote boundary which subdivides the study area into 24 cells. The 1:25,000 topographic map in the study area are from the Geospatial Information Authority of Japan. Black rectangles

enclose the studied Shikano, Iwatsubo area and Kuroki areas (see Figs. 3.10, 3.17 and 3.24, respectively). Broken black rectangles enclose the Satani, Saji and eastern part of the Iwatsubo areas shown as an example of the representative active fault trace and lineaments. The corresponding geological maps are shown in Fig. 3.2. and 3.9.

3.2. Overview of topography and geology

The Japan Sea is distributed in the northern part of the study area. The Tottroi sand-dune is located along the seacoast, designated as a natural monument area and a geosite of San-in geopark (UNESCO). In the eastern part of the study area, Tottori plane, which is composed of alluvial plains and river terraces formed by effects of Sendai river running toward the Japan sea, is distributed. Tributary rivers of the Sendai river (e.g., Haji river, Hattou river and Kisaichi river) is arisen from mountainous regions and formed the surrounding river terraces (e.g., Kuwamura and Yano, 2012). Greater part of the study area is constituting the mountainous regions (namely, Chugoku mountains).

The study area comprises three major active faults (the Shikano, Yoshioka and Iwatubo fault) and minor active faults (Tawara and Tsunogasen fault; Research Group for Active Faults of Japan, 1991; Fig. 3.1). The broad-scale geology of the SSZ is characterized by Suo metamorphic rocks, Mesozoic volcanic rocks, Granitoids, early to middle Miocene volcanic rocks, late Miocene volcanic rocks, Ningyo-toge formation, Pliocene volcanic rocks and Quaternary (e.g., Murayama et al., 1963; Fig. 3.2). The Suo metamorphic rocks are weakly recrystallized (metamorphosed) rocks, which is distributed from northern Kyushu to eastern Chugoku district. The rocks are distributed in the southern part of the study area. The Mesozoic volcanic rocks are composed of tuff, lapilli tuff and tuff breccia. Sasada et al. (1979) described the tuffaceous rocks in the study area and defined the rocks as Tottori-nambu volcanic rocks, which is equivalent to Late Mesozoic volcanic rocks shown in (Murayama et al., 1963). The Granitoids are subdivided into Imbi intrusive rocks and Hiroshima granite in the San-in district and the Imbi intrusive rocks are distributed in the study area (e.g., Nishida et al., 2005; Kamei, 2007). In the study area, such intrusive rocks are defined as Yoshioka granite, whose granite is comparatively fine graine and has phenocrysts of quartz, plagioclase and biotite (Sasada et al., 1963). On the other hand, coarse-grained granitic rocks (e.g., Murayama et al., 1963) and gabbroic mass (Ochigakochi gabbroic mass; Sasada, 1979) are also confirmed in the study area, whose subdivisions remains as yet unidentified. Early to middle Miocene volcanic rocks (mostly, Tottori group; Murayama et al., 1963) exposed in the

eastern part of the mapped area unconformably overlies the basement rocks (the Suo metamorphic rocks, the Mesozoic volcanic rocks and the Granitoids). It consists of basal conglomerate, volcanic formation, alteration of conglomerate, sandstone and mudstone in ascending order (e.g., Murayama et al., 1963). The Ningyo-toge formation is plant-bearing sedimentary rocks, located in the vicinity of the border between Tottori Prefecture and Okayama Prefecture (Hujita, 1972). According to Murayama et al. (1963), Pliocene volcanic rocks are composed of lower part (tuff-breccia, volcanic conglomerate and tuff of andesite and dacite) and upper part (lava flows of andesite, basalt, dacite). ENE-WSW striking geologic faults are also distributed in the northern part of the study area, corresponding to the Shikano and Yoshioka fault.

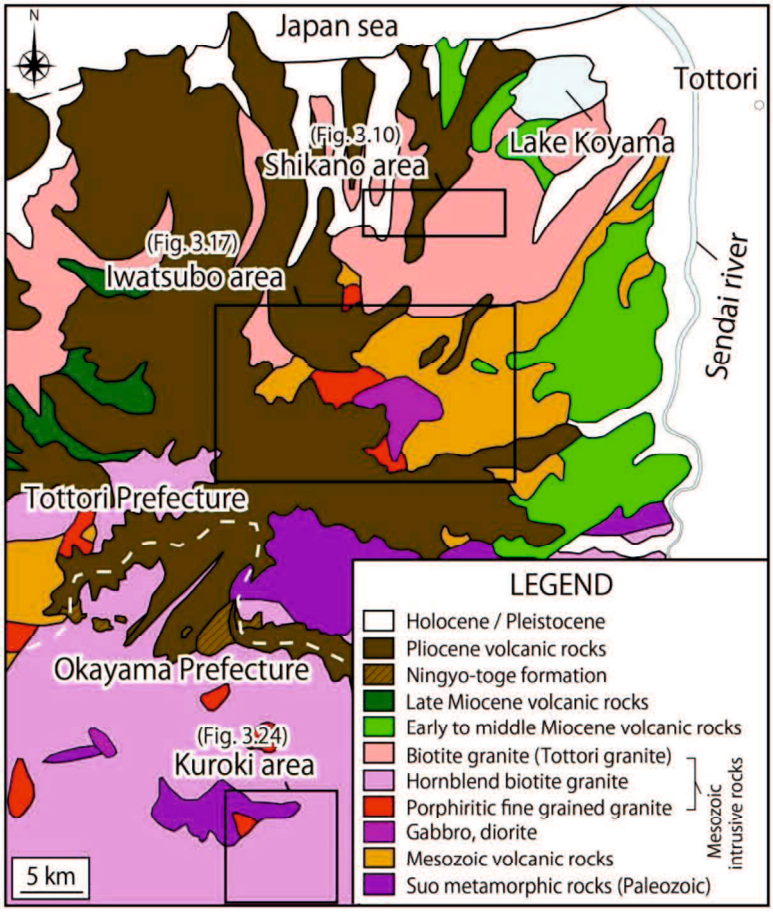

Figure 3. 2. Simplified geological map of the study area (after Murayama et al., 1963)

Black rectangles enclose the studied Shikano, Iwatsubo and Kuroki areas (see Figs. 3.10, 3.17 and 3.24, respectively). White dotted line indicates border between Tottori and Okayama Prefecture. Black rectangles are study area for field surveys. The location of an open circle shows location of Tottori city.

3.3. Method

In order to understand distribution and the density of the active fault traces and lineaments in and outside of the SSZ, topographical analysis was carried out using 1:10,000 to 1:50,000 aerial photography and digital elevation model (DEM), whose resolutions are higher than photographs and DEM data in the conventional topographic detections (Research Group for Active Faults of Japan, 1991; Nakata and Imaizumi, 2002; Takada et al., 2003; Imaizumi et al., 2018). Topographic maps (1 m and 10 m contour lines), stereopair images, slope maps were depicted using "Simple DEM Viewer" in accordance with Goto et al. (2012). The DEM 10 m and 0.5 m grid-cell DEM were obtained from Geospacial Information Authority of Japan and Tottori city, respectively. Detected active fault traces were subdivided into three ranks (active faults, presumed active faults and lineaments), which refer the reliability of the existence of the active faults, following to the guideline proposed by Nakata and Imaizumi (2002). During the field observation, strikes, dips, striations, sense of shears, host rocks, fault rocks of fault outcrops were described. Observations of polished slabs (XZ planes) from the field were also conducted in case of important outcrop. In accordance with Oohashi et al. (2008), incohesive fault rocks (fault gouge and fault breccia) were sampled and the polished slabs were made.

In order to determine the depositional age and latest activity, the carbon in the sand-gravel mixtures were sampled. The radiocarbon measurement was performed by accelerator mass spectrometry (AMS) (Paleo Lab compact AMS instrument) in Paleo Labo Co., Ltd. (Saitama, Japan). The radiocarbon age was measured based on a Libby half-life of 5568 years and was corrected for isotope fractionation using AMS-measured $\delta^{13}C$. The measured conventional age was calibrated using the OxCal 4.4 program (Bronk Ramsey, 2009) with the IntCal 20 calibration curve (Reimer et al., 2020).

Some fault gouges involved in faults were sampled and conducted X-ray diffraction (XRD) analysis to understand the mineral compositions. The samples were measured with a diffractometer, Rigaku MiniFlex 600 in Yamaguchi University. To examine the variety of clay minerals, particles of $< 2\ \mu m$ were extracted by sedimentation in distilled water after dispersion. The conditions of the XRD analysis are as follows; CuKα target, voltage; 40 kV, current; 15 mA, Step; 0.01° /min, Speed; 2° /min; measurement range; 3° –70° (3° –30° for particles of $< 2\ \mu m$). In addition, the $< 2\ \mu m$ fractions were treated with ethylene glycol. In addition, the samples were with corundum (25 wt.%) as an internal standard for the

RockJock program (Eberl, 2003). To estimate the paleostress field, Multiple Inverse Method Processer Version 6.02 (Produced by A. Yamaji, K. Sato and M. Otsubo, Kyoto University; Yamaji, 2000; Yamaji et al., 2011) was adopted. The multiple inverse method was applied in the Shikano area and Iwatsubo area to constrain the paleostress fields within the SSZ. In this study, the dike data in the Shikano area were processed using GArcmb software (Yamaji, 2016) to estimate the paleostress field during the intrusions.

3.4. Results

3.4.1. Active fault traces and lineaments in and outside of the SSZ

Previous inventories detected a total of 22 active fault traces (Certainty I and II) and lineaments (Certainty III) in the study area (Fig. 3.1; Research Group for Active Faults of Japan, 1991; Imaizumi et al., 2018). From this detailed aerial photograph interpretation and DEM analysis, a total of 86 active fault traces and/or lineaments were newly detected in the study area. The number of newly found active faults, presumed active faults, and lineaments was 1 (L33 in Satani area), 2 (L60 and 61 in Saji area) and 83, respectively (Fig. 3.1). The active fault traces and lineaments are detected based on the continuous presence of tectonic landforms (e.g., offset, fault saddle, displaced alluvial fan). Displaced rivers and ridges indicate dextral movement on the NE–SW to ENE-WSW-trending active fault traces and lineaments, whereas sinistral movement on the NW–SE-trending active fault traces and lineaments. The majority of the active fault traces and lineaments are oriented NE–SW and ENE–WSW. The NE–SW to ENE–WSW-trending active fault traces, lineaments and seismicity are distributed especially around the Shikano and Iwatsubo fault (Fig. 3.3. ~ 3.5.), while Saji area (corresponding to the subarea N and O; Fig. 3.1 and 3.2), which are located between the Iwatsubo area and Kuroki area, also possess ENE–WSW-trending active fault traces of Certainty II. The active fault traces and lineaments were not almost detected in the eastern part of the study area (especially in the eastern part of the subarea D, H, L, P and T). The active fault traces and lineaments may not have been detected due to the existence of the Tottori plane and the Sendai river, constituting the Quaternary landforms and geology (e.g., river terrace deposits, alluvium deposits, sand dunes and pumice bed) of the eastern part of the study area. These young facies can obscure the tectonic expression of minor faults unless there was remarkable repeated faulting after the formations. In addition, Tottori city, where more residential areas than any other regions are distributed, is located in the northeastern part of the study area, suggesting that the northeastern part of the study area can be mostly

affected by anthropogenic modifications. On the other hand, Tottori plane is not distributed in the southeastern part of the study area (subareas P and T), which should allow this study to easily detect lineaments and active fault trace. However, the lineaments and active fault traces cannot be detected well in the eastern part of the subareas P and T because more detailed aerial photos than those of previous inventories (Research Group for Active Faults of Japan, 1991; Imaizumi et al., 2018) are not provided. Hence, topographic detection of active fault traces and lineaments is thought to be difficult in the eastern part of the study area. In contrast, Research Group for Active Faults of Japan (1991) detected as much as 8 lineaments the in the subarea W and X outside of the SSZ, which are also corresponding to the eastern part of the study area. The southeastern part of the subarea W and X are located only a few to 7 km away from the Oohara fault and the Koegatawa fault. The Oohara fault is constituting the Yamazaki fault zone, which is one of the well-known major active faults in southwest Japan. The Koegatawa fault is a part of the Nagisen fault zone, representative active fault in the northern part of Okayama Prefecture. These facts suggest that subareas W and X might have affected by the activities of the Yamazaki and Nagisen fault zone. Thus, these subareas are inappropriate to simply regard as the regions outside of the SSZ due to the effects of the major active faults. Except for subarea W and X, the density of active fault traces and lineaments showed decreasing with increasing distance from the Shikano and Iwatsubo fault. This implies that structural reliefs are concentrated around the Shikano, Yoshioka and Iwatsubo fault, which may be related to topographical and geological factors (e.g., scarps, straight valleys, faults or joints, folds, bedding and dikes).

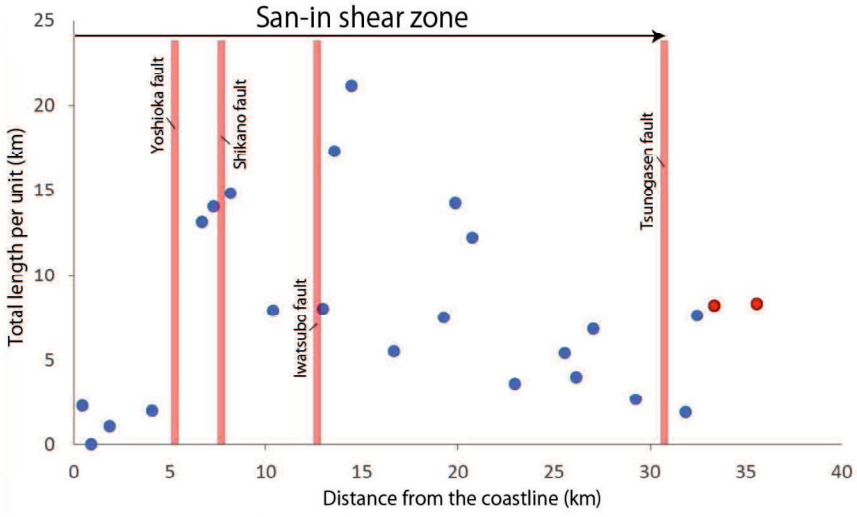

Figure 3. 3. Density of the active fault traces and lineaments

Red lines are the approximate location of the Shikano, Iwatsubo and Tsunogasen fault, respectively. Red plots show the total length of the active fault traces and lineaments in subarea W and X, which may be affected by the Nagisan fault zone and Yamazaki fault zone.

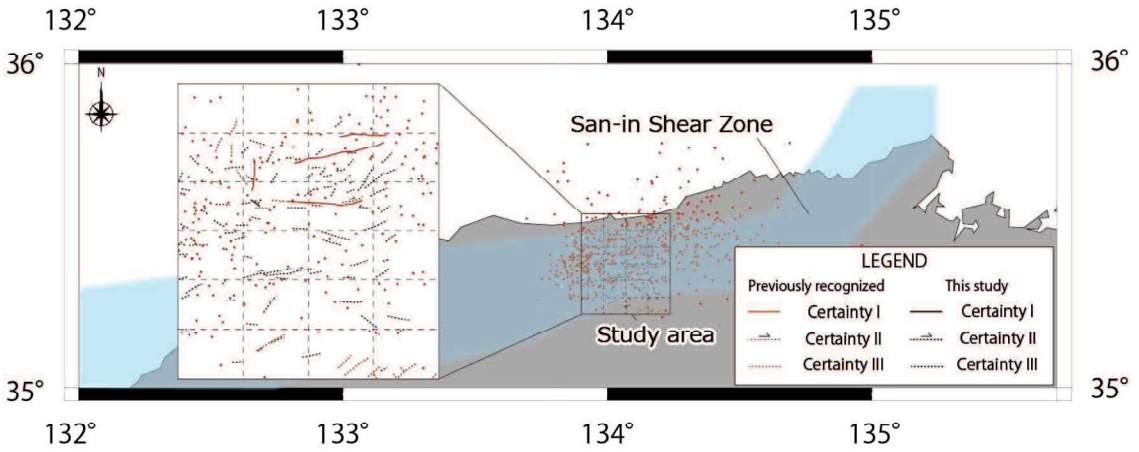

Figure 3. 4. Distribution of seismicity in 1943 and active fault traces and lineaments

The map shows the eastern part of the San-in district. The blue zone shows the San-in Shear Zone. The seismic information is from JMA.

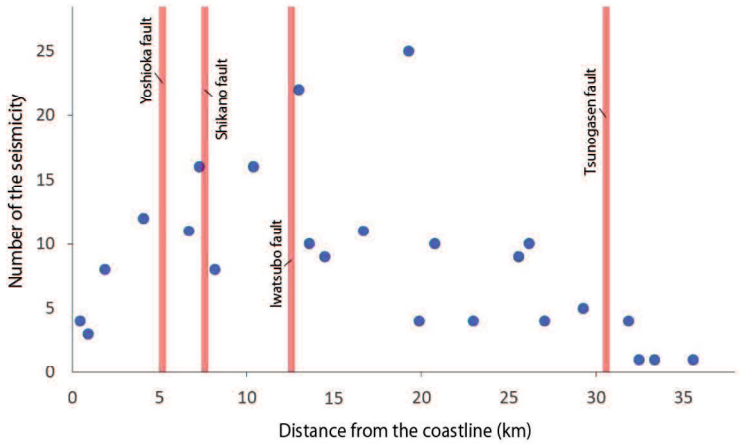

Figure 3. 5. The relation between distance and number of the seismicity

Red lines are the approximate location of the Shikano, Iwatsubo and Tsunogasen faults, respectively.

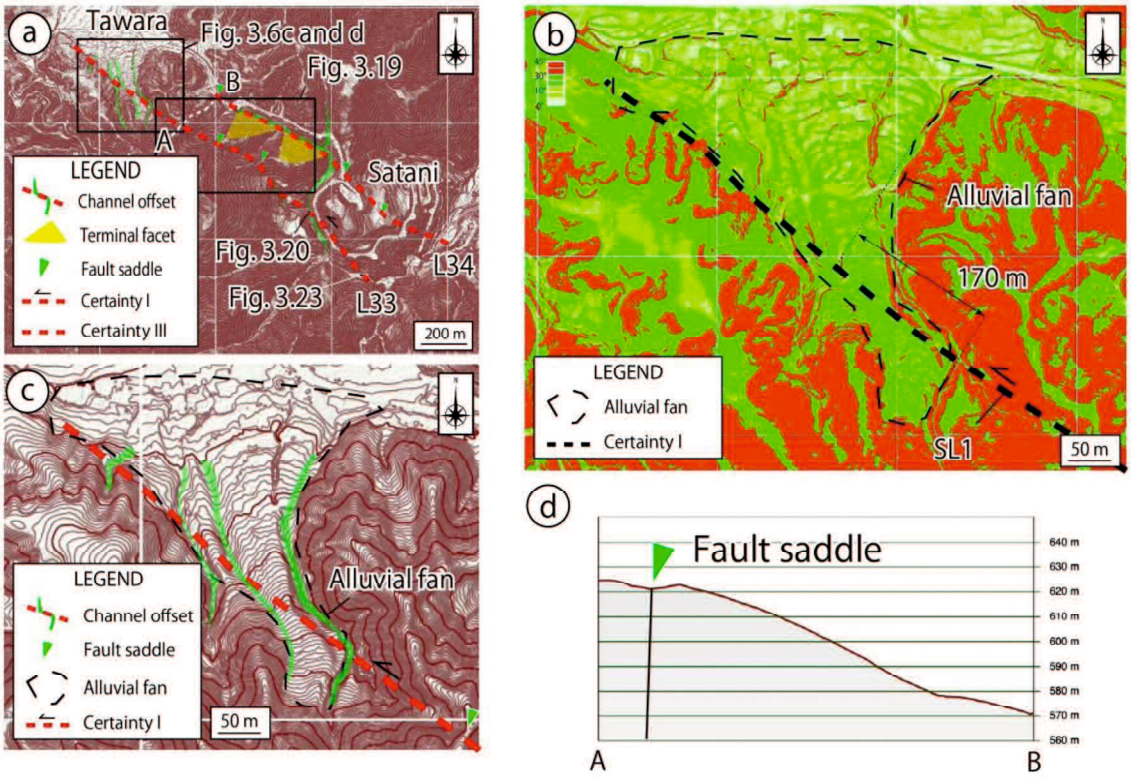

Figure 3. 6. Representative active fault trace and lineaments at the Satani region

(a) The topographic map and tectonic landforms in the Satani area. (b) Slope gradation map. (c) Sinistral offsets of an alluvial fan and its channels. (d) Transection of active fault trace and surrounding topography. The base topographic map was created using the 0.5-m-gridcell digital elevation model (DEM) provided by Tottori Prefectural Government.

In this study, the active fault trace L33 was recognized in the Satani area using the 0.5 m grid-cell DEM (Fig. 3.6). L33 is comprise of channel offsets, terminal facet and undulating topographies. Since the slope gradation map of the Tawara region shows the fan-shaped plane slopes gently down to the north (enclosed by black broken line in Fig. 3.6b and c), an alluvial fan turned out to be distributed in the southern part of the Tawara region. The small-scale channels are distributed in the alluvial fan and are displaced systematically, which implies that the alluvial fan was also displaced by L33 because the channels should be formed after the formational stage of the alluvial fan. Most of the displacements of the channels are few dozens of meters, whereas an upstream side of the channel shows the maximum right-laterall displacement (170 m offset; Fig. 3.6b). Thus, the cumulative displacements of the L33 may be 170 m. The undulating topographies, which could not be detected by conventional aerial photo interpretations due to its resolution, has depression a few dozens of meters. Since the

fault outcrops are often confirmed around these undulating topographies (see Section 3.4.3 for details), I identified them as the fault saddle. Thus, the clear tectonic landforms are frequently recognized, and the displacement is likely to have been generated after the formation of the alluvial fan. Hence, the fault trace L33 was categorized as the "active fault" in accordance with the criteria of Nakata and Imaizumi (2002) and Takada et al. (2003).

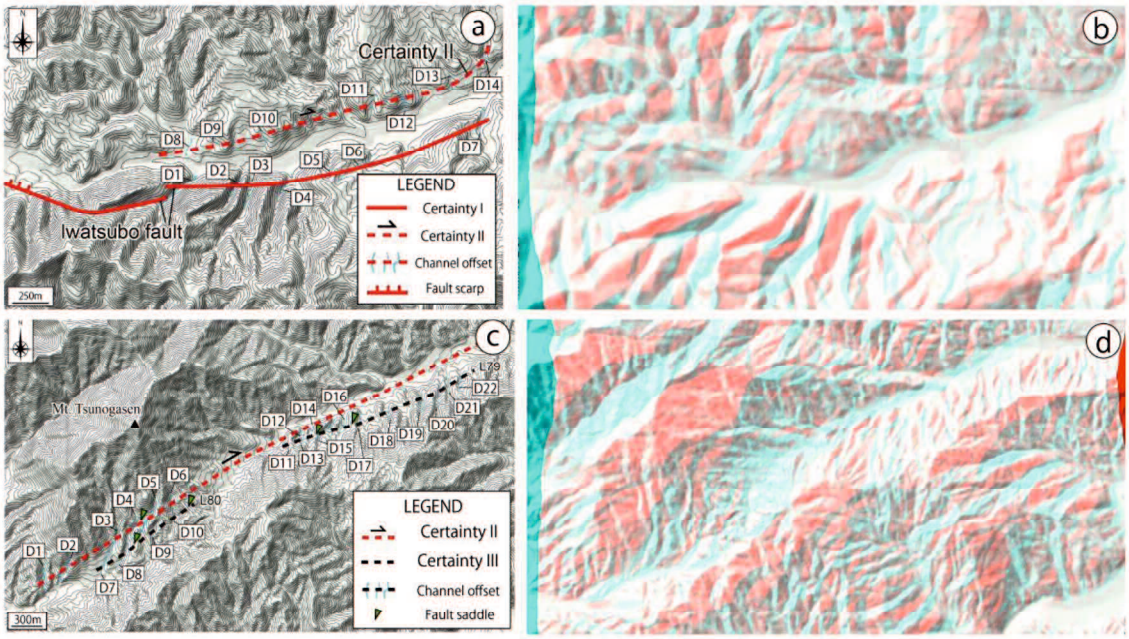

Figure 3. 7. Tectonic landforms of the active faults, presumed active faults and lineaments

(a) The Iwatsubo fault trace and a presumed active fault trace. (b) Anaglyph image around the Iwatsubo fault trace and a presumed active fault trace. (c) Tsunogasen fault trace and lineaments. (d) Anaglyph image around the Tsunogasen fault trace and lineaments. The base map was created using the 10-m-gridcell digital elevation model (DEM) provided by Geospacial Information Authority of Japan.

The Shikano fault have been known as active fault because it caused surface rupture during the 1943 Tottori earthquake. On the other hand, the Research Group for Active Faults of Japan (1991) and Imaizumi (2018) identified the Iwatsubo fault trace as "active fault" since these materials recognized not only dextral offset (D1 ~ 7 in Fig. 3.7a and b) but also fault scarps (Fig. 3.7a and b), which are one of the evidences of the activity during the Quaternary. Imaizumi et al. (2018) also recognized a presumed active fault trace, corresponding to Certainty II. In this study area, not only such presumed active fault but also an active fault trace of Certainty II (Tsunogasen fault trace) was recognized by Research Group for Active

Faults of Japan (1991). The presumed active fault trace detected by Imaizumi et al. (2018) is approximately 2.5 km in length and has 7 channel offsets (D8 ~ 14 in Fig. 3.7a and b), whereas there presumed active faults do not show any evidence of its activity during the Quaternary. The displacements of these offsets are a few dozens of meters. The Tunogasen fault trace is approximately 4.3 km in length and has 6 channel offsets (D1 ~ 6 in Fig. 3.7c and d), whereas this trace does not show any evidence of its activity during the Quaternary. The displacements of 6 channel offsets along the Tsunogasen fault trace were a few dozens to hundreds of meters. L79 and 80 have more consecutive tectonic landforms (D7 ~ 22 in Fig. 3.7c and d) than the presumed active fault trace detected by previous materials (Research Group for Active Faults of Japan, 1991; Imaizumi et al., 2018). However, L79 and 80 were identified as "lineament (Certainty III)" because the length of L79 and 80 is much shorter than any other active fault traces of Certainty II.

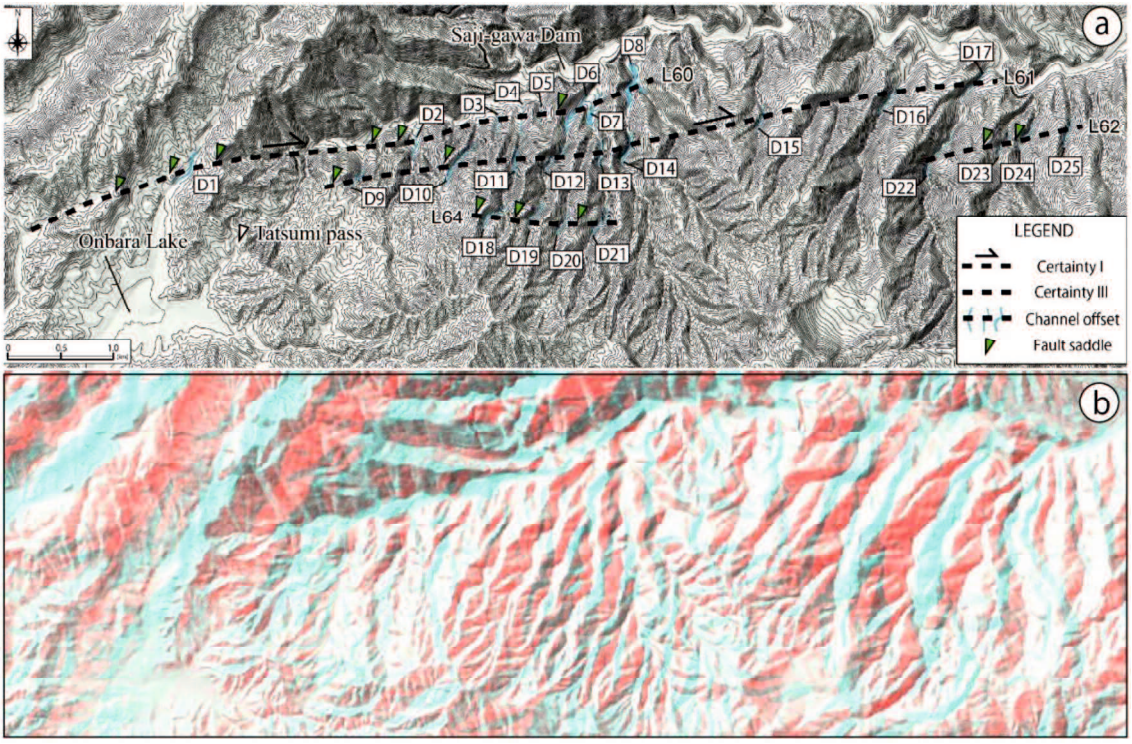

Figure 3. 8. Tectonic landforms in the Saji area

(a) Presumed active fault traces and lineaments in the Saji area. (b) Anaglyph image of the Saji area. The base map was created using the 10-m-gridcell digital elevation model (DEM) provided by Geospacial Information Authority of Japan.

When more consecutive tectonic landforms than presumed active fault traces shown in

previous materials (Research Group for Active Faults of Japan, 1991; Imaizumi et al., 2018) were recognized, I defined them as "Certainty II". In this study, active fault cannot be detected except for L33 due to no evidence of activity during the Quaternary. L60, 61, 62 and 64 was recognized in the Saji area using the 10 m grid-cell DEM and aerial photographs. L60 and 61 are approximately 6 km in length and these traces has 8 (D1 ~ 8) and 9 (D9 ~ 17) channel offsets, respectively (Fig. 3.8). Most of the displacements are a few dozens of meters, whereas some displacements show more than 100 m offset (D1, 6, 7, 8, 10, 12, 14, 17 in Fig. 3.8a). Thus, the L60 and 61 were interpretated as "Certainty II" because these have more consecutive tectonic landforms than the presumed active fault traces detected by previous materials (Research Group for Active Faults of Japan, 1991; Imaizumi et al., 2018). L62 and 64 are approximately 1.8 km in length and has only 4 channel offsets (Fig. 3.8a and b). Although the displacements of these channel offsets are a few dozens of meters, D18 and 22 show dextral offset of more than 100 m. L62 and 64 have shorter length and less consecutive tectonic landforms than the active fault traces of Certainty II detected by previous materials (Research Group for Active Faults of Japan, 1991; Imaizumi et al., 2018). Thus, L64 and 66 were identified as "lineament (Certainty III)". The Shikano, Yoshioka and Tsunogasen fault traces are distributed on the geological faults (Fig. 3.9). In addition, the Iwatsubo fault trace and Tunogasen fault trace are partly distributed on the geological boundaries. As for lineaments (Certainty III) detected by previous materials (Research Group for Active Faults of Japan, 1991), PL2, 8 and 13 are adjacent to the geological faults (Fig. 3.9). PL5 and PL8 are partly distributed on the geologic boundary (Fig. 3.9). In addition to the previous lineaments detected by previous materials (Research Group for Active Faults of Japan, 1991: Imaizumi et al., 2018), L63, 70 and 81 are adjacent to the geological faults (Fig. 3.9 and Table. A1). L1, 7, 9, 13, 16, 19, 20, 21, 34, 36, 37, 39, 43, 55, 60, 63, 65, 66, 67 are also partly distributed on the geological boundaries (Fig. 3.9 and Table. A1). These active fault traces and lineaments may be controlled by the existence of the geological fault and geological boundaries.

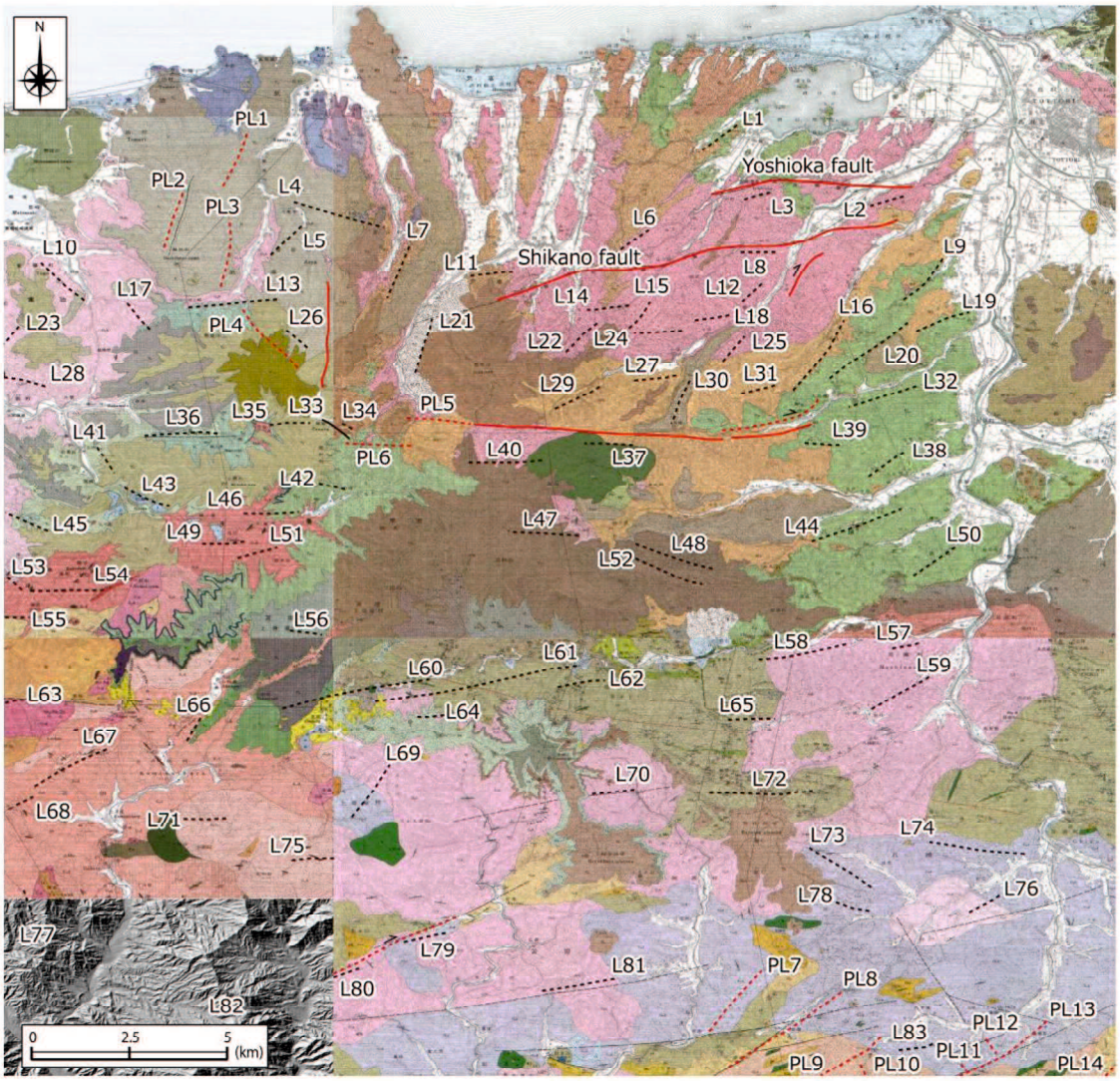

Figure 3. 9. Distribution of geology, active fault traces, lineaments.

The basemap is from 1:50,000 geological maps of Murayama and Oosawa (1961), Murayama et al. (1963), Yamada (1961) and Yamada (1965). The legend of this figure is shown in Fig. A1.

3.4.2. Fault occurrences in the Shikano area

The Shikano area mainly has the granite and the Pliocene volcanic rocks (Fig. 3.10). In the central and eastern part of the Shikano area, the Pliocene volcanic rocks unconformably overlie the Tottori granite. Of these, volcanic rocks in the central part of the study area are identified as Hakuto formation (Okada et al., 1981). The Quaternary deposits are distributed along the rivers in the Shikano area. Murayama et al. (1963) mapped two geologic faults in the northern part of the study area, corresponding to the Shikano and Yoshioka fault. A displacement at 40 cm ~ 1m dextral offset of a channel is conserved at the Suemochi area,

where the Shikano fault displaced it along with the 1943 Tottori earthquake (Nishida et al., 1993). Other surface ruptures of the 1943 Tottori earthquake are also confirmed, striking E-W to ENE-WSW direction along the geologic faults (Kaneda and Okada, 2002). Since the outcropping in the Shikano area is not always recognized frequently, the field survey and structural analysis was mainly conducted along two well-exposured trails in Horaya region and Kuchihosomi region, respectively (Fig. 3.11 ~ 3.15). Myotokuji outcrop is an only one fault outcrop intensively described as an exception to the Horaya region and Kuchihosomi region, which is approximately 1 km away from the Shikano fault (Fig. 3.16).

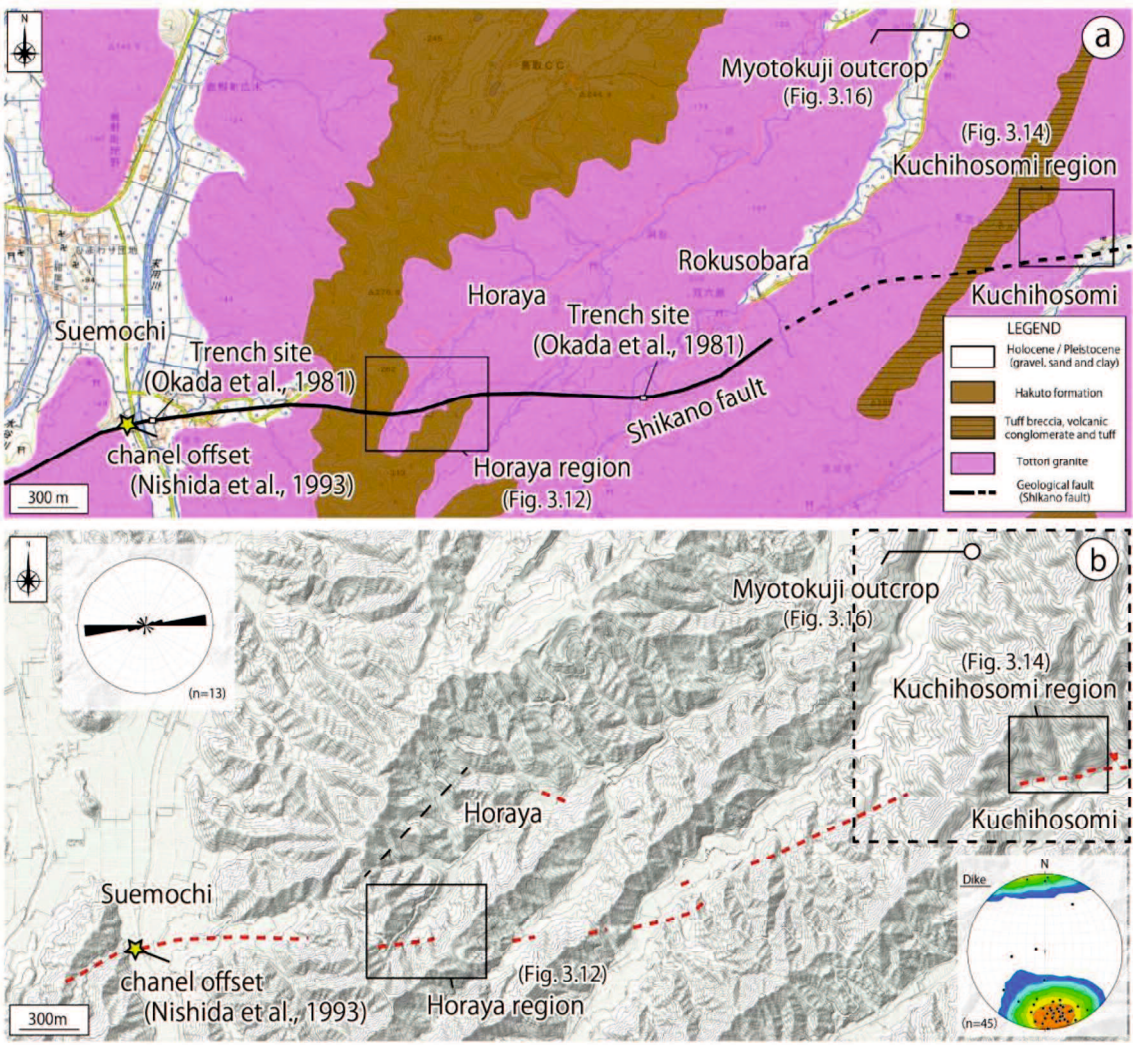

Figure 3. 10. Geological and topographical map of the Shikano area

The base topographic map was created using the 0.5-m-gridcell digital elevation model (DEM) provided by Tottori Prefectural Government, whereas the 10-m-gridcell digital elevation model (DEM) provided by Geospatial Information Authority of Japan was applied in dotted black flame. Black rectangles denote the

intensively surveyed units. The rose diagram shows the orientation of the surface ruptures given by (Kaneda and Okada, 2002). The stereo diagram shows equal area, lower hemisphere projection of the poles of dikes in the Shikano area.

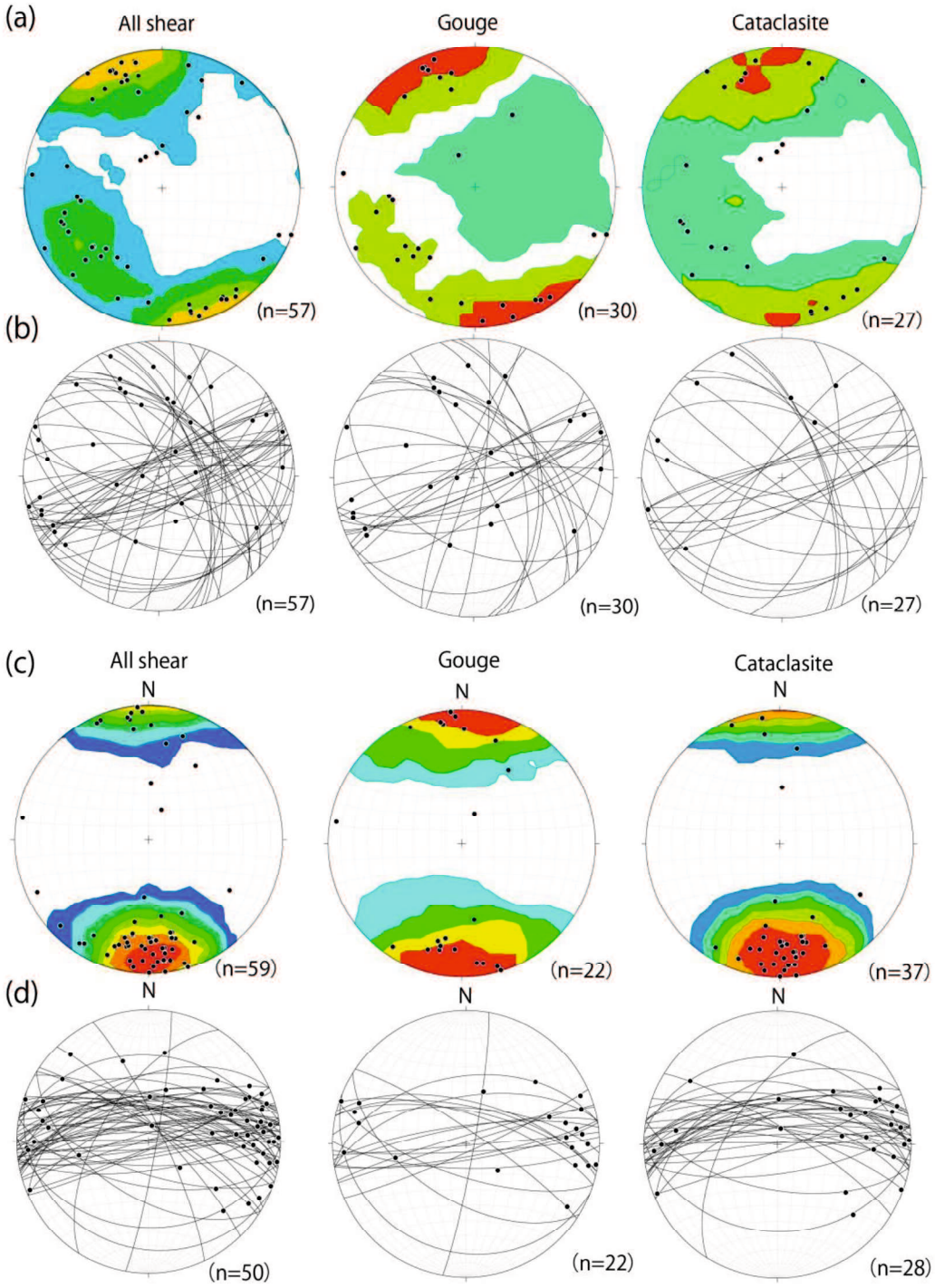

Figure 3. 11. Equal area, lower hemisphere projection of the poles of faults in the Shikano area

(a) fault planes in the Horaya region. (b) fault striations in the Horaya region. (c) fault planes in the Kuchihosomi region. (d) fault striations in the Kuchihosomi region. The great circles indicate attitude. Black dots show plots of the fault surfaces (a and c) or striations (b and d).

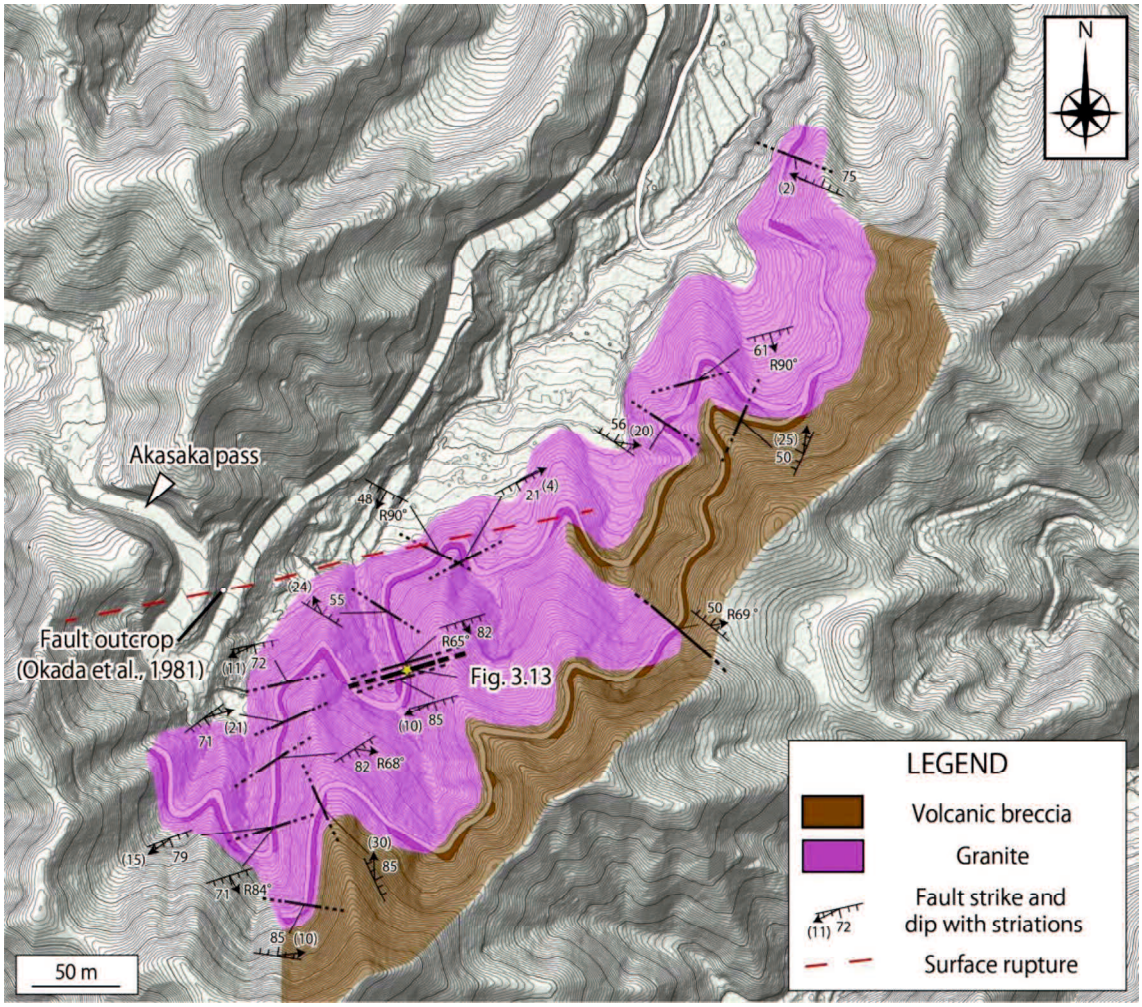

Figure 3. 12. Detailed geological maps in the Shikano area

The base topographic map was created using the 10-m-gridcell digital elevation model (DEM) provided Geospacial Information Authority of Japan. The distribution of the surface ruptures is depicted in accordance with Kaneda and Okada (2002).

The trail in Horaya region is running across the Shikano fault and a total of 57 faults were recognized along the trail (Fig. 3.12). These faults should be related to the Shikano fault because the trail is located in the vicinity of Shikano fault, which is only 0 ~ 200 m away from its active fault trace. Most of the faults has a few millimeters to several centimeters in width and consists of fault gouge zone, fault breccia zone and cataclasite zone. In addition, most of

the faults strikes ENE–WSW or NW–SE directions and dipping steeply (Fig. 3.11). The striations tend to plunge low to high angle, indicating strike-slip faulting or dip-slip faulting. On the other hand, the Horaya outcrop, which consists of fault gouge zone and fault breccia zone, has 20–30 centimeters in width and strikes ENE–WSW direction (Fig. 3.13). The striations on the slickenside were nearly vertical rake angle (R82° to 90°) or horizontal plunging (14° to the west). The core zone of the Shikano fault likely to be exposed at the trail since the Shikano fault trace passes through the trail. However, no large-scale fault zone, which is suitable for regarding as core zone of the Shikano fault, was confirmed except for the Horaya outcrop. The strike of the fault zone of the Horaya outcrop is consistent to that of the Shikano fault inferred from the topographic analysis, whereas other fault gouge/breccia zones trending ENE–WSW directions range in only a few millitimeters to several centimeters, despite the continuous outcropping. Therefore, the Horaya outcrop is interpretated as the core zone of the Shikano fault.

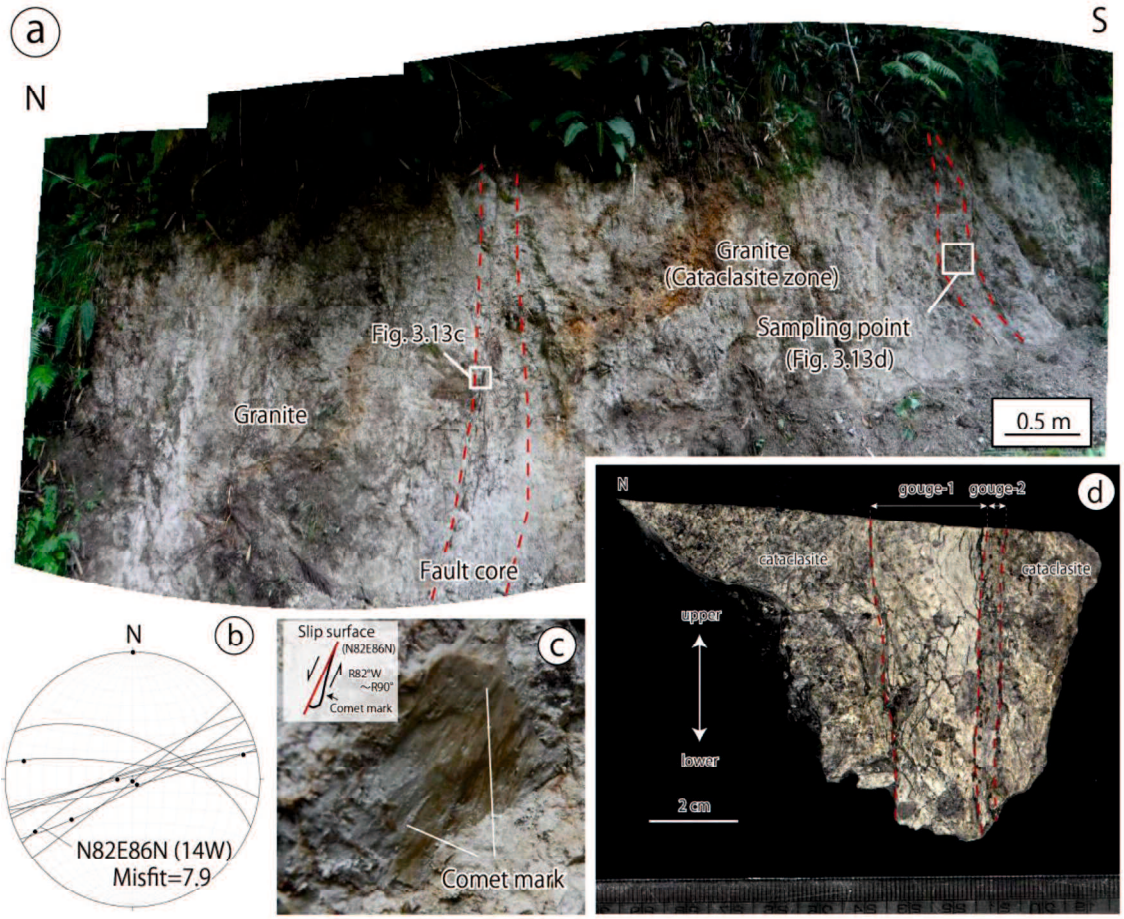

Figure 3. 13. Fault core zone of the Shikano fault at the Horaya region

(a) Annotated photograph outcrops showing fault core zone of the Shikano fault with a secondary fault. (b) Plots to fault planes of the fault core zone and its secondary faults, with lower-hemisphere, equal-area projections. (c) Representative slip surface with shear sense indicators. (d) Polished fault rock sample collected from the secondary fault.

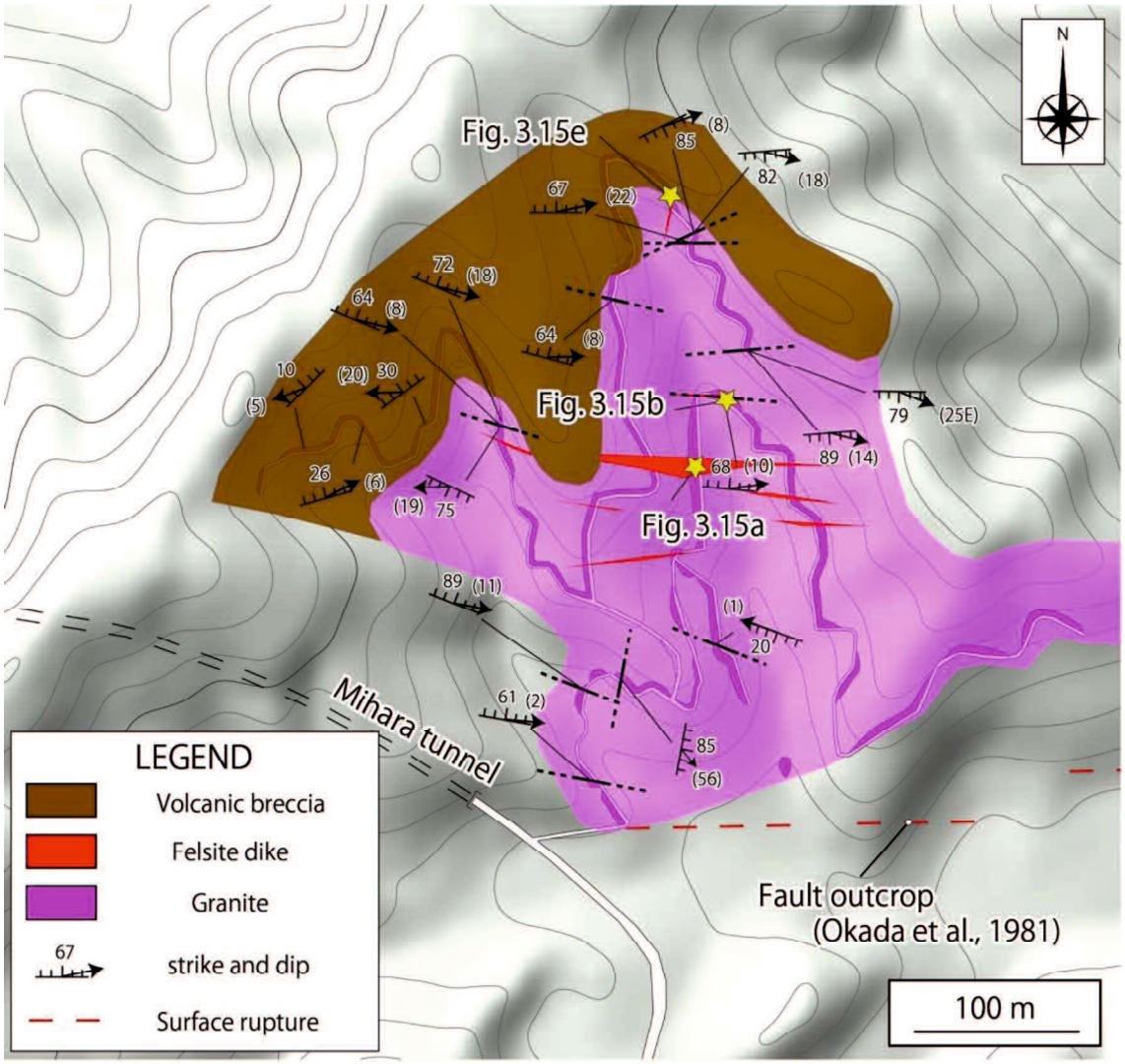

Figure 3. 14. Detailed geological maps in the Kuchihosomi area

The base topographic map was created using the 10-m-gridcell digital elevation model (DEM) provided Geospacial Information Authority of Japan. The distribution of the surface ruptures is depicted in accordance with Kaneda and Okada (2002).

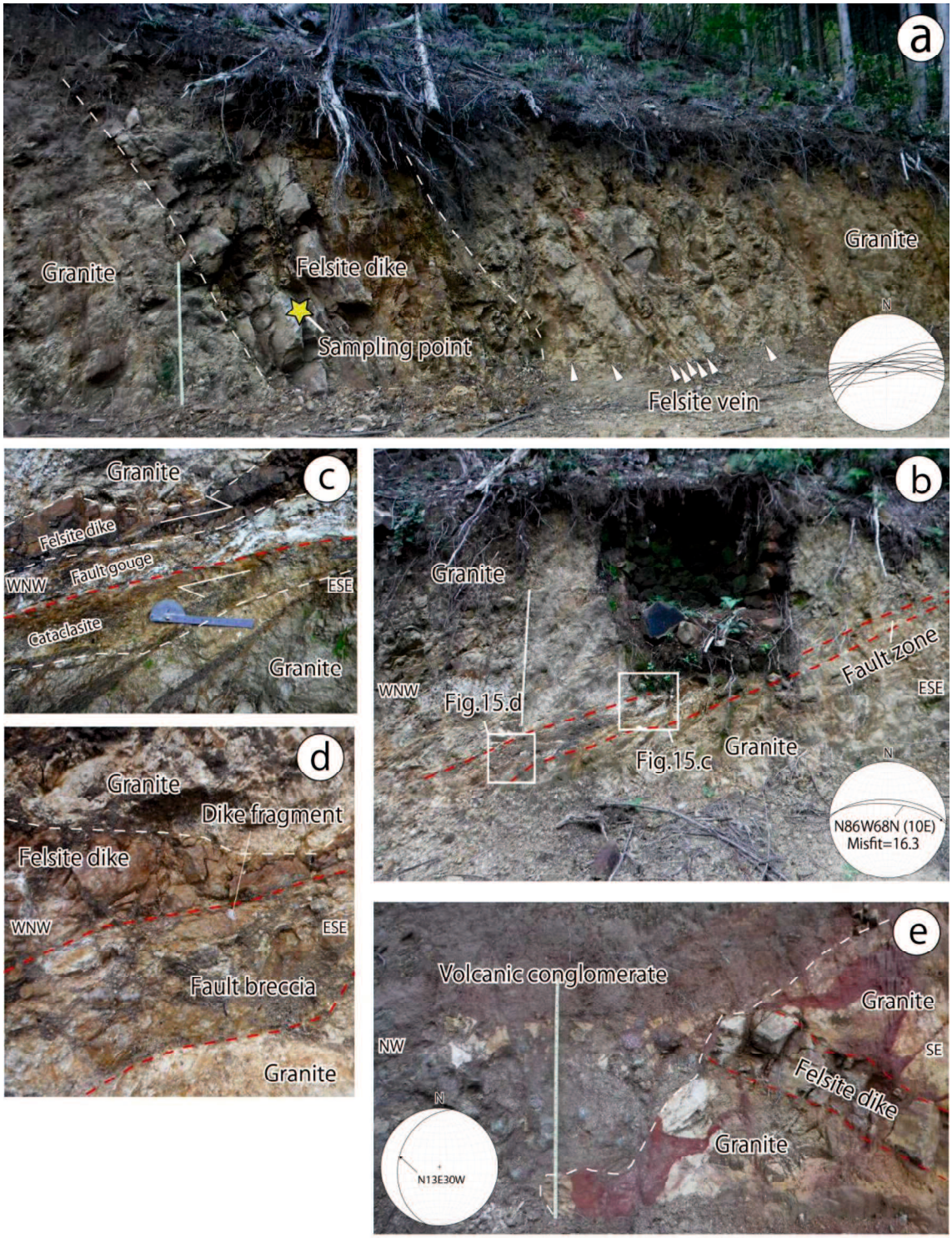

Figure 3. 15. Geological characteristics of the Kuchihosomi region

(a) Felsite dikes and veins. (b) Representative fault outcrop in the Kuchihosomi area. (c) Fault gouge zone accompanied with dike. (d) Fault breccia zone accompanied with dike. (e) Unconformity between the granite and volcanic breccia. The sampling in (a) is conducted for the zircon U-Pb dating (see detail for Fig. A2).

The trail in the Kuchihosomi region is located in the vicinity of the Shikano fault, which ranges a few meters to 300 meters away from the surface ruptures of the 1943 Tottori earthquake (Fig. 3.14). A total of 59 faults were recognized along the trail. All faults along the trail have a few millimeters to several centimeters in width and consists of fault gouge zone, fault breccia zone and cataclasite zone. The majority of the strikes and dips of the faults are E–W direction and dipping steeply to the north. The slickenlines on the fault surface plunge low angle while some of the faults have high angle plunging. Although NW–SE striking and steeply dipping faults were not confirmed unlike the Horaya region, the approximate attitudes of the faults are consistent with the Shikano fault. Thus, faults in Kuchihosomi region are also thought to be associated with the Shikano fault since those faults are nearly same attitude of the Shikano fault and distributed near the Shikano fault trace. In addition to the faults, quartz vein and/or dikes intruding the granite are frequently confirmed (Fig. 3.14 and 3.15). The majority of the veins and dikes strike E–W directions, and dips steeply to the north, which is good agreement with the attitudes of the faults in the Kuchihosomi region. However, no veins and dikes were found in the Pliocene volcanic rocks unconformably overlying the granite. The volcanic breccia, which is one of the Pliocene volcanic rocks found in the Kuchihosomi region, are unconformably overlies these veins and dikes, suggesting that the dikes and veins intruded before the formational age of the volcanic breccia.

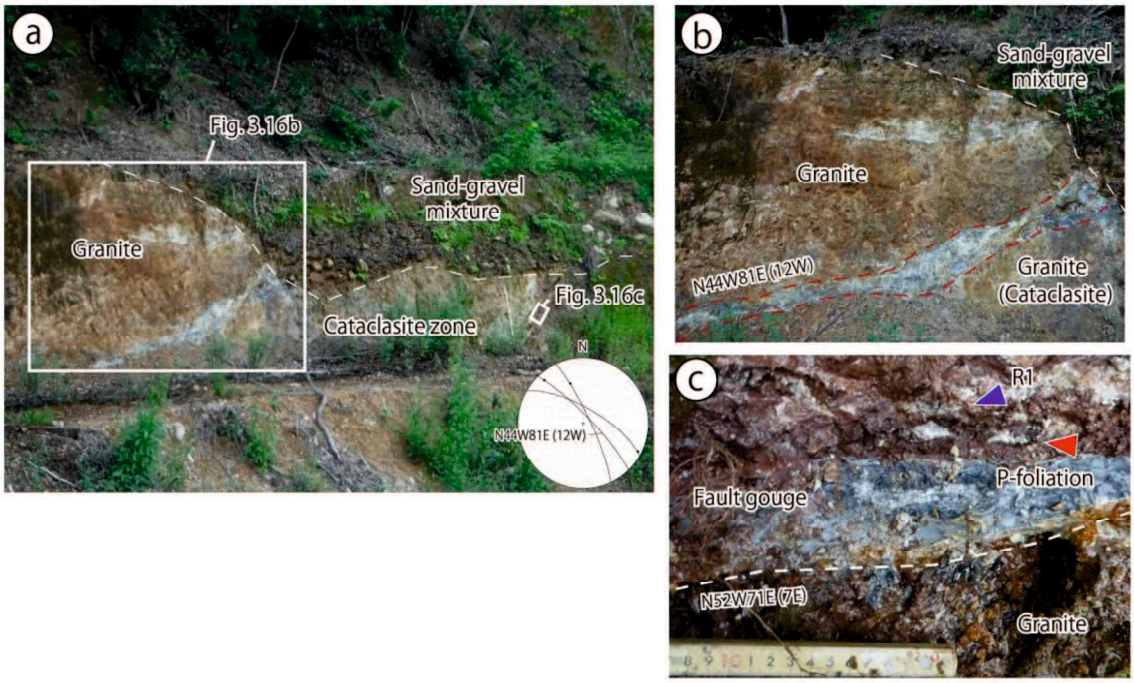

Figure 3. 16. Representative occurrence of faults away from the Shikano fault

(a) Photographs of outcrop showing the whole fault zone. (b) The widest gouge zone away from the Shikano fault. (c) Composite planar fabrics in the fault gouge zone.

Myotokuji outcrop occurs three fault zones, consisting of dozens of centimeters thick cohesive sticky gouge/breccia zone and cataclasite zone, and are black, gray, white, brownish red in color (Fig. 3.16). Approximate strikes and dips are NW–SE directions and steeply dipping, inconsistent with the attitude of the Shikano and Yoshioka fault. The composite planar fabrics in the gouge zone shows sinistral sense of movements, which is also incongruous sense of shears to that of the Shikano and Yoshioka fault. Although such faults are enough large-scale to express the tectonic landforms, neither of lineaments nor active fault traces were depicted.

3.4.3. Fault occurrences in the Iwatsubo area

Iwatsubo area is mainly composed of Tottori-nambu volcanic rocks (tuff, lapilli tuff, tuff breccia), intrusive rocks (granite, granodiorite, gabbro), Pliocene volcanic rocks (tuff breccia, volcanic conglomerate, tuff of andesite and dacite, lava flows of andesite, basalt, dacite) (Murayama et al., 1963; Fig. 3.17). In the central part of the Iwatsubo area, the Iwatsubo fault are distributed, and the Tawara fault are distributed in the northwestern part of the area. Both faults are detected from topographic analysis, whereas the direct evidence have never been

confirmed. Since the outcropping in the Iwatsubo area is frequently confirmed, field survey was conducted as widely as possible, which result in a total of 268 faults can be observed in the Iwatsubo area (Fig. 3.18). While the strikes and dips of the faults are mostly NW–SE to NNW–SSE striking and dipping steeply, E–W striking and dipping steeply faults are also confirmed. These faults indicate dextral sense of shear on the E–W to ENE-WSW striking, whereas sinistral sense of shear on the NW–SE to NNW–SSE-trending faults. The majority of the active fault traces and lineaments are oriented NE–SW and ENE–WSW. Most slickenlines on the faults shows low to moderate angle plunging (R0° ~ 45°). The greater part of the faults typically ranges in thickness from a few millimeters to centimeters. Although most of such minor faults are distributed around the active fault traces and lineaments, there are also minor faults away from the active fault traces and lineaments.

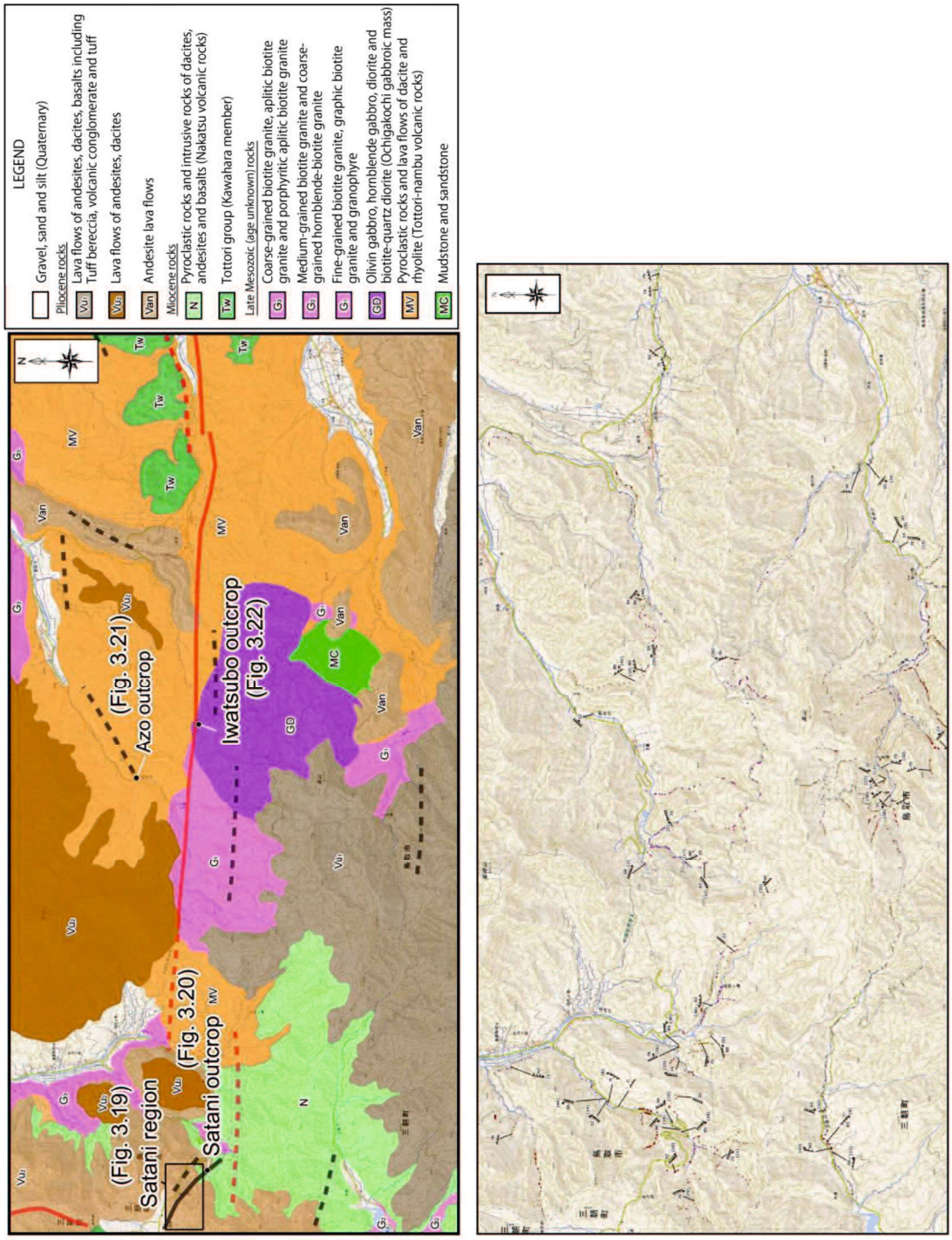

Figure 3. 17. Distribution of the geology and minor faults in the Iwatsubo area

(a) Geological map of the Iwatsubo area (after Murayama et al., 1963). (b) Route map of the Iwatsubo area. The 1:25,000 topographic map is from Geospacial Information Authority of Japan.

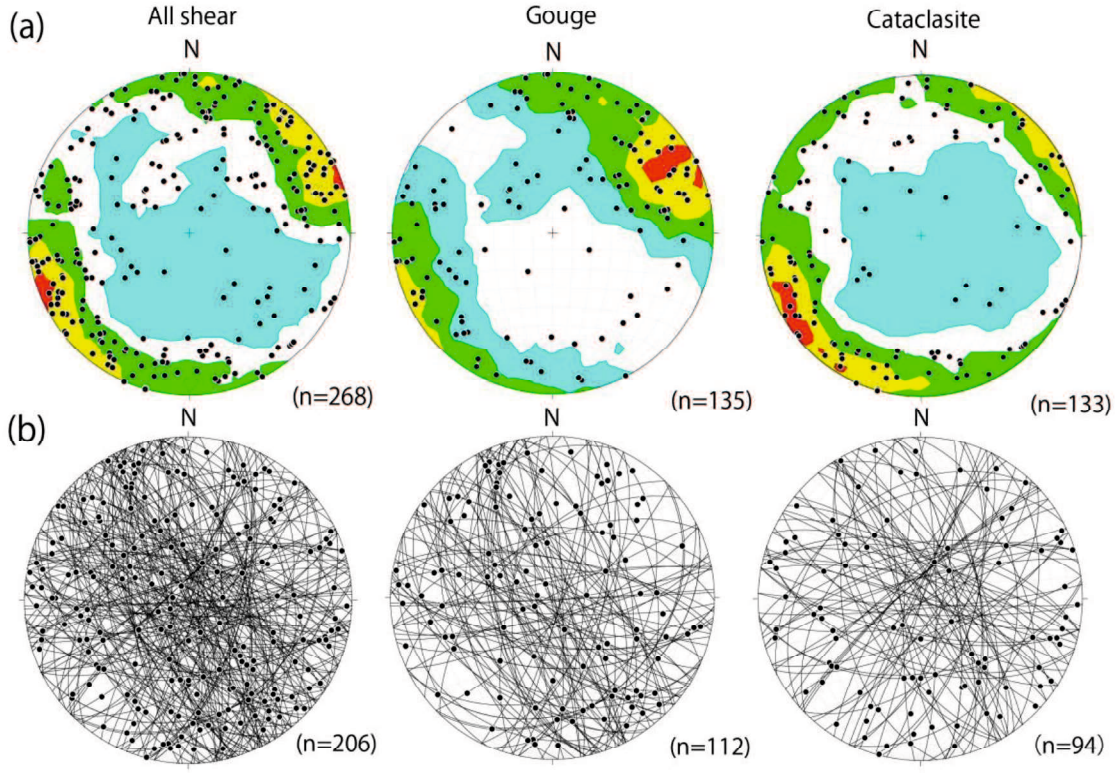

Figure 3. 18. Equal area, lower hemisphere projection of the poles of faults

(a) Fault planes in the Iwatsubo area. (b) Fault striations in the Iwatsubo area. The great circles indicate attitude. Black dots show plots of the fault surfaces or striations.

At the Satani region, a total of 42 faults striking mostly NW–SE-trending were recognized through the field observations around a trail (Fig. 3.19). Most of the slickenlines on the faults plunge at low to moderate angle (R0° ~ 45°) on steeply to moderately dipping fault planes. The faults exposed around the trail typically ranges in thickness from a few millimeters to several centimeters except for 5 fault outcrops accompanied with thick gouge/breccia zone (> 10 cm in width). Satani outcrop possesses 12–18 cm gouge/breccia zone accompanied with 2 m cataclasite zone, derived from andesitic host rock (Fig. 3.20). The fault gouges/breccia zone are white, pale purple, purple, red and ocher in color. Such shear planes in the gouge zone strikes NW–SE directions and dips steeply, with composite planar fabrics showing the sinistral sense of shear. This fault outcrop is located on an NW–SE trending active fault trace with sinistral sense of displacement, suggesting that the fault is corresponding to the core zone of active fault trace L33.

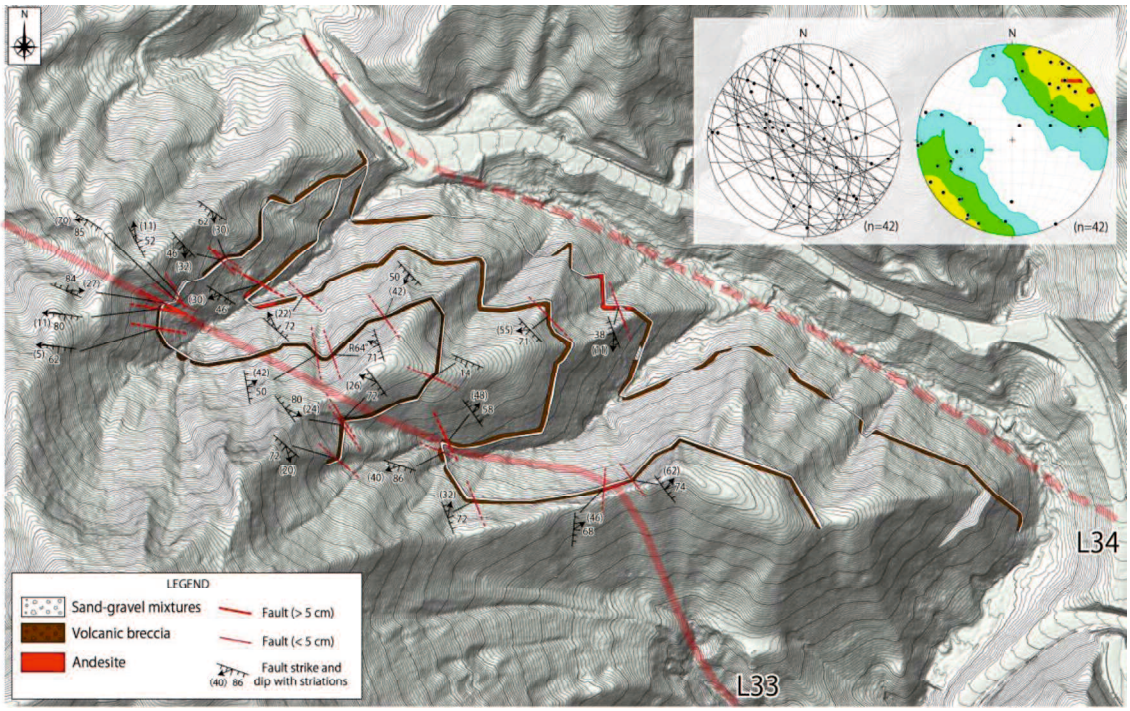

Figure 3. 19. Detailed route map around the Satani region

The base topographic map was created using the 0.5-m-gridcell digital elevation model (DEM) provided by Tottori Prefectural Government. Solid pale red line denotes active fault trace, whereas Dashed red line shows lineament. Diagrams indicate the fault planes and striations in this region.

The Azo outcrop (Fig. 3.21) is located at the southwestern extension of the NE–SW trending lineament with tectonic landforms of dextral offsets ("L29", hereafter; Fig. 3.1). The fault outcrop is marked by fault gouge zone and cataclasite zone. The cataclasite zone is 0.6 m in width, which has fragments with random fabrics derived from tuffaceous host rock. The fault gouge zone strikes N72° E, dips 30° S, and is 0.5–4 cm in width. Slickenlines on the fault plane 26° to the southeast. The gouge zone deforms unconformably overlying sand-gravel mixtures because of a granitic gravel (Fig. 3.21h) in the gouge zone, injected gouge zone into the sand-gravel mixtures (Fig. 3.21a, b and c) and deformed brownish layer (Fig. 3.21g and h). R_1 shear plane and P-foliations defined by fragments in the gouge zone indicates that the fault gouge underwent right-lateral reverse faulting (Fig. 3.21d ~ f). Radiocarbon age of humus sample from the sand-gravel mixtures showed 18648–16313 cal. BC, indicating that the sand-gravel mixtures was deposited in late Pleistocene (Table 3.1). Since the Azo outcrop is located at the southwestern extension of the L29 and its attitude has good agreement with that of the lineament, such fault gouge zone may be corresponding to the L29 shown as one

of the topographic expressions of dextral offsets in the study area.

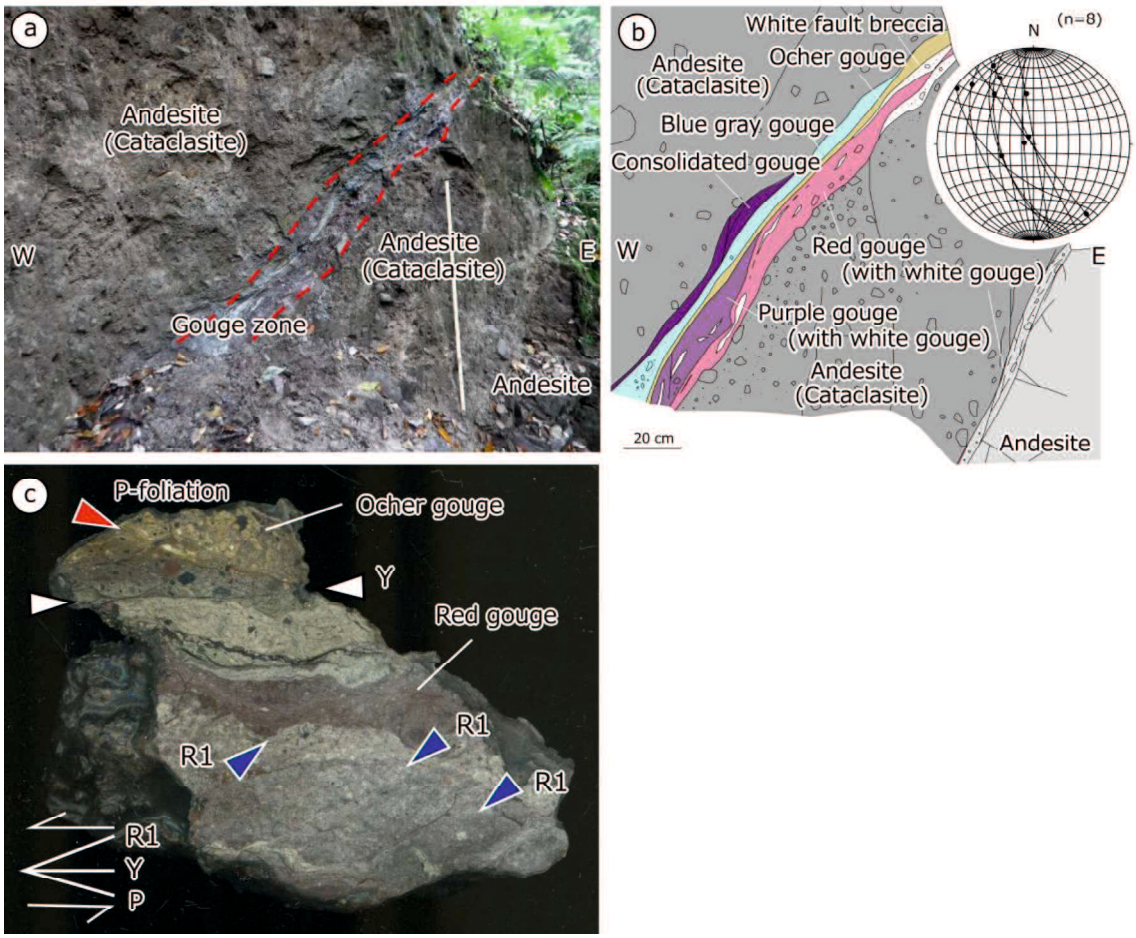

Figure 3. 20. Characteristics of the Satani outcrop

(a) Photograph of the fault zone. (b) Sketch of the fault zone. (c) Hand-specimen photograph of a sample from the outcrop shown in (a). The length of the yellow ruler in (a) is 1 m. Diagrams indicate the fault planes and striations in this region. R1=Riedel shear; Y=Y plane; P=P-foliation of composite planar fabric.

Table 3. 1. Radiocarbon age of humus sample at Azo outcrop

The 1 σ and 2 σ uncertainties represent the 68.27% and 95.45% confidence intervals of the calibrated age based on the high-probability density range method, respectively. The age between brackets shows conventional ^{14}C age rounded off to the nearest ten. The percentages attached with the calibrated age show the probabilities of the calibrated age on the basis of the high-probability density range method.

Sample	$\delta\ ^{13}C$ (‰)	Conventional ^{14}C age (yrBP±1σ)	^{14}C age (yrBP±1σ)	Calibrated age (Cal AD)	
				1σ	2σ
Humus soil	-22.71±0.21	15142±45	15140±45	16674-16515 cal BC (53.94%) 16381-16336 cal BC (14.33%) 18623-18464 cal BC (53.94%) 18330-18285 cal BC (14.33%)	16699-16461 cal BC (67.39%) 16440-16313 cal BC (28.06%) 18648-18410 cal BC (67.39%) 18389-18262 cal BC (28.06%)

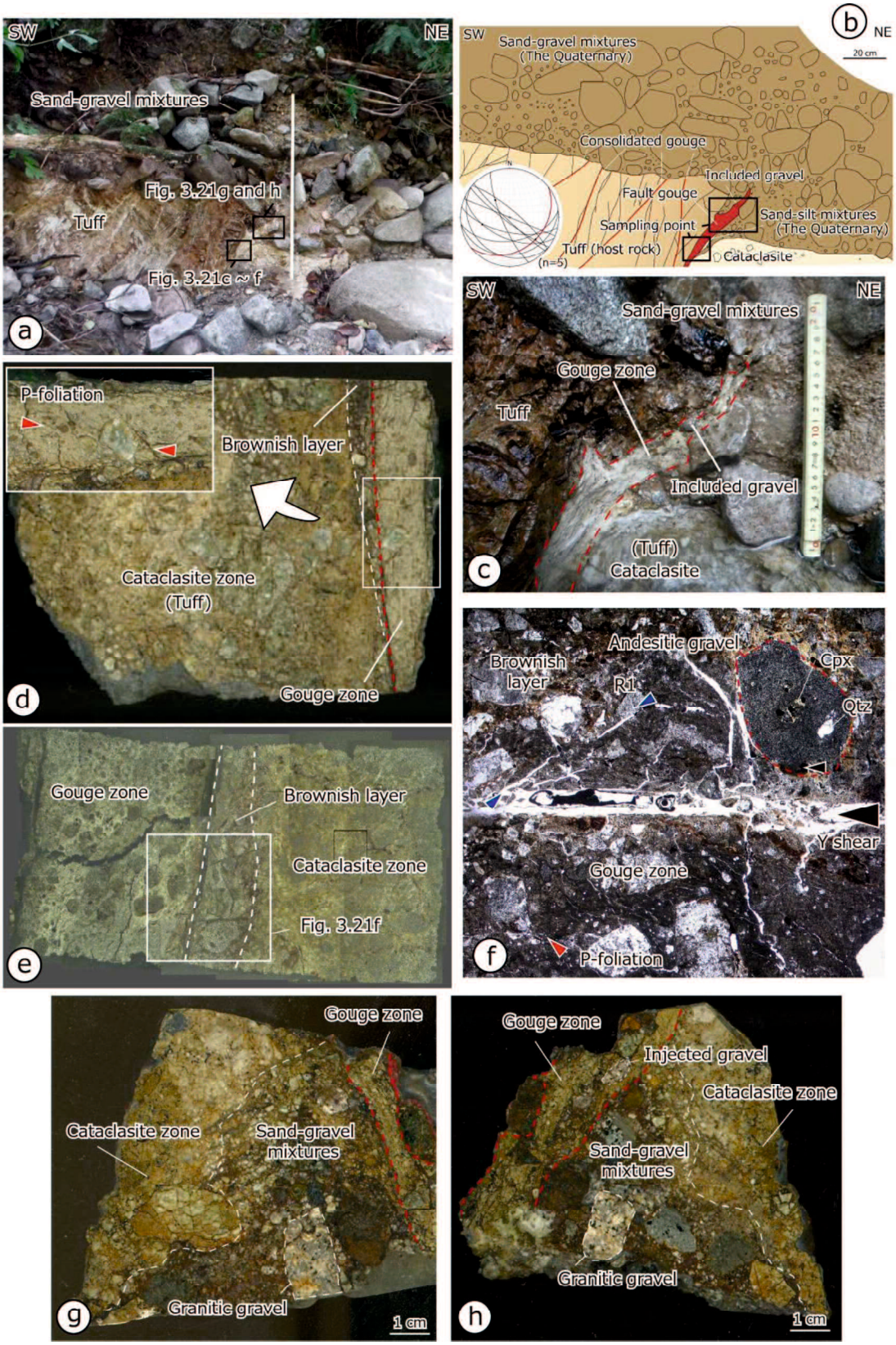

Figure 3. 21. Representative occurrence of minor fault at the Azo outcrop

(a) Photograph of the fault zone. The length of the yellow ruler in (a) is 1 m. (b) Sketch of the fault zone. (c)

Closed section of the fault zone. The length of the yellow ruler in (c) is 20 cm. Diagrams indicate the fault planes and striations in this region. (d) Fault slab. (e) Thin section. (f) Microscopic view of the thin section. (g) Fault slab containing sand-gravel mixtures. (h) Counter part of (g).

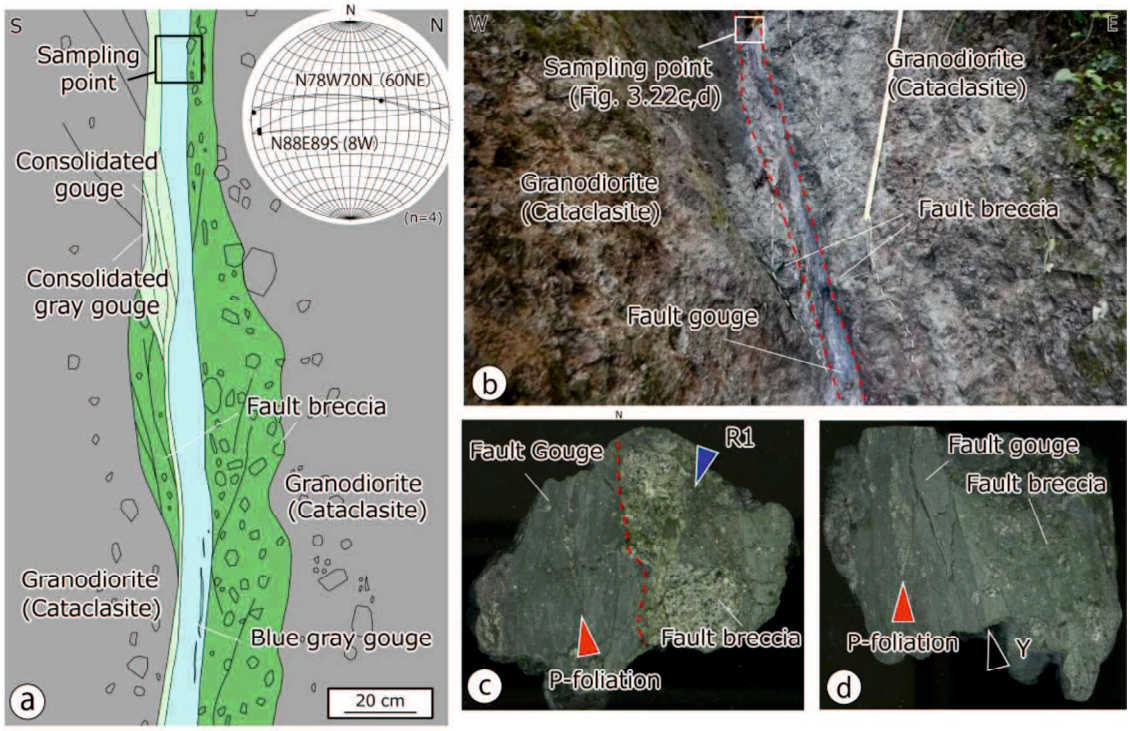

Figure 3. 22. Fault core zone of the Iwatsubo fault

(a) Sketch of the fault zone. (b) Photograph of the fault zone. (c) Hand-specimen photograph of a sample (XZ plane for N88° E89° S, with striation 60° plunging to the west) from the outcrop shown in (b). (d) Hand-specimen photograph of a sample (XZ plane for N78° W70° N, with striation 60° plunging to the NE) from the outcrop shown in (b).

The Iwatsubo outcrop is composed of fault gouge zone, fault breccia zone and cataclasite zone and is marked by a gouge/breccia zone that is 30 centimeters thick (Fig. 3.22). The shear plane in the gouge zone strikes N88° E, dips south at 89° , whose striation plunges 8° to the west. The orientation of a boundary between the gouge zone and breccia zone is N78° W/70° N and its striations plunge 60° to the east. The former fault surface was measured in the gouge zone, plunging 8° to the west. The latter was boundary between the gouge zone and breccia zone, whose plane plunges 60° to the east. From the observation of fault rocks (XZ plane along both of the slickenlines), the composite planar fabrics showed that the planes experienced right-lateral normal (horizontal component is dominant) or left-lateral

reverse (vertical component is dominant) slip. The Iwatubo outcrop is interpretated as a fault core zone of the Iwatsubo fault because of its occurrence, fault attitude and location.

In the southern part of the Satani region, an outcrop of unconsolidated sand-gravel mixtures was recognized (Fig. 3.23). The sand-gravel mixtures are estimated to be deformed since the tail-like clasts and gravels having rearranged orientations in the mixture were confirmed. Although the location of the outcrop is on the active fault trace L33, whether or not the sand-gravel mixtures were deformed by faulting was not identified.

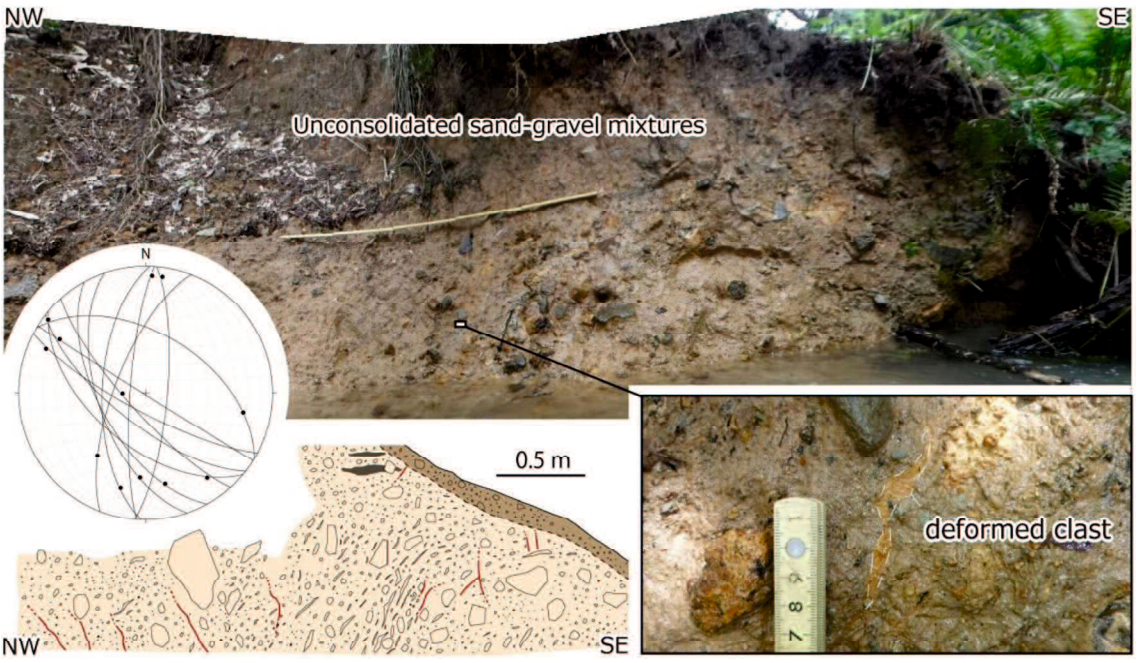

Figure 3. 23. Outcrop of the Quaternary deposits in Satani region.

The length of the yellow ruler is 1 m. Stereogram shows the attitudes of shear planes in the unconsolidated sand-gravel mixtures. Although the basement rock cannot be seen, the granite outcrop is found in the vicinity of this outcrop.

3.4.4. Fault occurrences in the Kuroki area

Kuroki area is mainly consisted of the Suo metamorphic rocks and the intrusive granitoids (Fig. 3.24). The southern Tunogasen fault, identified by Research Group for Active Faults of Japan (1991) based on the existence of dextral offsets, is NE–SW trending active fault and is 18.5 km away from the Iwatubo fault. The Tsunogasen fault, 18.5 km away from the nearly central portion of the SSZ, was regarded as the marginal line for the southern side of the SSZ because Menesess-Gutierrez and Nishimura (2020) showed 15–22.5 km in half width of the

SSZ. NE–SW to ENE–WSW trending geologic faults are distributed in northern part and central southern part of the Kuroki area. One geologic fault is distributed along the Tsunogasen fault, while another is running from northwestern part of Dogahara region to northeastern part of Kuredoko region.

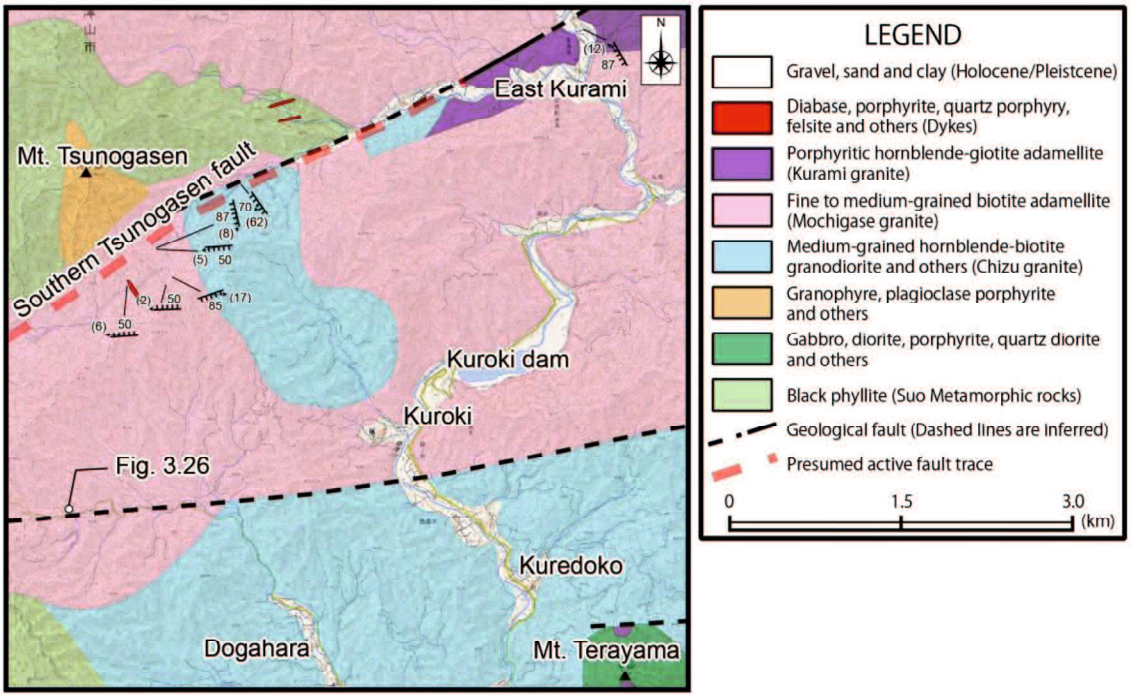

Figure 3. 24. Detailed geological map of the Kuroki area (modified after Yamada, 1965)
Dashed red line shows Tsunogasen fault trace given by Research Group for Active faults (1991). The strikes and slips shown in the geological map indicates the attitudes of the gouge planes.

A total of 26 faults were found and shows that the NW–SE striking and steeply dipping faults or NE–SW striking, and moderate dipping faults were often recognized (Fig. 3.25). NW–SE striking, and steeply dipping faults tend to appear as the consolidated shear plane or in the cataclasite zone (Fig. 3.25). On the other hand, NE–SW-striking and moderate dipping faults are mostly confirmed in the fault gouge zone, whose strikes are consistent with trend of the Tsunogasen fault (Fig. 3.25). The fault zone has only a few millimeters to several centimeters in width. The distribution of the gouge zone is in vicinity of the Tsunogasen fault, whereas only one fault gouge zone, which has only 1 mm in width, can be recognized away from the Tsunogasen fault (Dogahara outcrop, hereafter; Fig. 3.26). The Dagahara outcrop has dip-slip reverse fault with striking N83° E and northward dip of 50° , whose slickensteps

on the slip surface of the gouge zone indicates the reverse sense of shear. This suggests that the fault does not contribute to the dextral motion of the SSZ. Since this fault outcrop is located near the geologic fault, the gouge zone can be associated with the geologic fault.

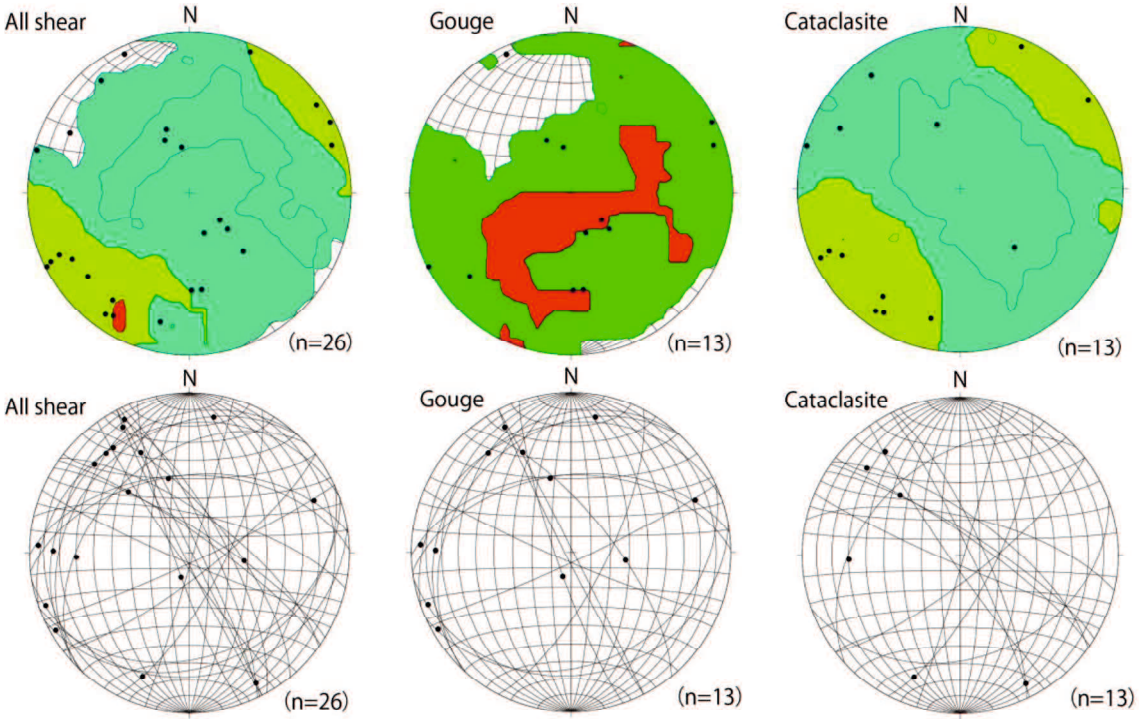

Figure 3. 25. Equal area, lower hemisphere projection of the poles of faults in the Kuroki area

The great circles indicate attitude. Black dots show plots of the fault surfaces or striations.

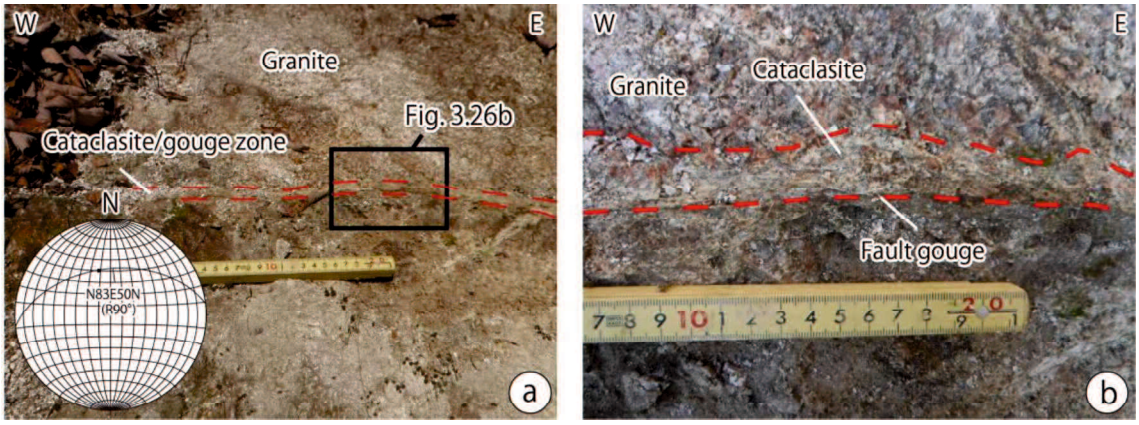

Figure 3. 26. Representative fault occurrences (Dogahara outcrop) in the Kuroki area

(a) Photograph of Dogahara outcrop. (b) Closed section of the fault zone. The stereogram shows the attitude of the fault gouge zone.

3.4.5. Mineral compositions

Analyzed fault gouges and cataclasite are mainly composed of quartz, plagioclase, k-feldspar, as major minerals, and smectite as a clay mineral. Although quartz, plagioclase and k-feldspar are often contained in most of the fault gouges, amount of quartz, plagioclase and k-feldspar of the Satani fault outcrop are comparatively less than any other fault gouges (Table 3.2). Clay mineral of the fault gouges typically includes smectite regardless of fault rocks, host rocks, fault widths and locations.

Table 3. 2. Results of XRD analysis for fault rocks

Qt=Quartz, Pl=Plagioclase, ksp=k-feldespar, Au=Augite, He=Hematite, Sm=Smectite, Ill=Illite, Ka=Kaolinite, Ch=Chlorite, DOF=Degree of fit.

Sample name	Location	Fault material	Host rock	Mineral Composition									
				Qt	Pl	ksp	Au	He	Sm	Ill	Ka	Ch	DOF
20052201	Minor fault	Fault gouge	Granite	28.9	17.8	8.6			35.0	9.7			0.0931
20052202	Minor fault	Cataclasite	Granite	26.5	19.3	29.5			15.0	9.6			0.1524
20100201	Azo core	Fault gouge	Rhyolite	32.4	18.8	15.7			22.3	10.1	0.7		0.1138
20100202	Azo core	Fault gouge	Rhyolite	40.1	15.7	11.6			27.0	5.4	0.1		0.1285
20100503	Satani core	Fault gouge	Andesite	2.1	42.4		0.9		48.2	2.8		3.6	0.0638
20100504	Satani core	Fault gouge	Andesite	13.1	12.9	16.2	2.7	1.1	50.0			4.0	0.0404
20100505	Satani core	Fault gouge	Andesite	13.6	9.1		3.9	1.6	69.8			2.0	0.0417
20100701	Iwatubo core	Fault gouge	Granodiorite	28.5	18.8	24.3		0.1	2.6	11.4		14.2	0.1053
20100702	Iwatubo core	Fault gouge	Granodiorite	27.0	13.2	14.6			19.5	9.5		16.1	0.0731
20100703	Iwatubo core	Fault breccia	Granodiorite	29.4	16.2	24.4			9.1			21.0	0.1075

3.4.6. Paleostress fields

A total of 17 entire slip data in the Shikano area were applied for the calculation of the stress field. The results utilizing the entire slip data of the gouge zone shows σ_1 trends NW–SE direction; σ_3 trends NE–SW direction, and σ_1 trends E–W direction; σ_3 trends N–S direction (Fig. 3.27). Both clusters are well concentrated, but the latter cluster has only low stress ratio. Since the former cluster has a wider variety of stress ratio and plunge directions, the former is considered to be major stress field. Dike method using the Bingham fitting (Yamaji, 2016) yielded σ_3 trending N–S direction in all cases (k = 1 ~ 5; Fig. 3.28). According to the calculated Bayesian information criterion (BIC), whose minimum value indicates the best fitting of the Bingham distributions, the results of the k =1 is the most reasonable. Thus, dikes in the Shikano area are thought to be intruded under the showing σ_1 trending NE–SW direction; σ_3 trending N–S direction.

A total of 49 entire slip data (17 slip data in gouge zone and 32 slip data in cataclasite zone

or consolidated shear plane) in the Iwatsubo area were obtained for multiple inverse method. The calculation results applying the entire slip data of the gouge zone shows σ_1 trends NW–SE direction; σ_3 trends NE–SW direction (Fig. 3.29). A cluster, which is reverse faulting paleostress regime with a northeast-trending σ_3, is also recognized. The former has scattered directions of the plunge, a wide variety of stress ratio and well concentrated clusters. However, the latter has comparatively minor cluster and the uniform stress ratio (0.4 ~ 0.6). Hence the former is thought to be major stress field. The results using the fault plane within cataclasite zone and shear planes without fault rocks shows σ_1 trends ENE–WSW direction; σ_3 trends N–S direction (Fig. 3.29). A cluster normal-faulting paleostress regime with E–W-trending σ_3 is also confirmed although the former cluster is interpretated to be major stress field because of well concentrated cluster.

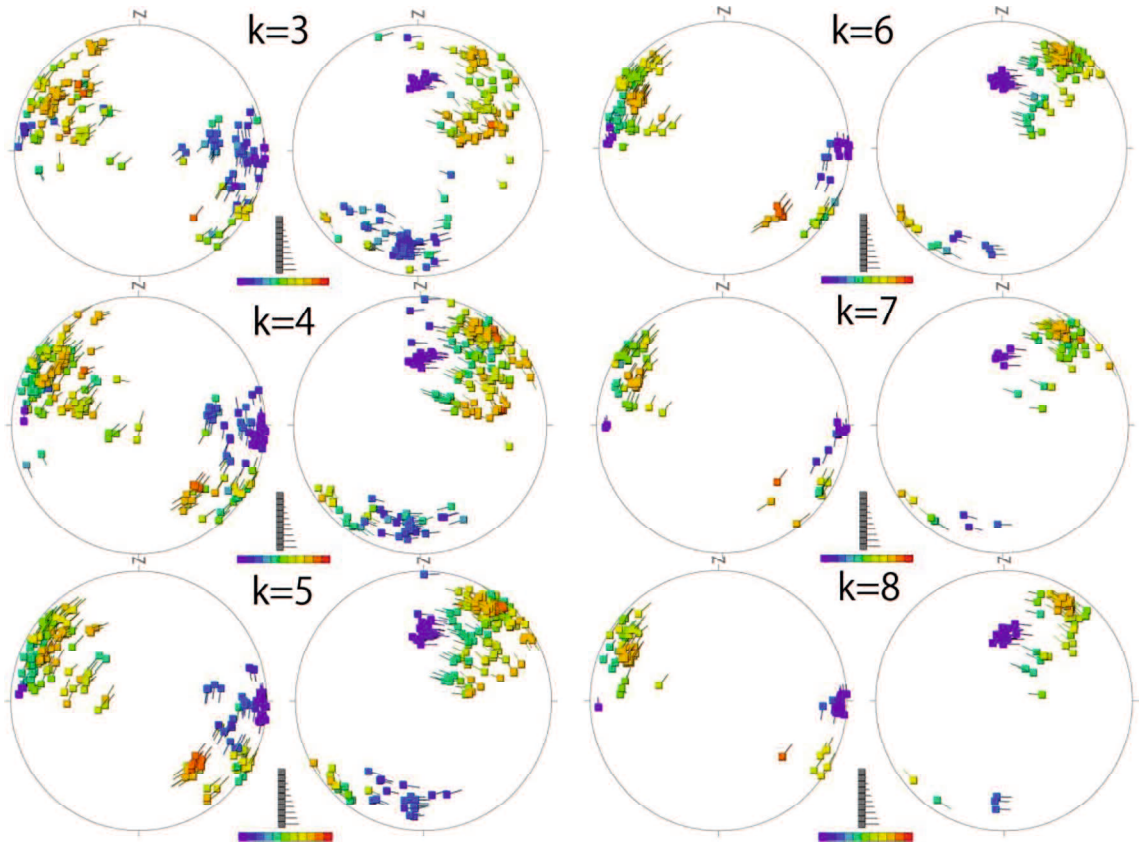

Figure 3. 27. Paleostress fields estimated from slip data of gouge zone in the Shikano area

Parameter "k" indicates fault combination number. Tadpole-like symbols depicts the with the head and tail representing the position of the σ_1 axis and the direction of the σ_3 axis, respectively in the left stereograms, and opposite in the counter parts. Color of the symbols shows the degree of stress ratio, given by $(\sigma_2-\sigma_3)/(\sigma_1-\sigma_3)$.

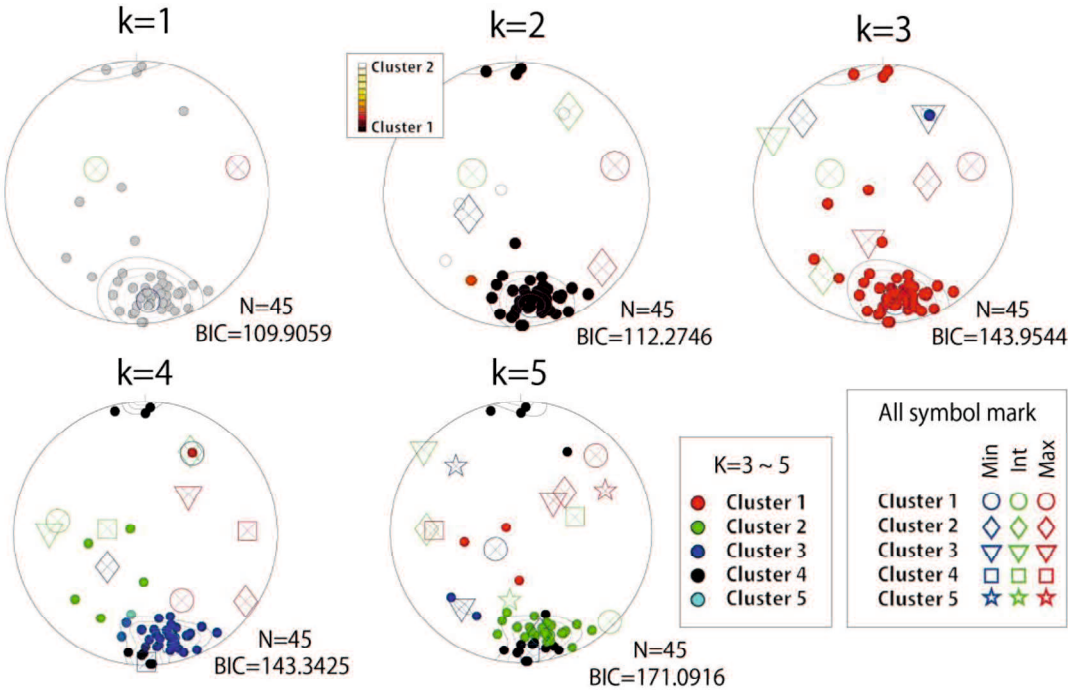

Figure 3. 28. Paleostress fields calculated from dikes in the Shikano area

Parameter "k" indicates number of the mixed Bingham distributions. The minimum Bayesian information criterion (BIC) indicates the best fitting of the Bingham distributions.

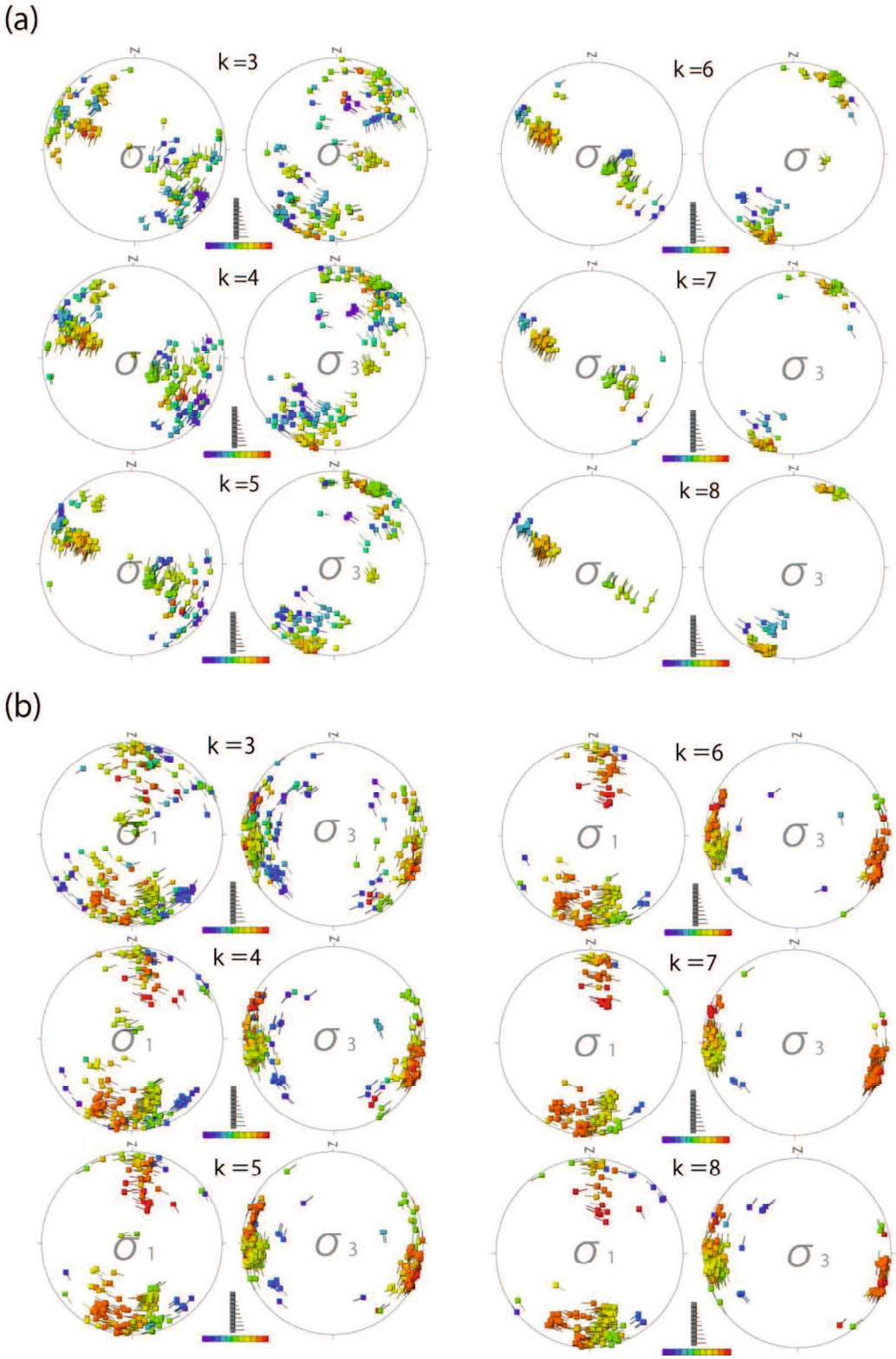

Figure 3. 29. Paleostress fields of the Iwatsubo area

The paleo-stress fields estimated from slip data of (a) gouge zone and (b) combination of cataclasite zone and cohesive shear planes without fault rocks. Parameter "k" indicates fault combination number. Tadpole-

like symbols depicts the with the head and tail representing the position of the σ_1 axis and the direction of the σ_3 axis, respectively in the left stereograms, and opposite in the counter parts. Color of the symbols shows the degree of stress ratio, given by $(\sigma_2-\sigma_3)/(\sigma_1-\sigma_3)$.

Table 3. 3. Geological feature in and outside of the SSZ.

	Geological features in the SSZ	Geological features outside of the SSZ
Distribution	Broad distribution	Limited distribution
Occurrence	~ a few dozens of cm	~ a few cm
Attitude	NNW-SSE Low to moderate plunge	NW-SE (dipping high angle) NE-SW (dipping low angle)

3.5. Discussion

3.5.1. Hierarchical structure of the SSZ

The occurrence and distribution of faults in the Shikano and Iwatsubo areas can be summarized as follows: (1) Most of the faults have a few millimeters to centimeters in width while some faults, as shown in the Iwatsubo fault core, have a few dozen centimeters in width, (2) Minor faults are distributed not only around the major active faults but also away from the major active faults, (3) ENE–WSW trending and steeply dipping faults with dextral sense of shear are confirmed, suggesting that the fault within the SSZ can contribute to the dextral motion of the SSZ. On the other hand, the occurrence and distribution of faults in the Kuroki area showed that: (1) Most of the faults have only a few millimeters to several centimeters in width, (2) Faults are only distributed around the geologic faults and Tsunogasen fault, (3) The fault gouge zone away from the Tsunogasen fault is dip-slip fault, suggesting that the fault outside of the SSZ cannot contribute to the dextral motion of the SSZ. Therefore, there are clear difference between faults within the SSZ and faults outside of the zone from the sight of the occurrence and distribution of faults (Table 3.3). As for the contribution to the dextral motion of the SSZ, faults within the SSZ have positive contribution but outside of the SSZ have no contribution to the deformation of the SSZ. In general, the fault zone structure is composed of the fault core and damage zone (e.g., Chester and Logan, 1987; Mitchel and Faulkner, 2009). However, this study clearly demonstrates there are minor faults away from active faults, suggesting that the traditional fault zone model can only explain deformation in the vicinity of active faults, and is not enough to explain overall upper crustal deformation in

the SSZ. Here, I constructed the hierarchical structure model of the SSZ as follows based on fault distribution, fault occurrence, contribution for the deformation of the SSZ: (1) faults core, (2) damage zone, (3) incipient brittle shear zone (or active background; the area beyond the damage zone but in the SSZ), (4) inactive background (Fig. 3.30).

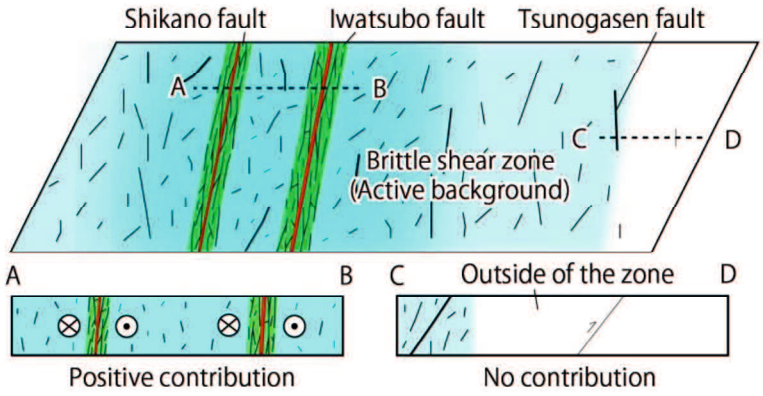

Figure 3. 30. Schematic illustration of characteristic structures across the SSZ

The blue zone denotes active zone of concentrated minor faults. The Shikano and Iwatsubo faults are composed of the damage zone (green zone) and fault core (red lines). Minor faults developed away from the active faults are given by blackish lines.

Except for the Shikano fault, the slip rates of the faults in the SSZ are unknown, whereas slip rates of faults with clear tectonic landforms can be estimated by applying the concept of "threshold of geomorphic detectability" (Kaneda, 2003 and Kaneda, 2006). The threshold of geomorphic detectability is slip rate exceeding in order that progressive coseismic surface offset can be preserved as detectable tectonic landforms that may be otherwise erased by surface processes (Kaneda, 2003; 2006). The threshold of geomorphic detectability in the San-in area is estimated to be 0.1 mm/y by surface rupture of the Shikano, Yoshioka and Gomura faults (Kaneda, 2003; 2006). Therefore, the threshold of geomorphic detectability in the study area including the Shikano and Yoshioka faults are assumed to be 0.1 mm/y. In this study, the slip rates of active fault traces (Certainty I and II) were regarded as larger slip rate than the threshold of geomorphic detectability since the active fault traces have clear and continuous tectonic landforms. The Tsunogasen fault trace (Fig. 3.7), L60, L61 (Fig. 3.8) are active fault traces of Certainty II, which locate in the area sufficiently away from the major active faults. Such faults are thought to play a role of the deformation in the brittle shear zone (or active background) because it is difficult to consider that these are related to the major

active faults due to their distance. Thus, the total slip rate of faults in the brittle shear zone (or active background) is expected to be at least 0.3 mm/y, implying that this zone can store more than 5 ~ 7.5 % of the crustal strain.

As shown in Azo outcrop, some lineaments can be regarded as active faults. The density distribution of the lineaments shows similar characteristic to that of the seismicity. Thus, a total of 42 lineaments (L2, 3, 6, 8, 9, 11, 12, 14, 15, 18, 22, 24, 25, 27, 29, 31, 32, 38, 40, 44, 46, 47, 49, 50, 51, 54, 55, 56, 57, 58, 59, 62, 63, 64, 65, 67, 68, 70, 71, 72, 75) which are difficult to interpret as a geological boundary could also be explained by active faults. Since lineaments have unclear tectonic landforms, long-term slip rates of these faults are thought to be less than 0.1 mm/y (C class active faults; Matsuda, 1975) due to the threshold of geomorphic detectability of 0.1 mm/y in San-in area. Thus, the slip rates of these faults might range from 0.01 to 0.1 mm/y. The sampling areas (area W, C and E) were set oriented N10° W, perpendicular to the approximate strike of the SSZ, to avoid double counting of fault. The width of the area is 1.57 km, corresponding to the average length of the lineaments. The total slip rate of faults in the area W is 0.04 ~ 0.4 mm/y because the area includes 4 lineaments (L46, 49, 51, 75). As for area C, the total slip rate of the faults is 0.07 ~ 0.7 mm/y because of 7 lineaments (L11, 22, 29, 40, 47, 62, 70) in the area. Since 8 lineaments are distributed in the area E, the total slip rate of faults in the area will be 0.08 ~ 0.8 mm/y. Combining these results, the total slip rate estimated from the lineaments are 0.04 ~ 0.8 mm/y. This indicates ~40 % of the crustal strain in the SSZ can be explained by the major active faults and minor faults away from the Shikano, Yoshioka and Iwatsubo faults (Certainty II and III).

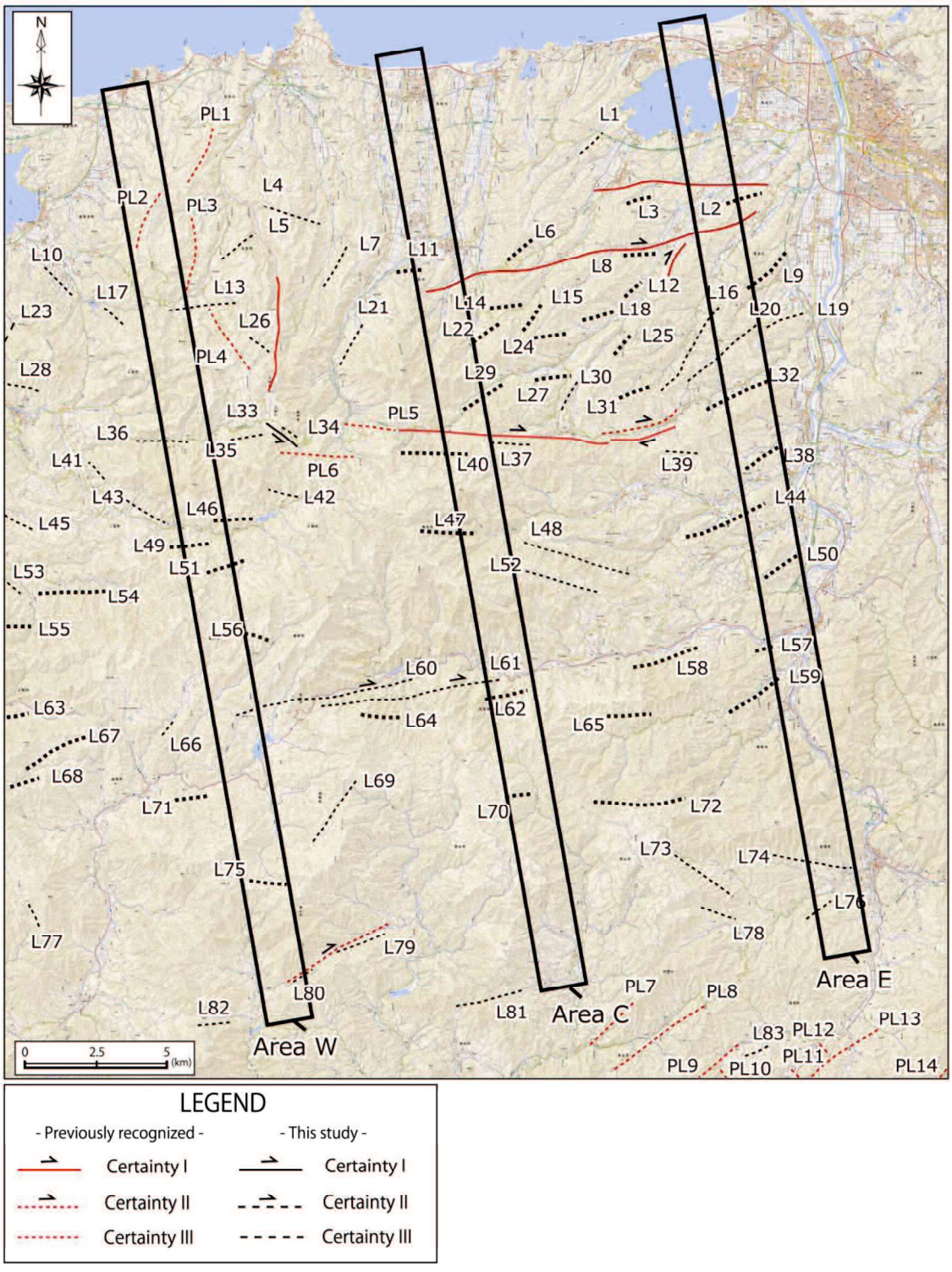

Figure 3. 31. The sampling areas of the lineaments.

Thick dotted black lines are lineaments interpretated as faults. The Thick black rectangles are sampling areas.

3.5.2. Evolutional process of faults the in the SSZ

The attitudes of dikes are quite similar to those of faults especially in the Kuchihosomi region. These faults are thought to be a part of the Shikano fault in that region since these are located < 300 m from the surface rupture. The noteworthy features of the minor faults are not only nearly same attitudes as those of the dikes but also their occurrences accompanied with dikes, suggesting that the Shikano faults are controlled by dikes. These minor faults may be activated after the intrusion of the dikes (after 31.4 ~34.7 Ma; see Fig. A2 for detail) because the dikes were crushed or cut by the faults. In addition, the dikes are thought to be formed under the N–S-trending tensile stress field in present-day geographic coordinate, which was confirmed based on the dike method using Bingham fitting (Yamaji, 2016; Stage 1 in Fig. 3.32). Thus, dikes intruded in granite under N–S-trending tensile stress field after 32 Ma, and then incipient faults with same attitudes of the dikes were prepared in the granitic basement rocks as a framework of the Shikano fault (Stage 2 in Fig. 3.32). According to Hoshi et al. (2015), 40° clockwise rotation of SW Japan was happened during the 16~18 Ma, which results in rotation of dikes and faults to E-W direction (Stage 3 in Fig. 3.32). Some of these faults are thought to have caused the 1943 Tottori earthquake under the present stress field (Stage 4 in Fig. 3.32). Therefore, the Shikano fault have grown by repeated activity using the pre-existed dikes. On the other hand, the attitudes of dikes in the Iwatsubo area are different from that of the Iwatsubo fault, suggesting that the Iwatsubo faults are not controlled by dikes. One possibility of the evolutional factor may be geologic boundary since the Iwatsubo fault trace is partly passing through the boundary between Tottori-nambu volcanic rocks and granitic rocks. This suggests that the Iwatsubo fault may have grown by repeated activity using the pre-existed geological boundary. Although the evolutional process between the Shikano and Iwatsubo faults may be different, it can be considered that such pre-existed structures have grown and resulted in the present major active faults in the SSZ.

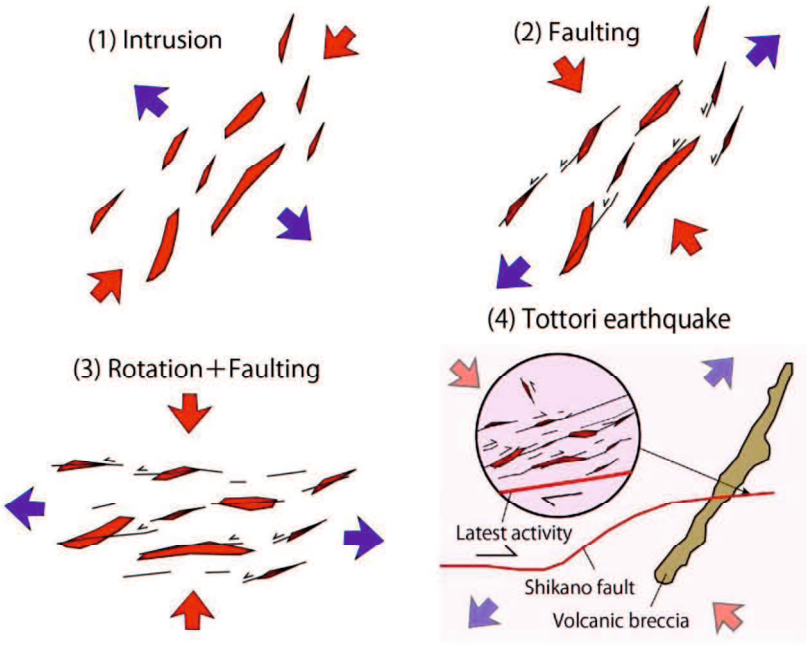

Figure 3. 32. Evolutional process of the Shikano fault

Estimated paleo-stress fields in these stages are based on the calculation results of the multiple inverse method (Yamaji, 2000) and dike method (Yamaji, 2016).

3.6. Conclusion

The main conclusions of my study in the SSZ are:

1. Field survey and topographic analysis conducted within the SSZ showed the existence of faults even away from the major active faults. Although most of the trends of faults (or lineaments) detected based on the topographic interpretations are subparallel to the trend of the SSZ, NNW–SSE to NW–SE-striking and steeply dipping fault found in the field survey is dominant.

2. Since there is apparent difference between contribution of faults to the crustal deformation in and outside of the SSZ, the brittle shear zone (or active background) that is characterized by concentrated minor faults are newly defined as the deformation zone outside of the damage zone but inside of the SSZ. Therefore, the SSZ has four hierarchical deformation zone: fault core of major active faults, damage zone of major active faults, brittle shear zone (or active background) and inactive background.

4. Overall discussions

4.1. The characteristics of the minor faults in the high strain-rate zone.

In this chapter, three points are discussed as follows: (1) Common features and differences between NKTZ and SSZ, (2) universal hierarchical structural model of the high strain-rate zones and its relation to the ongoing crustal deformation, (3) Academic and social implications.

The common characteristics of the NKTZ and SSZ were confirmed through the topographical and geological investigations. Minor faults turned out to be existed not only around the major active faults but also away from the major active faults. The density of the lineaments and active fault traces are increasing with decreasing the distance from the major active faults, implying that faults in the high strain-rate zone may be concentrated around the major active faults. These minor faults can contribute to the dextral motion of the high strain-rate zones. Thus, minor faults are thought to be one of the significant structure to explain the deformation of the high strain-rate zones.

On the other hand, the differences between the NKTZ and SSZ are also confirmed (Fig. 4.1). The major active faults in the SSZ have 10 to 30 centimeters thick fault core zone and have10 to 26 km length, whereas the major active faults range in thickness from a few meters to dozens of meters and range in length from 20 to 69 km in the NKTZ. In addition to the length and width, slip rate of the Shikano fault, one of the major active faults in the SSZ, is only 0.3-0.6 mm/y, whereas the slip rate of the Atotsugawa and Ushikubi fault is expected to be at least more than 1 mm/y [URL 2]. While the minor faults in the SSZ consist of a few millimeters to dozens of centimeters thick fault gouge/breccia zone, the minor faults in the NKTZ consist of a few millimeters to 5 m thick fault gouge/breccia zone. It might be speculated that these differences are reflecting the degree of maturations for faults in the high strain-rate zones. As for insight from the topography, Okada (2002) also anticipated that the active faults in the San-in district is immature and low activity due to lack of the tectonic landforms. On the other hand, geologic insight also provides evolutional process of the SSZ and NKTZ. According to Uchida et al. (2021), the fault gouge zone distributed in the aftershock area of the 2000 Western Tottori earthquake is considered to be formed at ~ 25 Ma based on the K-Ar dating of fault gouge, and the evolution process of these fault gouge zones are proved to be divided into 5 stages since 25 Ma. In this study, dikes in the Kuchihosomi region, which are thought to form incipient faults of the Shikano fault, should

intrude after the Oligocene because the K-Ar age of the granite yielded about 32 Ma (Imaoka et al., 2011). In contrast, the Atotsugawa fault system in the NKTZ is known that it has originated from tensile cracks formed in the Cretaceous (Takeuchi, 1983; Oohashi and Kobayashi, 2008; Niwa et al., 2011). Thus, it may be considered that faults in the SSZ are comparatively younger than those of the NKTZ (Fig. 4.1).

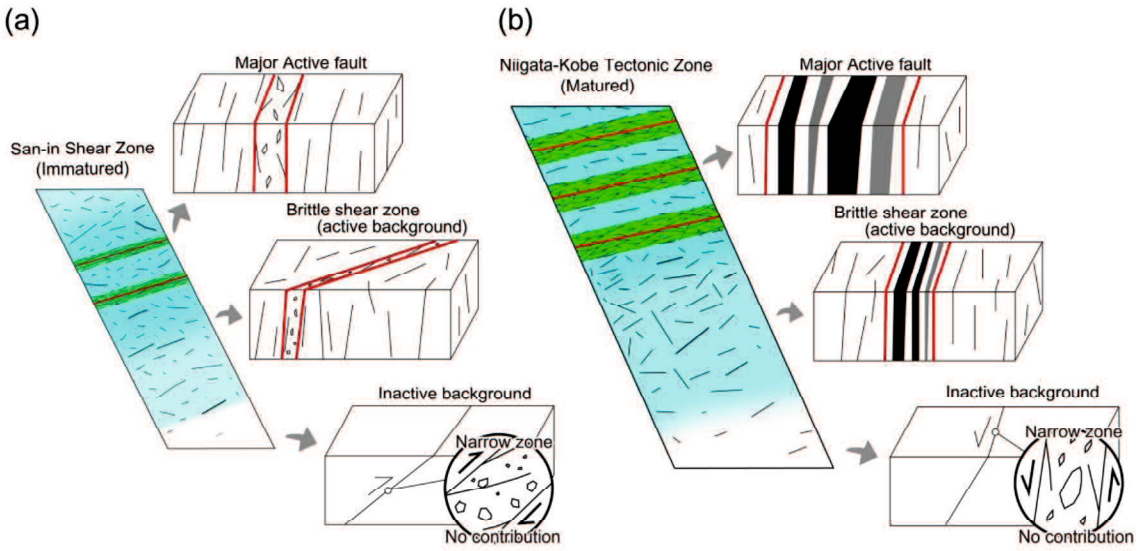

Figure 4. 1. Integrated structure model of the high strain-rate zone

(a) The structural model of the SSZ. (b) The structural model of the NKTZ. The blue zone denotes brittle shear zone. Green zone shows the damage zone of the major active faults. Red lines in the green zone shows the core zone of major active fault.

As for explanations of inelastic strain stored in the upper crust, block rotations, microcracking, tensile/shear fractures, shifted/deformed veins (sigmoidal carbonate vein), granular flow, folding, pressure solution and dislocation creep have been suggested (Shelef and Oskin, 2010; Ohzono et al., 2011; Otsubo et al., 2020; Karabacak et al., 2020). In the ECSZ, one of the well-known high strain-rate zones, Shelf and Oskin (2010) considered block rotations and offsets of secondary faults as off-fault deformations near the master fault. In addition, Karabacak et al. (2020) investigated around the master fault and described deformed vein in the NAFZ, which is also well-known high strain-rate zone. These previous studies show these geological structures adjacent to the master fault (~ a few km) can contribute to the deformation of these high strain-rate zones, whereas minor faults in the area a few km away from the major active faults turned out to also be significant factor from this study. As

shown in Chapter 2 and 3 (Tamura, 2018 MS; Tamura et al., 2020), both high strain-rate zones possess unique hierarchical deformation zone, which is marked by fault core zone, damage zones, incipient brittle shear zones (or active background; these are beyond the damage zone but in the high strain-rate zone) and inactive backgrounds (beyond the high strain-rate zone). Although the general structure of fault zone is composed of the fault core zone and damage zone (e.g., Chester and Logan, 1987; Mitchel and Faulkner, 2009), it appears that additional deformation is also expected to be assumed within high strain-rate zones because of the existence of minor faults away from active faults. Tamura (2018 MS) considered that the total slip rate of minor faults can be equal to that of A class active fault (> 1 mm/y), suggesting that the total deformation of minor faults is not negligible on a crustal deformation budget. Thus, further deformation zone should be defined for constructing general model of high strain-rate zone because the minor faults, which are often ignored in most of studies, are also significant structures for the contribution to the dextral motions of the high strain-rate zones. Combining the similar structures of the NKTZ and SSZ, it is therefore reasonable to conclude that the specific structures of high strain-rate zones is suggested as follows: (1) fault core zones, (2) damage zones, (3) incipient brittle shear zone (or active background) and (4) inactive background.

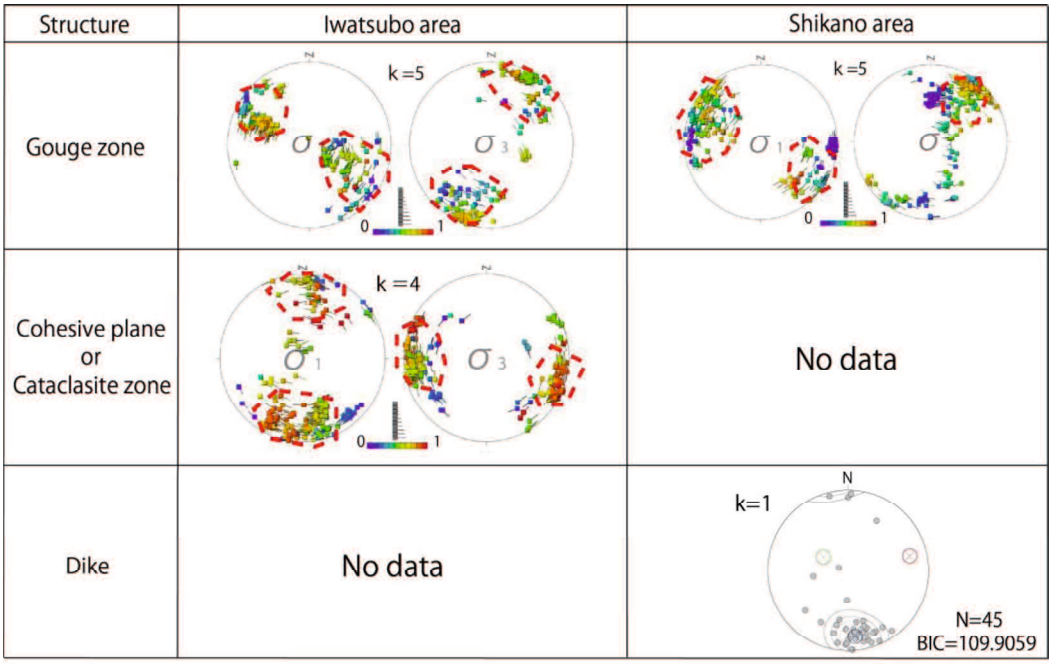

Figure 4. 2. Figure 4.2. Paleo-stress histories of the study area.

The stereo pairs in the table show paleo-stress fields obtained from the multiple inverse method (Yamaji,

2000). The stereo projection at the lower column shows paleo-stress fields obtained from the dike method using mixed Bingham distributions (Yamaji, 2016)

In addition, the distribution and evolutional process of each fault may be different and associated with local geological history (structural evolution) even in an identical high strain-rate zone. As shown in Fig. 4.2, the paleo-stress history obtained from gouge data in the Shikano area is nearly same as that of the Iwatsubo area. However, the evolutional process of the Shikano is thought to be different from that of the Iwatsubo fault (see section 3.5.2). The fault gouge zone and catacalasite zone were also discovered in the aftershock area of the 2000 Western Tottori earthquake, which is located in the western part of the SSZ (e.g., Kobayashi, 2004; Aizawa et al., 2005; Uchida et al., 2021). Aizawa et al. (2005) confirmed dikes, whose attitudes are nearly same as those of studied faults, and thought that the distribution of the dikes is related to the evolution of faults in the aftershock area. Uchida et al. (2021) concluded that the majority of such pre-existed structures in the San-in region, including fault gouge zones in the aftershock area, are considered to have grown through served tectonic stress conditions. Since the paleo-stress fields of the study area of the 2000 Western Tottori earthquake are not fully consistent to those of aftershock area, evolutional processes of major active faults in the study area are also thought to be different from that of the faults in the aftershock area as suggested by Uchida et al. (2021). Additionally, paleo-stress fields of study area and the aftershock area of the 2000 Western Tottori earthquake are not consistent to that of the Tajima-Myokenzan area located in the eastern part of the SSZ (Haji and Yamaji, 2021). Haji and Yamaji (2021) considered that faulting of the map-scale faults and minor faults ceased until 13.5 Ma, implying that their evolutional processes are clearly different from those of the faults in the western part of the SSZ and this study area. Thus, it is thought that some faults were grown and can contribute to the dextral deformation of the SSZ, while other faults were abandoned. These facts suggest that evolutional processes of faults may depend on local tectonic background of each region even in the same high strain-rate zone. One possibility of the difference between abandoned fault and ongoing active fault may be controlled by the regional stress fields. The approximate stress fields in the SSZ is thought to be σ_1 trending NW–SE ~ E–W direction; σ_3 trending NE–SW ~ N–S direction (Imanishi et al., 2021), whereas local tress fields are also recognized (Yukutake et al., 2020). In addition, multiple inverse method in the Shikano and Iwatsubo area yielded minor paleo-stress fields (Fig. 3.27 and 3.29), suggesting that some of the faults are also controlled by minor stress fields. Another

possibility may be each frictional property of faults. Coefficient of frictions of the minor faults in the aftershock area of 2000 Western Tottori earthquake are known to be 0.15 ~ 0.3 based on friction experiments (Mori, 2020 BS; Mori, 2022 MS). Mori (2020 BS) considered that these low coefficients of frictions are related to the clay minerals of fault gouge zone, which mainly includes smectite. Most of the faults in this study area also includes smectites (Table 1), indicating that these clay minerals may contribute to the frictional property. Therefore, these faults, which are controlled by minor stress fields and/or low coefficients of frictions, may contribute to whether faults can be active or not.

On the other hand, there are also common process between the faults of each region. The Shikano fault, Iwatsubo fault, and minor faults in the aftershock area of 2000 Tottori earthquake are commonly derived from pre-existed structures (e.g., dike geological boundary). According to Nishimura and Takada (2017), the evolutional process of the SSZ is progressive deformation based on the sand-box experiments (Tchelenko, 1970), which indicates NNW-SSE-trending faults in the SSZ are similar to the Riedel shears in the initial stage. However, they regarded the NNW-SSE-trending faults as R2 shear planes, whereas the shear planes exposed in the initial stage of the shear experiments shown in Tchelenko (1970) is thought to be R1 planes. Additionally, an initial condition of the sand-box before the shear experiments was filled with homogeneous clay, whereas the upper crust along the SSZ is thought to be heterogeneous due to the existence of the pre-existed structures. Thus, it is not reasonable to consider the evolutional process of the SSZ based on progressive deformation. In this study, the evolutional process of the faults is thought to be repeated reactivation of the pre-existed structures. In addition to the example of the SSZ, the Atotsugawa fault system in the NKTZ is known that it has grown by repeated faulting along tensile cracks (Takeuchi, 1983; Oohashi and Kobayashi, 2008; Niwa et al., 2011). Therefore, it can be concluded that faults in the high strain-rate zones were originated along pre-existed structure (e.g., dike, geological boundary and tensile cracks) and grown in response to local and regional stress fields that generate shear stress to faults (Fig. 4.3).

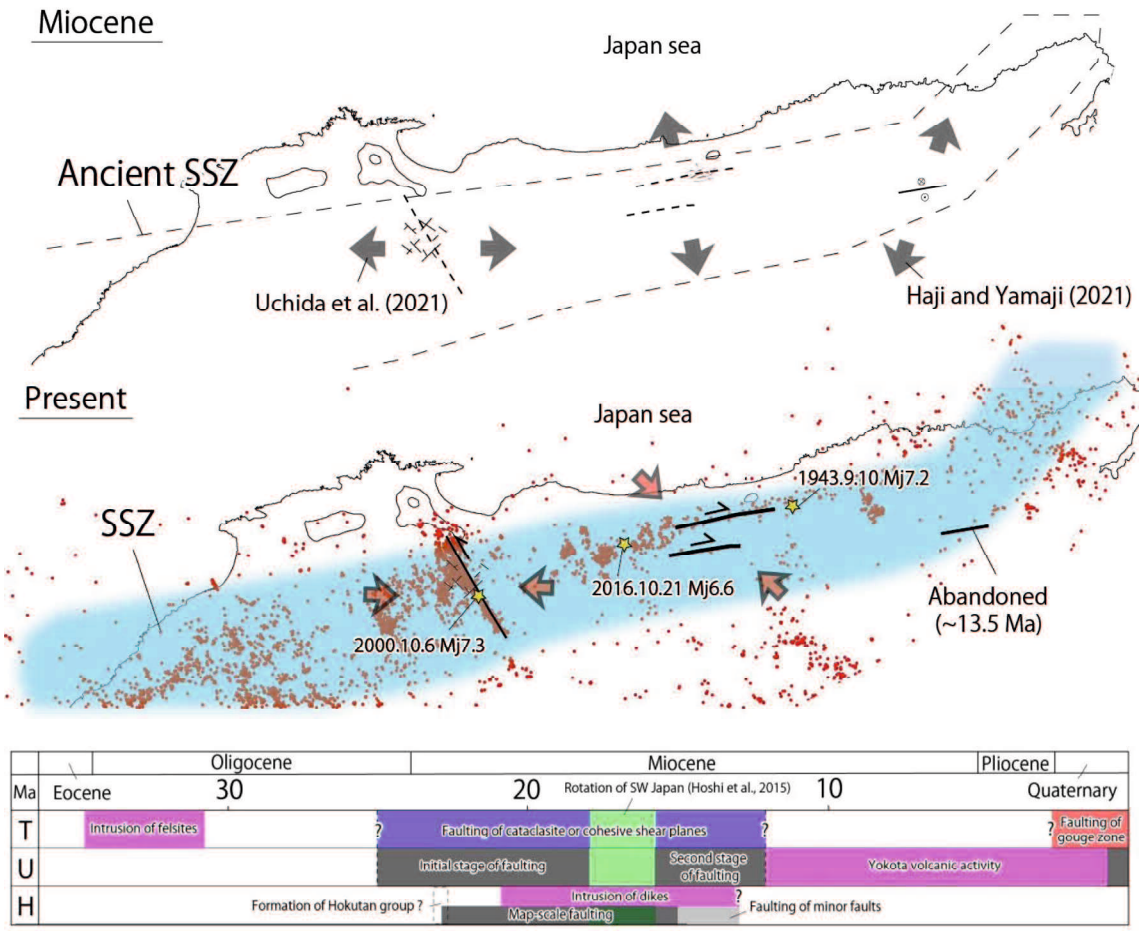

Figure 4. 3. Evolutional model of the high strain rate zone

The red dots show microearthquakes during 2005 ~ 2009 from Japan Metrological Agency (JMA). The blue zone shows the San-in Shear Zone. T=This study, U=Uchida et al. (2021), H=Haji and Yamaji (2021).

4.2. Academic and social impacts of new structural model of high strain-rate zones

The strain-rate paradox is one of the significant issues of the crustal deformation and has not been solved yet. In this study, the brittle shear zone (or active background) was proposed by focusing on the existence of minor faults, which can contribute to the dextral deformation of the high strain-rate zones. The brittle shear zone (or active background) of the NKTZ can store 4 ~ 24 % of crustal strain (Tamura, 2018 MS; Tamura et al., 2020) and the zone of the SSZ can explain at least 5 ~7.5 % of crustal strain (See chapter 3). Thus, the strain rate paradox can partly be solved by applying this new model "brittle shear zone (or active background)". Additionally, previous studies attempted to construct the models of the high strain-rate zones (e.g., Iio et al., 2004; Iio, 2009), whereas these models have not been taking the effects of the minor faults into account. Thus, it can be better understanding for crustal

deformation by introducing the new concept "brittle shear zone (active background)" into the previous crustal models (e.g., Iio et al., 2004; Iio, 2009). Further, it will be needed to analyze the brittle shear zone insight from the geodesy and seismology.

In addition to the academic role of the minor fault, focusing on minor faults can also provide beneficial data for regional disaster preventions in high strain-rate zones. As suggested by Uchida et al. (2021), knowledge of minor faults in areas where no active faults or geological structures are known (namely, "blind active fault") may provide understanding of seismic hazards because they recognized 1066 minor faults in the aftershock area of the 2000 Western Tottori earthquake (corresponding to the western part of the SSZ). In this study, minor faults also recognized away from effects of active faults (e.g., deformation in aftershock area, on-and off-fault deformation) within the high strain-rate zones, suggesting that they are generally distributed within the zone. Moreover, outcrops of active faults were newly recognized through the investigations targeting on minor faults, which implies that at least some parts of widespread faults in the high strain-rate zone are active. Generally, revealing not only distributions but also activities of faults are one of the quite significant works for assessing the future earthquakes. As shown in the case study of the Inagoe fault, which is smaller-scale active fault than Atotsugawa fault system (see Chapter 3), fault gouge zone is interpretated to be clearly active because of the field evidence of faulting during the Quaternary. Such information cannot be negligible for sustainable maintenance of Hida tunnel and basic data of seismic hazard in Hida city. However, this example succeeded in obtaining beneficial data for the Hida area, whereas other minor faults, which have not been assessed and may have potential for earthquake disaster, are likely to be distributed along the high strain-rate zone. Thus, analyzing not only major active faults but also minor faults will enhance the disaster prevention. In addition, maintenance of the Hida tunnel will be needed to take the effects of the Inagoe fault into account. Therefore, it can be concluded that further active fault studies taking effects of minor faults into account for seismic hazard and tunnel constructions are needed, especially in high strain-rate zone.

5. Conclusions

The main outcomes of this study in the NKTZ are summarized as follows.

(1) The fault core, consisting of 5 m fault gouge/breccia zone in width, of the Inagoe fault was described in detail. Unconsolidated sand-gravel mixtures unconformably overlying the fault zone were sandwiched within the fault gouge zone, implying the latest activity after the Quaternary. Dating of a radiocarbon age from a humus sample in the sand-gravel mixtures showed the formational age of AD 1521–1658. This suggests that the western segment of the Inagoe fault might have ruptured during one of the four historical earthquakes in the northern part of the Gifu Prefecture.

(2) A total of 13 faults in the Kurumijima area, located outside of the NKTZ, are NE-SW to ENE-WSW striking, whose slickenlines on fault planes plunge at low to moderate angles (R0° ~ 45°). The senses of movements of the faults are inconsistent with the dextral motion of the NKTZ, suggesting that the faults in the Kurumijima area cannot contribute to the deformation of the NKTZ.

(3) From the investigation in the Kurumijima area, the characteristics of faults distributed in and outside of the NKTZ turned out to be different. Integrating such facts and previous works, an enhanced version of hierarchical structure model of the NKTZ was reconstructed as follows: 1) fault core, 2) damage zone, 3) incipient brittle shear zone (or active background), 4) inactive background.

The main outcomes of this study in the SSZ are summarized as follows.

(1) Field survey and topographic analysis conducted in the SSZ showed the existence of minor faults even away from the major active faults. Although the majority of the trends of active fault traces and lineaments detected by means of topographic interpretations are subparallel to the trend of the SSZ, faults in the field also have NNW–SSE- to NW–SE-trending and E–W-trending strikes with steep dips in the Shikano and Iwatsubo areas.

(2) The faults in the Kuroki area typically range in thickness from a few millimeters to centimeters. These minor faults are mostly distributed around the Tsunogasen fault, whereas fault gouge zone is also recognized outside of the SSZ. However, the fault, consisting of only a few millimeters thick gouge zone, has incongruous sense of shear to the dextral motion of the SSZ. Such occurrence and limited distribution suggest that minor faults possess clear difference between the faults in and outside of the SSZ.

(3) The hierarchical structure model of the SSZ was constructed in terms of fault distribution, fault occurrence, contribution to strain concentrated on the SSZ as follows: 1) fault core, 2) damage zone, 3) incipient brittle shear zone (or active background; the area beyond the damage zone but in the SSZ), 4) inactive background.

The hierarchical structure of the NKTZ is quite similar to that of the SSZ. It can be therefore concluded that high strain-rate zones consist of fault core, damage zone, incipient brittle shear zone (or active background) and inactive background as a general structure model. In addition, faults in the high strain-rate zones develop using pre-existed structure and grown faults result in dextral deformation element of the high strain-rate zones. As shown in the ECSZ and NAFZ, deformation elements in high-strain rate zones are thought to be secondary faults and they form a rotation of mylonite and deformed vein. However, minor faults in the high strain-rate zone but away from the major active faults are also thought to be significant deformation element from the topographical and geological insight.

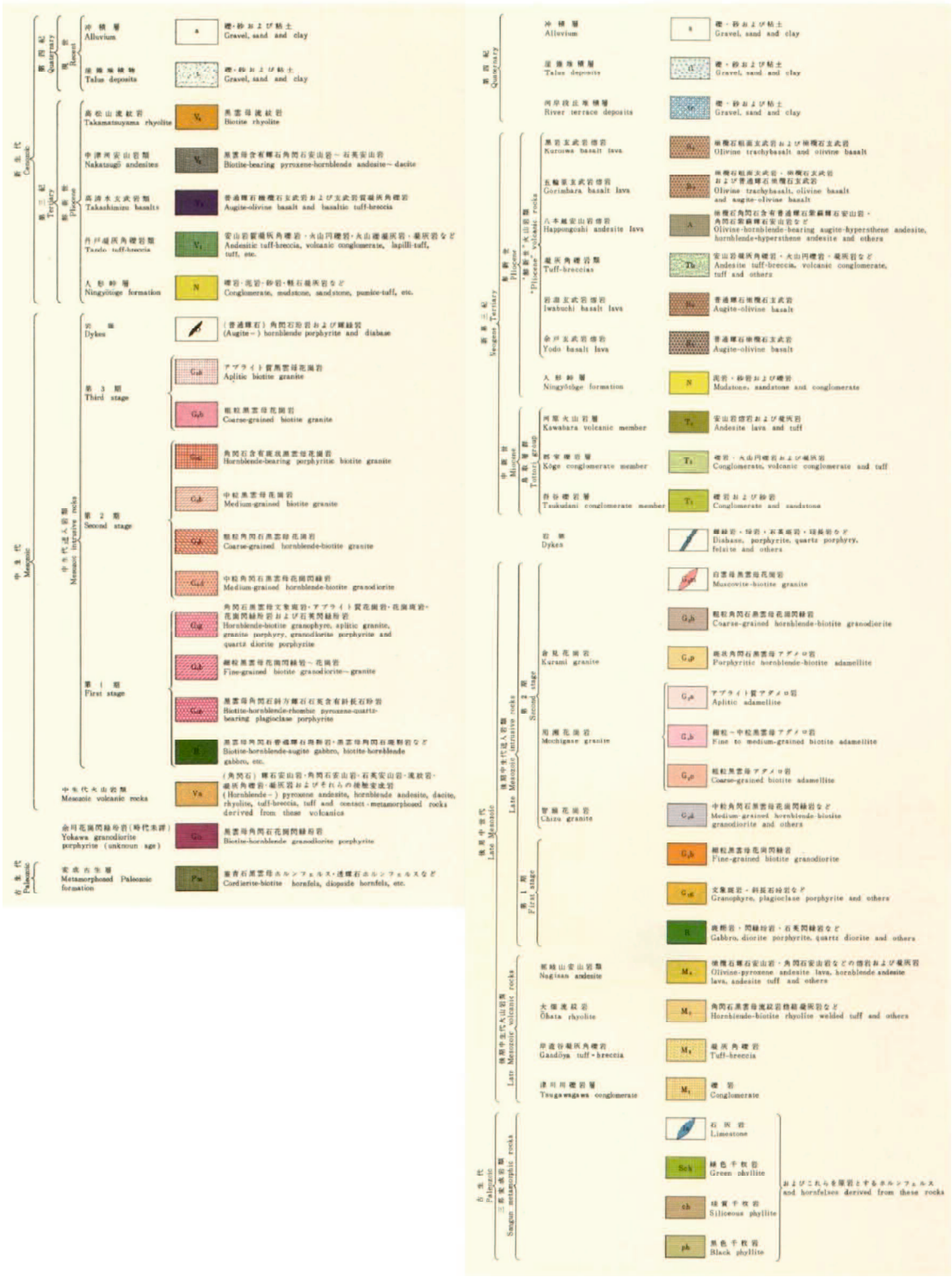

Figure A1. Compiled legends of the geological maps in Figure 3.9.

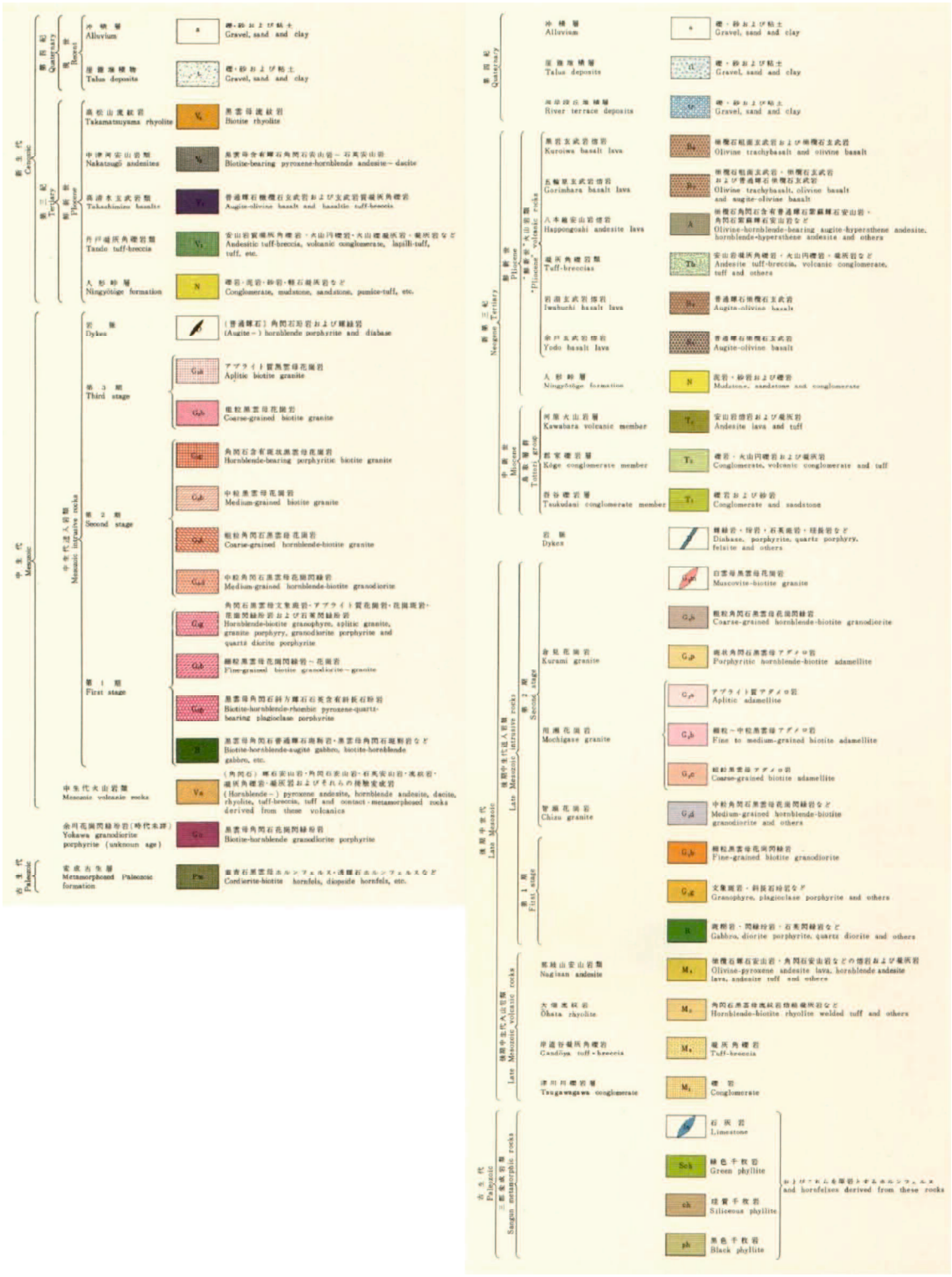

Figure A1. Compiled legends of the geological maps in Figure 3.9 (Continued).

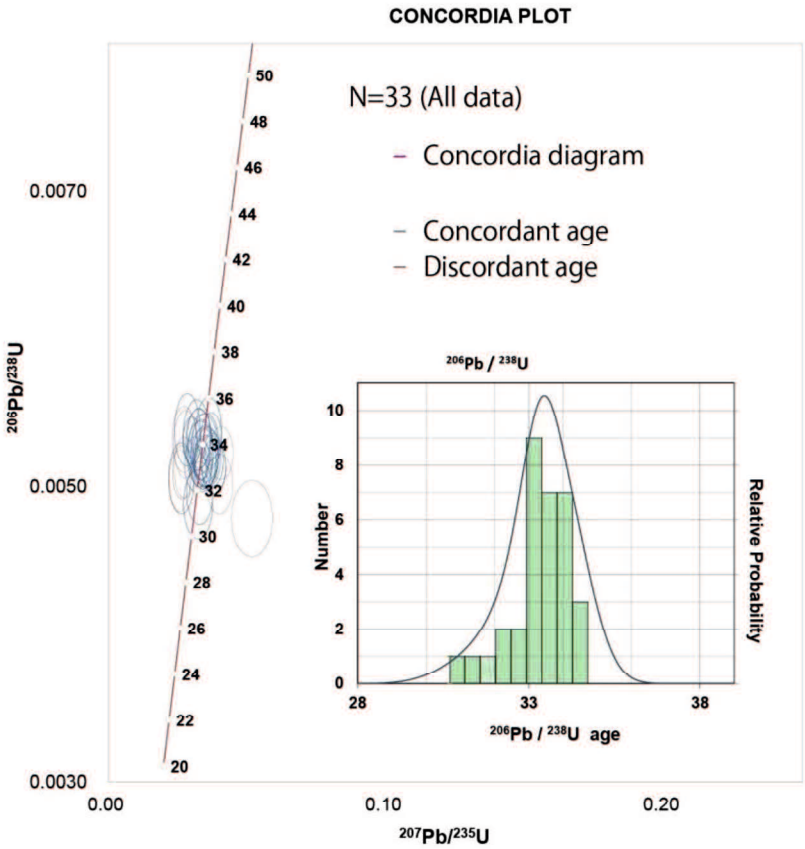

Figure A2. The The results of the zircon U-Pb dating

The zircon U-Pb dating was conducted at the premises of Kyoto Fission-Track Co., Ltd. (Kyoto, Japan). The sampling point of the felsite dike was shown in Fig.3.15a. The detected zircon of the felsite was homogeneous crystal habit, automorphic shape, unimodal age of 30 concordant grains, indicating intrusion age of the dike. The whole age of the zircon U-Pb dating range from 31.4 ~34.7 Ma.

Table A1. Basic information for active fault traces and lineaments.

Number	Length	Direction	Category	Tectonic landforms	Factor	Number	Length	Direction	Category	Tectonic landforms	Factor
L1	1.1 km	N48° E	Lineament	Dextral offset	Geological boundary	L43	1.6 km	N57° W	Lineament	Dextral offset	Geological boundary
L2	1.4 km	N76° E	Lineament	Dextral offset		L44	3.1 km	N66° E	Lineament		
L3	0.94 km	N78° E	Lineament	Dextral offset		L45	1.1 km	N64° W	Lineament		
L4	2.2 km	N73° W	Lineament	Sinistral offset		L46	1.4 km	N88° E	Lineament		
L5	1.1 km	N56° E	Lineament			L47	1.9 km	N88° W	Lineament		
L6	1.1 km	N52° E	Lineament			L48	3.2 km	N74° W	Lineament		
L7	1.7 km	N30° E	Lineament		Geological boundary	L49	1.4 km	N80° W	Lineament		
L8	1.3 km	N87° E	Lineament			L50	1.5 km	N55° E	Lineament		
L9	1.3 km	N47° E	Lineament		Geological boundary	L51	1.4 km	N72° E	Lineament		
L10	1.4 km	N43° W	Lineament			L52	2.7 km	N77° W	Lineament		
L11	0.94 km	N78° E	Lineament			L53	0.63 km	N48° W	Lineament		
L12	0.78 km	N48° E	Lineament			L54	2.3 km	N88° E	Lineament		
L13	2.5 km	N48° E	Lineament		Geological boundary	L55	0.94 km	N88° E	Lineament		Geological boundary
L14	1.1 km	N80° E	Lineament			L56	0.94 km	N75° W	Lineament		
L15	1.1 km	N35° E	Lineament			L57	0.67 km	N73° E	Lineament		
L16	3.3 km	N35° E	Lineament		Geological boundary	L58	2.3 km	N73° E	Lineament		
L17	0.94 km	N47° W	Lineament			L59	2.0 km	N53° E	Lineament		
L18	1.1 km	N35° E	Lineament			L60	6.3 km	N79° E	Presumed Active fault	Dextral offset	Geological boundary
L19	1.4 km	N71° E	Lineament		Geological boundary	L61	9.4 km	N81° E	Presumed Active fault	Dextral offset	
L20	3.1 km	N51° E	Lineament			L62	1.6 km	N77° E	Lineament		
L21	1.7 km	N19° E	Lineament		Geological boundary	L63	0.78 km	N78° E	Lineament		Geological boundary Geological fault
L22	1.3 km	N55° E	Lineament			L64	1.6 km	N86° W	Lineament		
L23	0.78 km	N26° E	Lineament			L65	1.6 km	N87° E	Lineament		Geological boundary
L24	1.1 km	N26° E	Lineament			L66	0.67 km	N33° E	Lineament		Geological boundary
L25	0.78 km	N26° E	Lineament			L67	2.3 km	N61° E	Lineament		Geological boundary
L26	0.86 km	N54° W	Lineament			L68	1.1 km	N73° E	Lineament		
L27	1.3 km	N54° W	Lineament			L69	2.7 km	N35° E	Lineament		
L28	1.3 km	N78° W	Lineament			L70	0.94 km	N77° E	Lineament		Geological fault
L29	1.6 km	N56° E	Lineament			L71	1.3 km	N85° E	Lineament		
L30	1.1 km	N27° E	Lineament			L72	4.3 km	N87° E	Lineament		
L31	1.3 km	N70° E	Lineament			L73	2.5 km	N55° W	Lineament		
L32	2.3 km	N67° E	Lineament			L74	2.8 km	N81° W	Lineament		
L33	1.4 km	N52° W	Active fault			L75	1.3 km	N83° W	Lineament		
L34	0.67 km	N56° W	Lineament		Geological boundary	L76	1.1 km	N52° E	Lineament		
L35	1.1 km	N82° E	Lineament			L77	0.94 km	N23° W	Lineament		
L36	1.9 km	N88° W	Lineament		Geological boundary	L78	1.1 km	N72° W	Lineament		
L37	1.4 km	N87° W	Lineament		Geological boundary	L79	1.9 km	N68° E	Lineament		
L38	1.3 km	N56° E	Lineament			L80	0.83 km	N59° E	Lineament		
L39	1.1 km	N82° W	Lineament		Geological boundary	L81	2.5 km	N78° E	Lineament		Geological fault
L40	2.3 km	N88° W	Lineament			L82	1.0 km	N81° E	Lineament		
L41	0.86 km	N40° W	Lineament			L83	0.94 km	N65° E	Lineament		
L42	1.1 km	N74° W	Lineament								

The average length of the lineaments detected by Research Group for Active Faults (1991) and this study is 1.57 km. Most of the detected lineaments and fault trace of L60 and L61 are trending ENE-WSW ~ E-W directions. The category of the presumed active fault and lineaments are corresponding to the Certainty II and III, respectively.

Reference

Aizawa, Y., Kobayashi, K., Umetsu, K. and Yamamoto, R., 2005, Fault rocks in the aftershock area and the neighborhood of 2000 Tottori-ken Seibu earthquake, *J. Geol. Soc. Japan*, **111**, 12, 737-750 (in Japanese, with English abstract).

Bronk Ramsey, C., 2009, Bayesian analysis of radiocarbon dates, *Radiocarbon*, **51**, 1, 337–360.

Cello, G., Roberto, G., Stefano, M., Andrew, R., Emanuele, T. and Vittorio, Z., 2000, Fault zone characteristics and scaling properties of the Val d'Agri Fault System (Southern Apennines, Italy), *J. Geodynamics*, **29**, 293–307. https://doi.org/10.1016/S0264-3707(99)00043-5

Chester, F.M. and Logan, J.M., 1987, Composite planar fabric of gouge from the Punchbowl Fault, California. *J. Stcuct. Geol.*, 9, 809-817. 307.

Childs, C., Manzocchi, T., Walsh, JJ., Bonson, CG., Nicol, A. and Schopfer. MPJ., 2009, A geometric model of fault zone and fault rock thickness variations, *J Struct Geol*, **31**, 2, 117–127.

Crowell, J, C, 1974, Origin of late Cenozoic basins in southern California, *Spec. Publ. Soc. Econ. Palaeont. Miner. Tulsa.*, **22**, 190–204.

Doke, R. and Takeuchi, A., 2009, The latest event at the eastern part of the Atotsugawa fault, inferred from the outcrops at Sako, Hida city, central Japan, *Quatern. Res.*, **48**, 11–17 (in Japanese, with English abstract).

Dolan. JF., Bowman, DD. and Sammis, CG., 2007, Long-range and long-term fault interactions in Southern California, *Geology*, **35**, 9. 855–858. doi:10.1130/G23789A.1.

Eberl, D.D., 2003, User's Guide to RockJock -A program for determining quantitative mineralogy from power X-ray diffraction data, *USGS Open-file Report*, 03-78.

Fossen, H., 2010, Structural geology. Cambridge University Press, *Cambridge*, p463.

Fukui, K., Okubo, S., Moriyama, M., Aoki, T., Kozuka, T. and Matsubara, M., 2007, Disc-Cutter Wear of TBM at Hida Tunnel, *J. Min. Metall. Inst. Japan*, **123**, 467–474 (in Japanese, with English abstract).

Fuseshima, Y., Imura, R., Morino, M., Sugiyama, Y. and Mizuno, K., 2002, Trenching surveys of surface ruptures associated with the 2000 Tottori-ken-seibu earthquake, *Ann. Rep. Active Fault and Paleoearthquake Res.*, **2**, 183–208 (in Japanese, with English abstract).

Goto, A., Sasaki, A, Komatsu, T., Miwa, A., Terusawa, S., Kagohara, K. and Shimada, K.,2020,

A catalog showing distribution and features of lineaments and related landforms in an active shear zone with unclear fault displacement topography; An example of an active left-lateral shear zone in southern Kyushu Island, southwest Japan, *JAEA-Report-2020-013*, 88p (in Japanese).

Haji, T. and Yamaji, A., 2021 Post - rift stress history of Southwest Japan inferred from early to middle Miocene intrusions and meso - scale faults in the Tajima–Myokensan area, IslandArc,30,e12412, https://doi.org/10.1111/iar.12412

Hashimoto, T., Hoshino, K. and Kato, H., 1980, Active faults in eastern Shimane and western Tottori Prefectures, *Bull. Geol. Surv. Japan*, **31**, 2, 93-97 (in Japanese, with English abstract).

Hasi, B., Takeuchi, A., Sakogaichi, K., Takebe, A., Ito, T., Niimi, K., Kinoshita, H. and Nohara, T., 2000, Activity of the Atotsugawa fault and Mozumi-Sukenobe fault, *extra. Earth Monthly*, **28**, 113–118 (in Japanese, with English abstract).

Hoshi, H., Kato, D., Ando, Y. and Nakashima, K., 2015, Timing of clockwise rotation of Southwest Japan: constraints from new middle Miocene paleomagnetic results, Earth Planets Space, 67, 10.1186/s40623-015-0266-3

Hubert-Ferrari, A., Armijo, R., King, G., Meyer, B., Barka, A.A., 2002. Morphology, displacement, and slip rates along the North Anatolian Fault, Turkey. *J. Geoph. Res.*, **107**, https://doi.org/10.1029/2001JB000393

Hujita, T., 1972, Volcanostratigraphy of the Misasa Group in the Vicinity of Ningyo-toge - Studies of the Misasa Group (I) -, *J. Geol. Soc. Japan*, 78, 1, 13-28 (in Japanese with English abstract).

Ichimura, M. and Mukoyoshi, H., 2020, The relationship between fault rocks and seismic activities in the aftershock area of 2016 central Tottori earthquake, *Bull. Geol. Soc. Shimane Pref.*, 35, 15-20 (in Japanese).

Iio, Y., 2009, The process by which interpolate earthquakes are generated, *Jour. Seismol. Soc. Japan, 2nd Ser.* , **61**, S365-S377.

Iio, Y., Sagiya, T., Kobayashi, Y. and Shiozaki, I., 2002, Water-weakened lower crust and its role in the concentrated deformation in the Japanese Islands, *Earth Planetary Science Letters*, **203**, 1, 15, 245–-253.

Iio, Y., Sagiya, T., Kobayashi, Y., 2004, What controls the occurrence of shallow interpolate earthquakes?, Earth Planets Space, **56**, 1077–1086.

Ikeda, Y., Okada, S. and Tajikara, M., 2012, Long-term strain buildup in the Northeast Japan

arc-trench system and its implications for gigantic strain-release events, *Jour. Geol. Soc. Japan*, **118**, 5, 294–312. (in Japanese with English abstract)

Imaizumi, T., Miyaushi, T, Tsutasumi, H. and Nakata, T., eds., 2018, New Edition: Digital active fault map of Japan, *University of Tokyo Press*, 154p (in Japanese).

Imanishi, K., Ushide, T., Shiina, T., Matsushita, R. and Nakai, M., 2021, Rep. Geol. Surv., **72**, 1, 23-40 (in Japanese, with English abstract).

Imanishi. K., Kuwahara, Y., Takeda, T., Mizuno, T., Ito, H., Ito, K., Wada, H. and Haryu, Y., 2011, Depth-dependent stress field in and around the Atotsugawa fault, central Japan, deduced from microearthquake focal mechanisms: Evidence for localized aseismic deformation in the downward extension of the fault, *J Geophys Res*, **116**, B1. doi:10.1029/2010JB007900.

Imaoka, T., Kiminami, K., Nishida, K., Takemoto, M., Iwata, T., Itaya, T., Kagami, H., Iizumi, S., 2011, K-Ar age and geochemistry of the SW Japan Paleogene cauldron cluster: Implications for Eocene-Oligocene thermo tectonic reactivation, *Jour. Asian. Earth. Sci*, **40**, 509-533.

Inoue, D., Miyakoshi, K., Ueta, K., Miyawaki, A. and Matsuura, K., 2002, Active Fault Study in the 2000 Tottori-ken Seibu Earthquake Area, *Jour. Seismol. Soc. Japan, 2nd Ser.*, **54**, 557-573 (in Japanese, with English abstract)

Isozaki, Y., Maruyama, S., Aoki, K., Nakama, T., Miyashita, A. and Otoh, S., 2010, Geotectonic subdivision of the Japanese Islands revisited: Categorization and definition of elements and boundaries of Pacific-type (Miyashiro type) orogen, *J Geogr*, **119**, 6. 999–1053 (in Japanese, with English abstract).

Ito. T., Tsumura, N., Takeuchi, A., Ishimuru, T., Takami, A., Ikawa, H., Komada, N., Yamamoto, S., Miyauchi, S., Kawanaka, T. and Ikawa, T., 2007, Imaging of the Mozumi–Sukenobe fault, Hida district, central Japan, by the seismic reflection method. In: Ando, M. (ed), *Geodynamics of Atotsugawa Fault System*. Terrapub.

Itoh, Y., Kimura, H. and Doshida, S., 2004, Active strike-slip faulting and macroscopically nonrigid deformation of volcanic rocks in central Japan inferred from a paleomagnetic study, Tectonophysics, **374**, 81–98.

Kamei, A, 2007, Overview on the granitic rocks and ore deposits in San-in district, *Geol. Sci. Rep. Shimane Univ.*, Special Issue, 27-30 (in Japanese, with English abstract).

Kaneda, H., 2003, Threshold of geomorphic detectability estimated from geologic observations of active low slip-rate strike-slip faults, *Geophysical Research Letters*, **30**, 5,

1238, doi: 10.1029/2002GL016280.

Kaneda, H., 2006, Threshold of geomorphic detectability of strike-slip active fault, *Chikyu monthly*, **54**, 78–84.

Kaneda, H. and Okada, A., 2002, Surface rupture associated with the 1943 Tottori earthquake: compilation of previous reports and its tectonic geomorphological implications, *Act. Fault Res.*, **21**, 73-91 (in Japanese, with English abstract).

Kano, T., 1983, Origin of augen gneiss and related mylonitic rocks in the eastern part of the Hida metamorphic region, central Japan (Part 1) – Mode of occurrences, petrographical and mineralogical properties of rocks and potash-feldspar megacrysts –, *Jour. Geol. Soc. Japan*, **89**, 7, 375–393.

Katagawa, H., Anata, F., Yoshida, S. and Ito, T., 2002, The Time of the latest Activity along the Eastern Part of the Atotsugawa Fault, *Quatern. Res.*, **41**, 73–83 (in Japanese, with English abstract).

Katsumata, K., Kosuga, M, Katao, H. and University Group of the Joint Seismic Observations at NKTZ., 2010, Focal mechanisms and stress field in the Atotsugawa fault area, central Honshu, Japan, *Earth Planets Space*, **62**, 367–380.

Kawansihi, R., Iio, Y., Yukutake, Y., Shibutani, T. and Katao, H., 2009, Local stress concentration in the seismic belt along the Japan Sea coast inferred from precise focal mechanisms: Implications for the stress accumulation process on intraplate earthquake faults, Jour. Geoph. Res., **114**, B01309, https://doi.org/10.1029/2008JB005765

Kim, Y., Peacock, D. and Sanderson, D., 2004, Fault damage zones, *J. Stru. Geol.*, **26**, 503–517.

Kimura, H., Itoh, Y. and Tsutsumi, H., 2004, Quaternary strike-slip crustal deformation around an active fault based on paleomagnetic analysis: a case study of the Enako fault in central Japan, *Earth Planet Sci Lett*, **226**, 321–334. doi:10.1016/j.epsl.2004.08.003.

Kobayashi, K., Aizawa, Y., Umetsu, K., Oyama, A. and Yamamoto, R., 2003, Geological structure of the epicentral area of the 2000 Tottori-ken Seibu earthquake, *Ann. Rep. Active Fault and Paleoearthquake Res.*, **3**, 163-174 (in Japanese, with English abstract).

Koide, H., 1983, Seismotectonic Problem of en Echelon Fault System and Earthquake Source Mechanism, *J. Tokyo Geogr. Soc.*, **92**, 3, 33–52 (in Japanese, with English abstract).

Kumahara, Y., Okada, A., Goto, H., Tsutsumi, H. and Matta, N., 2019, HIDAFURUKAWA: Sheet map of active faults of Ushikubi fault zone and its vicinity, scale 1:25,000, *Geos Info Auth of Japan* (in Japanese).

Kumahara, Y., 2019, HIDAFURUKAWA: Sheet map of active faults of Ushikubi fault zone, Atotsugawa fault zone and its vicinity, scale 1:25,000, *Tech. Material GSI: D1-No.931*, 13p (in Japanese).

Kuwamura, M. and Yano, T., 2012, Formative process of the Kuninaka Plain, eastern Tottori Prefectrue, *Mem. Fac. Reg. Sci., Tottori Univ.*, 75-87.

Ma, K., Brodsky, E., Mori, J., Ji, C., Song, T. and Kanamori, H., 2003, 1999, Evidence for fault lubrication during the 1999 Chi-Chi, Taiwan, earthquake (Mw 7.6), *Geophys. Res. Lett.*, **30**, 5, 1244.

Maeda, S., 1958, Stratigraphy and Geological Structure of the Tetori Group in the Hida Mountainland, *J. Geol. Soc. Japan*, **64**, 755, 388–398 (in Japanese, with English abstract).

Matsuda, T., 1975, Magnitude and Recurrence Interval of Earthquakes from a Fault, *Jour. Seismol. Soc. Japan, 2nd Ser.* , **28**, 269-283.

Matsuda, T., Okada, S. and Watanabe, T., 2004, Development of active faults in Chugoku and Chubu districts – the comparison of cumulative slip, length of faults and width of crushed zones, *Active Fault Res*, **24**, 1–12 (in Japanese, with English abstract).

Matsukawa, M., Koarai, K., Shionoya, S., Shinkai, T., Nakada, K., Matsui, T., Aono, H., Kobayashi, N., Okubo, A., Hayashi, K. and Ito, M., 2003, Stratigraphy and sedimentary basin developments of the Tetori Group in its main area, central Japan, *J. Geol. Soc. Japan*, **109**, 7, 383–398 (in Japanese, with English abstract).

Matsu'ura, R., 2011, What is reliable and physically plausible about 1586 Tensho eaethquake from historical materials? -The latest research on historical seismicity -, **35**, 29–39 (in Japanese, with English abstract).

Meade, B., J. and Hager, B., H., 2005, Block models of crustal motion in southern California constrained by GPS measurements, *J. Geoph. Res.*, 110, B03403, doi:10.1029/2004JB003209.

Menesess-Gutierrez, A. and Nishimura, T., 2020, Inelastic deformation zone in the lower crust for the San-in Shear Zone, Southwest Japan, as observed by a dense GNSS network, *Earth, Planets and Space*, **72**, 10.

Meneses-Gutierrez, A. and Sagiya, T., 2016, Persistent inelastic deformation in central Japan revealed by GPS observation before and after the Tohoku-Oki earthquake, *Earth Planet Sci Lett*, **450**, 366–371. doi:10.1016/j.epsl.2016.06.055.

Menesess-Gutierrez, A., Sagiya, T. and Sekine, S., 2018, Crustal Deformation Process in the Mid-Niigata Region of the Niigata-Kobe Tectonic Zone as Observed by Dense GPS

Network Before, During, and After the Tohoku-Oki Earthquake, *Journal of Geophysical Research*, **123**, doi:10.1029/2018JB015567.

Mitchell, T, M. and Faulkner, D, R., 2009, The nature and origin of off-fault damage surrounding strike-slip fault zones with a wide range of displacements: A field study from the Atacama fault system, northern Chile, *J Struct Geol*, **31**, 8, 802–816.

Miura, S., Sato, T., Hasegawa, A., Suwa, Y., Tachibana, K. and Yui, S., 2004, Strain concentrate zone along the volcanic front derived by GPS observations in NE Japan arc, *Earth Planets and Space*, **56**, 1347–1355.

Miura, S., Sato, T., Tachibana, K., Satake, Y. and Hasegawa, A., 2002, Strain accumulation in and around Ou Backborn Range, northern Japan as observed by a dense GPS network, *Earth Planets and Space*, **54**, 1071–1076.

Miyashita, Y., Nikaido, M. and Takase. S., 2008, Earthquake history of the Mozumi-Sukenobe fault, northern central Japan, *Abstr. JPGU. Meet. 2008*, S141–P016 (in Japanese, with English abstract).

Mori, Y., 2020 BS, The frictional property of the fault gouge occurred in the aftershock area of 2000 Western Tottori earthquake, B.S. Thesis of Yamaguchi University, Japan, pp51 (in Japanese).

Mori, Y., 2022 MS, The relationship between frictional property of the minor faults and the seismicity distributed in the San-in shear zone, M.S. Thesis of Yamaguchi University, Japan, pp94 (in Japanese).

Murayama, M., Isshiki, N. and Sakamoto, T., 1963, Geological sheet map at the scale of 1: 50,000, "TOTTORIHOKUBU and TOTTORINAMBU", and its explanatory text, Geological Survey of Japan, 66p. (in Japanese, with English abstract)

Murayama, M. and Oosawa, A., 1961, Geological sheet map at the scale of 1: 50,000, "AOYA and KURAYOSHI", and its explanatory text, Geological Survey of Japan, 91p. (in Japanese, with English abstract)

Nakata, T. and Imaizumi, T., 2002, Digital active fault map of Japan. University of Tokyo Press, Tokyo. (in Japanese, with English abstract)

Nishida, K., Imaoka, T. and Iizumi, S., 2005, Cretaceous-Paleogene magmatism in the central San-in district, Southwest Japan: an examination based on Rb-Sr isochron ages, *J. Geol. Soc. Japan*,

Nishida, R., Kurokawa, Y. and Akagi, S., 1993, 1943 Tottori earthquake accompanied with the Yoshino-Shikano fault and the surface ruptures, *Jour. Fac. Liberal. Arts. Tottori Univ.*,

27, 187-226 (in Japanese, with English abstract).

Nishimura, T., 2017, Strain concentration zones in the Japanese Islands clarified form GNSS data and its relation with active faults and inland earthquakes, *Act. Fault Res.*, **46**, 33–39. (in Japanese with English abstract)

Nishimura, T. and Takada, Y., 2017, San-in shear zone in southwest Japan, revealed by GNSS observations, *Earth Planets and Space*, **69**, 85, doi:10.1186/s40623-017-0673-8.

Niwa. M., Kurosawa, H. and Ishimaru, T., 2011, Spatial distribution and characteristics of fracture zones near a long-lived active fault: A field-based study for understanding changes in underground environment caused by long-term fault activities, *Eng Geol*, **119**(1–2), 31–50.

Nozawa. T., Kawada, K. and Kawai, M., 1975, Geology of the Hida–Furukawa district. Quadrangle series scale 1:50,000, *Geol Surv Jpn*, 79p.

Okada, A., 2002, Characteristics of the active faults in the San' in district, western Japan, *Act. Fault Res.*, **22**, 17-32.

Okada, A., 2011, The 1586 Tensho earthquake and associated active faults, *Act. Fault Res.* **35**, 1–13 (in Japanese, with English abstract).

Okada, A., Ando, M. and Tsukuda, T., 1981, Trenches, Late Holocene Displacement and Seismicity of the Shikano Fault Asocciated with the 1943 Tottori Earthquake, *Ann. Rep. Nat. Res. Inst. Earth Sci. Disaster Prev.*, **24**, B1, 105-126.

Okada, A. and Tsutsumi, H., 1997, Holocene Activity of the Chichio Fault, the Median Tectonic Line Active Fault System, Southwest Japan, based on Trenching Studies, *J. Geography (Chigaku Zasshi)*, **106**, 644–659 (in Japanese, with English abstract).

Ohzono, M., Sagiya, T., Hirahara, K., Hashimoto, M., Takeuchi, A., Hoso, Y., Wada, Y., Onoue, K., Ohya, F. and Doke, R., 2011, Strain accumulation process around the Atotsugawa fault system in the Niigata–Kobe Tectonic Zone, central Japan, *Geophys J Int.* doi:10.1111/j.1365-246X.2010.04876.x.

Oohashi, K. and Kobayashi, K., 2008, Fault geometry and paleo-movement of the central part of the Ushikubi fault, northern central Japan, *J Geol Soc Jpn*, **114**, 16–30 (in Japanese, with English abstract).

Oohashi K, Otsubo M, Miyakawa A, Niwa M, Tamura T., 2016, Geological and morphological features of the high-strain rate zone around the Atostugawa fault system, central Japan: Distribution and nature of minor faults. Annual meeting, Geol Soc Jpn, R14-P1 (in Japanese).

Oskin, M., Perg, L., Shelef, E., Strane, M., Gurney, E., Singer, B., Zhang, X., 2008, Elevated shear zone loading rate during an earthquake cluster in eastern California, *Geology*, **36**, 6, 507–510. doi:10.1130/G24814A.1.

Otsubo, M., Katayama, I., Miyakawa, A. and Sagiya, T., 2020, Inelastic behavior and mechanical strength of the shallow upper crust controlled by layer-parallel slip in the high-strain zone of the Niigata region, Japan, *Earth Planets and Space* , 72, 30, doi.org/10.1186/s40623-020-01154-w.

Otsuki, K., Uduki, T., Monzawa, N. and Tanaka, H., 2005, Fractal size and spatial distributions of fault zones: An investigation into the seismic Chelungpu Fault, Taiwan, *Island Arc*, **14**, 12–21. https://doi.org/10.1111/j.1440-1738.2004.00454.x

Reid, H, F., The California earthquake of April 18, 1906 ,1910, *Report of the State Eartquake Investigation Commission*, **2**, 16–18.

Reimer, P.J., Austin, W.E.N., Bard, E., Bayliss, A., Blackwell, P.G., Bronk Ramsey, C., Butzin, M., Cheng, H., Edwards, R.L., Friedrich, M., Grootes, P.M., Guilderson, T.P., Hajdas, I., Heaton, T.J., Hogg, A.G., Hughen, K.A., Kromer, B., Manning, S.W., Muscheler, R., Palmer, J.G., Pearson, C., van der Plicht, J., Reimer, R.W., Richards, D.A., Scott, E.M., Southon, J.R., Turney, C.S.M., Wacker, L., Adolphi, F., Büntgen, U., Capano, M., Fahrni, S.M., Fogtmann-Schulz, A., Friedrich, R., Köhler, P., Kudsk, S., Miyake, F., Olsen, J., Reinig, F., Sakamoto, M., Sookdeo, A. and Talamo, S., 2020, The IntCal20 Northern Hemisphere radiocarbon age calibration curve (0-55 cal kBP), *Radiocarbon*, **62**, 4, 725–757.

Reilinger, R., McClusky, S., Vernant, P., Lawrence, S., Ergintav, S., Cakmak, R., Ozener, H., Kadirov, F., Guliev, I., Stepanyan, R., Nadariya, M., Hahubia, G.,Mahmoud, S., Sakr, K., ArRajehi, A., Paradissis, D., Al-Aydrus, A., Prilepin, M., Guseva, T., Evren, E., Dmitrotsa, A., Filikov, S.V., Gomez, F., Al-Ghazzi, R., Karam, G., 2006. GPS constraints on continental deformation in the Africa–Arabia–Eurasia continental collision zone and implications for the dynamics of plate interactions. *J. Geoph. Res.,* Solid Earth **111**, B05411. https://doi.org/10.1029/2005JB00405

Research Group for Active Faults of Gifu Prefecture, 2008, Active Faults in Gifu, *Gifu newspaper publ.*, 202p (in Japanese, with English abstract).

Research Group for Active Faults of Japan, 1980, Active Faults in Japan, Distribution Map and the Related Materials, *Univ. Tokyo Press*, 363p (in Japanese, with English abstract).

Research Group for Active Faults of Japan, 1991, Sheet Maps and Inventories, Revised Edition.

University of Tokyo Press, Tokyo, 437p (in Japanese, with English summary).

Research Group for Active Faults of Gifu Prefecture, 2008, Active faults in Gifu, *Gifu Newspaper Gifu*, 201p (in Japanese).

Research Group for the Atotsugawa Fault, Okada, A., Takeuchi, A., Tsukuda, T., Ikeda, Y., Watanabe, M., Hirfano, S., Masumoto, S., Takehana, Y., Okumura, K., Takumura, T., Kobayashi, T. and Ando, M., 1989, Trenching study of the Atotsugawa Fault at Nokubi, Miyagawa Village, Gifu Prefecture, central Japan, *J Geogr*, **98**, 4, 62–85 (in Japanese, with English abstract).

Sagiya, T., 2009, Seismotectonics of the Japanese Islands Based on GPS Observation, J. Seismol. Soc. Japan, 2nd Ser, 61, Special issue, 479–487 (in Japanese, with English abstract).

Sagiya, T., Miyazaki, S. and Tada, T., 2000, Continuous GPS array and present-day crustal deformation of Japan. *Pure Appl. Geophys.*, **157**, 2302–2322.

Sagiya, T. and Meneses-Gutierrez, A., 2016, Crustal strain rate paradoxes of the Japan Islands: Their resolution and implications. Taiwan–Japan Workshop: Crustal dynamics 2016 – Unified understanding of geodynamic processes at different time and length scales, 19–22.

Shipton, Z, K., Soden, A, M. and Kirkpatrick, J, D, 2006, How thick is a fault? Fault displacement–thickness scaling revisited. In: Abercrombie, R. (ed) Radiated energy and the physics of faulting. American Geophysical Union.

Shelef, E., and Oskin, M., 2010, Deformation process adjacent to active faults: Examples from eastern California, *J. Geoph. Res.*, **115**, B05308, doi:10.1029/2009JB006289.

Soh, W., Tanikawa, W., Hirose, T., Lin, W., Tanimizu, M., Ishikawa, T., Hirono, T., Nakamura, N., Mishima, T., Yeh, E., Song, S. and Ma, K., 2009, Overview of scientific results of the deep drilling project of the Chelungpu Fault, upon which the 1999 Chi-Chi (Taiwan) earthquake occurred: Main findings and Future research, *J. Geol. Soc. Japan*, **115**, 9, 488–500 (in Japanese, with English abstract).

Sohma, T. and Kunugiza, K., 1993, The formation of the Hida nappe and the tectonics of Mesozoic sediments: The tectonic evolution of the Hida region, Central Japan, *Mem. Geol. Japan*, **42**, 1–20 (in Japanese, with English abstract).

Sueoka, S., Simada, K., Terusawa, S., Iwano, H., Danbara, T., Ogita, Y. and Hirata, T., 2021, Dating of a fault zone distributed in the South Kyushu shear zone based on fission-track thermochronology and U-Pb dating, *Jour. Geol. Soc. Japan*, **127**, 1, 25–39. (in Japanese

with English abstract)

Sugiyama, Y., Awata, Y. and Tsukuda, A. 1991, Holocene Activity of the Miboro Fault System, Central Japan, and Its Implications for the Tensho Earthquake of 1586 - Verification by Excavation Survey -, *Jour. Seismol Soc. Japan, 2nd Ser*, **44**, 283–295 (in Japanese, with English abstract).

Suzuki, Y. and Sugito, N., 2010, Sheet map of active faults in Gifu Prefecture, scale 1:50,000, *Gifu Pref.*, 138p.

Sylvester, A, G., 1988, Strike-slip faults, *Geol. Soc. Am. Bull.*, **100**,1666–1703.

Taira, A., 2001, Tectonic evolution of the Japanese Island arc system, *Ann Rev Earth Planet Sci*, **29**, 109–134. doi:10.1146/annurev.earth.29.1.109.

Takada, K., Tanaka, T., Nohara, T., Haraguchi, T., Ikeda, Y., Ito, K., Imaizumi, T., Otsuki, K., Sagiya, T. and Tsutsumi, H., 2003, Evoluation of active faults and lineaments as potential seismic faults in Chugoku district, Southwest Japan, *Active Fault Research*, **23**, 77–91. (in Japanese, with English abstract).

Sasada, M., 1979, Geology and petrography of the Ochigakochi gabbroic mass, Tottori Prefecture, Southwest Japan, *Mem. Geol. Soc. Japan.*, 17, 231-237.

Takeuchi, A., Hasbaartor, O. and Takebe, A., 2003, Recurrence interval of big earthquakes along the Atotsugawa fault system, central Japan: Results of seismo-geological survey, *Gephys. Res. Lett.*, **30**, 6, 8011.

Takeuchi, A., Ongirad, H. and Takebe, A., 2003, Recurrence interval of big earthquakes along the Atostugawa fault system, central Japan: Results of seismo-geological survey, *Geophys Res Lett*, **30**, 6, 8011. doi:10.1029/2002GL014957.

Takeuchi, A., Takebe, A., Ongirad, H. and Doke, R., 2007, Seismology of the Atotsugawa strike-slip fault system in the Hida mountains, central Japan – with the special reference to the investigation gallery across the branch Mozumi–Sukenobe fault. Prof. M. Ando ed. "Geodynamics of Atotsugawa Fault System", *TERRAPUB*, 1–10.

Tamura, I., Yamazaki, H. and Nakamura, Y., 2010, The wide-spread tephra in the Hokuriku Group and the Quaternary tectonics of the Toyama Basin, *J. Geol. Soc. Japan*, **116**, Supplement, S1–S20 (in Japanese).

Tamura, T., 2018 MS, Topographical and geological analysis and estimation of total slip rate by minor faults in the Niigata-Kobe Tectonic Zone: An example of Hida area, M.S. Thesis of Yamaguchi University, Japan, pp90. (in Japanese)

Tamura, T., Oohashi, K., Otsubo, M., Miyakawa, A. and Niwa, M., 2020, Contribution to

crustal strain accumulation of minor faults: a case study across the Niigata-Kobe Tectonic Zone, Japan, *Earth Planets and Space* , **72**, 7, doi.org/10.1186/s40623-020-1132-5

Taniguchi, K., Watanabe, M., Suzuki, Y. and Sawa H., 2011, Newly-found Surface Faulting Event on the North-central Portion of the Itoigawa-Shizuoka Tectonic Line Active Fault System, *J. Seismol. Soc. Japan, 2nd Ser.*, **64**, 11–21 (in Japanese, with English abstract).

Tchalenco J., S., 1970, Similarities between Shear Zones of Different Magnitudes, Geol.Soc. Amer. Bull, 81, 1625-1640.

Toda, S., Inoue, D., Kubouchi, A., S, Takase. and Nikaido, M., 1995, Paleoseismicity of of the Atera Fault System and 1586 Tensho earthquake: Trenching studies at Ogo, Aonohara and Dendahara, Central Japan, *J. Seismol. Soc. Japan, 2nd Ser.*, **48**, 401–421 (in Japanese, with English abstract).

Tukiji, A., 1948, Some observations on the relation between topography and active faults after Tottori earthquake, 1943, *Geogr. Rev. Japan*, **21**, 7-8, 239-247 (in Japanese).

Tuya, T., 1944, Sikano-Yoshioka fault and the geology, Bull. Earthq. Res. Inst., **22**, 1-32 (in Japanse).

Uchida, H., Mukoyoshi, H., Tonai, S., Yamaguchi, M. and Kobayashi, K., 2021, Reactivation of minor faults in a blind active fault area: A case study of the aftershock area of the 2000 Western Tottori Earthquake, Japan, J. Asian Earth Sci., **X**, 5, 100053.

Ueta, K. and Tani K., 1999, Deformation of Quaternary Deposits and Ground Surface Caused by Bedrock Fault Movements (Part 3) -Strike-slip and Oblique-slip Fault Model Tests-, *CRIEPI Res. Report, No. U98049*, 42p (in Japanese, with English abstract).

Usami, T., 1979, Hietsu earthquake of April 9, 1958 and the Atotsugawa Fault, Seismol. *Soc. Japan, Abstr.*, **1**, 108 (in Japanese, with English abstract).

Usami, T., Ishii, H., Imamura, T., Takemura, M. and Matsuura, R., 2013, Material for Comprehensive List of Destructive Earthquakes in Japan, 599–2012, *Univ. Tokyo Press*, 694p (in Japanese, with English abstract).

Yamada, N., Adachi, N., Kajita, M., Harayama, S., Yamazaki, H. and Bunno, M., 1985, Geology of the Takayama district. Quadrangle Series, scale 1:50,000, *Geol Surv Jpn*, 111p (in Japanese, with English abstract).

Yamada, N., 1961, Geological sheet map at the scale of 1: 50,000, “OKUTSU”, and its explanatory text, Geological Survey of Japan, 76p. (in Japanese, with English abstract)

Yamada, N., 1965, Geological sheet map at the scale of 1: 50,000, “CHIZU”, and its explanatory text, Geological Survey of Japan, 100p. (in Japanese, with English abstract)

Yamaji, A., 2000, The multiple inverse method: a new technique to separate stresses from heterogeneous fault-slip data, *J Struct Geol*, **22**, 441–452. doi:10.1016/S0191-8141(99)00163-7.

Yamaji, A., 2016, Genetic algorithm for fitting a mixed Bingham distribution to 3D orientations: a tool for the statistical and paleostress analyses of fracture orientations, Island Arc, **25**, 72–83.

Yamaji, A., Sato, K. and Otsubo, M., 2011, Multiple inverse method software package user's guide, *Kyoto University*, p20 (in Japanese with English version).

Yoshioka, T., Hirouchi, D., Sugito, N. and Saito, M., 2009, Paleoseismicity of the Makigahora, Enako, Miyagawa and Nukuidami faults in the Takayama-Oppara fault zone, central Japan, *Ann. Rep. Active Fault and Paleoearthquake Res.*, **9**, 279–317 (in Japanese, with English abstract).

Yukutake, Y., Iwata., T. and Iio, Y., 2020, Estimation of the heterogeneity of stress fields using misfit angles in focal mechanisms, *tectonophysics*, **790**, doi.org/10.1016/j.tetco.2020.228553.

Wakita, K., 2013, Geology and tectonics of Japanese islands: A review – the key to understanding the geology of Asia. *J Asian Earth Sci*, **72**, 10, 75–87. doi:10.1016/j.jseaes.2012.04.014.

Wesnousky, S, G. and Scholz, C, H., 1982, Deformation of an island arc: rates of moment release and crustal shortening in intraplate Japan determined from seismicity and quaternary fault data, *J Geophys Res*, **87**, B8, 6829–6852.

[URL1] Headquarters for Earthquake Research Promotion (HERP), 2016, Long-term evaluation report of the Atotsugawa fault zones, https://www.jishin.go.jp/regional_seismicity/rs_chugoku-shikoku/p31_tottori/ (Accessed 2021.10.27) (in Japanese)

[URL2] Headquarters for Earthquake Research Promotion (HERP), 2004, Long-term evaluation report of the Atotsugawa fault zones, 28p, https://www.jishin.go.jp/main/chousa/katsudansou_pdf/47_atotsugawa.pdf (Accessed 2021.8.18) (in Japanese)

[URL3] Headquarters for Earthquake Research Promotion (HERP), 2003, Long-term evaluation report of the Takayama–Oppara fault zones, 27p, https://www.jishin.go.jp/main/chousa/katsudansou_pdf/48_takayama_oppara.pdf (Accessed 2021.8.18) (in Japanese)

[URL4] Gifu Prefectural Museum, Geological map of Gifu Prefecture “GEOLAND GIFU” https://geo-gifu.org/geoland/kakusetsu/contents_top.html (2021.3.4 confirmed).

Acknowledgements

I would like to extend my sincere appreciation to Dr. Kiyokazu Oohashi of Yamaguchi University for many helpful discussions, passionate guidance and encouragements. I thank Prof. Toshiaki Shimura, Takehiro Ota, Arito Sakaguchi, Dr. Tomohiro Tuji of Yamaguchi University for reviewing this dissertation. I am grateful to Dr. Makoto Otsubo of Geological survey of Japan, National Institute of Advanced Industrial Science and Technology (AIST), Dr. Ayumu Miyakawa of Geological survey of Japan, National Institute of Advanced Industrial Science and Technology (AIST) and Dr. Masakazu Niwa of Japan Atomic Energy Agency (JAEA) for many helpful comments and critical discussions. I thank Prof. Takeshi Sagiya of Nagoya University for his helpful comments and critical discussions. I wish to thank Dr. Kyoko Kagohara of Yamaguchi University for introducing me the QGIS and its way to use and for reviewing this dissertation. I would like to thank Dr. Ken-ichi Yasue of Toyama University for instructing me how to obtain LiDAR-derived DEM data of Tottori Prefecture. Thank Prof. Yoshihisa Iio and Hideki Mukoyoshi for helpful discussion of stress fields in San-in shear zone. I thank Dr. Osamu Tadai of Marin Works Japan Ltd. for instructing me how to use Rock Jock program and for instructing me how to use instruments at the KCC. I wish to thank Dr. Hiroyuki Noda and Takuya Nishimura of Kyoto University for beneficial discussions. I also thank Dr. Kenta Kobayashi of Niigata University and Shun Suzuki of former Niigata University for useful discussion regarding the Inagoe fault outcrop. I wish to thank Dr. Yoshiaki Sugamori of Tottori University for valuable discussions on Iwatsubo fault outcrops in the San' in district. I would like to thank Mr. Hideto Uchida of Shikoku Research Institute INC. for introducing me the information on geology of San'in district. I wish to thank Mr. Keisuke Eshima of Yamaguchi University for introducing me the Simple DEM viewer. I would like to thank Mr. Yo Mori of Yamaguchi University for introducing me GMT and for helpful discussions. I thank former Prof. Yuji Kanaori of Yamaguchi University and Dr. Kotaro Aiyama of Central Research Institute of Electoric Power Industry (CRIEPI) for his helpful comments and supports.

This work was financially supported by a Grant-in-aid for JSPS fellows by the Japan Society for Promotion of Science (JSPS). This study was supported by the Fukada grant-in-aid of the Fukada Geological Institute and the grant-in-aid for Scientific Research on Innovative Areas (KAKENHI No. 2608) during the investigation in Hida city. This study was also supported by the San'in Kaigan Geopark grant-in-aid for Scientific Research of the San'

in Kaigan UNESCO Global Geopark during the investigation in Tottori city.

Finally, I would like to express my sincere thanks to my parent for her supports.